Texas Medical Center Library
DigitalCommons@The Texas Medical Center

UT GSBS Dissertations and Theses (Open Access) | Graduate School of Biomedical Sciences

8-2014

EGFR Modulates MicroRNA Maturation In Response To Hypoxia Through Phosphorylation Of Argonaute2

Jia Shen

Follow this and additional works at: http://digitalcommons.library.tmc.edu/utgsbs_dissertations

 Part of the Cancer Biology Commons, Cell Biology Commons, and the Molecular Biology Commons

Recommended Citation

Shen, Jia, "EGFR Modulates MicroRNA Maturation In Response To Hypoxia Through Phosphorylation Of Argonaute2" (2014). *UT GSBS Dissertations and Theses (Open Access)*. Paper 495.

This Dissertation (PhD) is brought to you for free and open access by the Graduate School of Biomedical Sciences at DigitalCommons@The Texas Medical Center. It has been accepted for inclusion in UT GSBS Dissertations and Theses (Open Access) by an authorized administrator of DigitalCommons@The Texas Medical Center. For more information, please contact laurel.sanders@library.tmc.edu.

The TMC LIBRARY Health Sciences Resource Center

EGFR MODULATES MICRORNA MATURATION IN RESPONSE TO HYPOXIA THROUGH PHOSPHORYLATION OF ARGONAUTE2

by

Jia Shen, B.S.

APPROVED:

_____
Mien-Chie Hung, Ph.D., Supervisory Professor

_____
Dihua Yu, M.D., Ph.D.

_____
Ann-Bin Shyu, Ph.D.

_____
Min Gyu Lee, Ph.D.

_____
Zhen Fan, Ph.D.

APPROVED:

_____
Dean, The University of Texas

Graduate School of Biomedical Sciences at Houston

EGFR MODULATES MICRORNA MATURATION IN RESPONSE TO HYPOXIA THROUGH PHOSPHORYLATION OF ARGONAUTE2

A

DISSERTATION

Presented to the Faculty of
The University of Texas
Health Science Center at Houston
and
The University of Texas
MD Anderson Cancer Center
Graduate School of Biomedical Sciences
in Partial Fulfillment

of the Requirements

for the Degree of

DOCTOR OF PHILOSOPHY

by

Jia Shen, B.S.

Houston, Texas

August, 2014

Copyright from Nature Publishing Group

The authors of articles published by Nature Publishing Group, or the authors' designated agents, do not usually need to seek permission for re-use of their material as long as the journal is credited with initial publication. For further information about the terms of re-use for authors please see below.

Author Requests

If you are the author of this content (or his/her designated agent) please read the following. Since 2003, ownership of copyright in in original research articles remains with the Authors*, and provided that, when reproducing the Contribution or extracts from it, the Authors acknowledge first and reference publication in the Journal, the Authors retain the following non-exclusive rights:

a. To reproduce the Contribution in whole or in part in any printed volume (book or thesis) of which they are the author(s).
b. They and any academic institution where they work at the time may reproduce the Contribution for the purpose of course teaching.
c. To reuse figures or tables created by them and contained in the Contribution in other works created by them.
d. To post a copy of the Contribution as accepted for publication after peer review (in Word or Tex format) on the Author's own web site, or the Author's institutional repository, or the Author's funding body's archive, six months after publication of the printed or online edition of the Journal, provided that they also link to the Journal article on NPG's web site (eg through the DOI).

NPG encourages the self-archiving of the accepted version of your manuscript in your funding agency's or institution's repository, six months after publication. This policy complements the recently announced policies of the US National Institutes of Health, Wellcome Trust and other research funding bodies around the world. NPG recognizes the efforts of funding bodies to increase access to the research they fund, and we strongly encourage authors to participate in such efforts.

Authors wishing to use the published version of their article for promotional use or on a web site must request in the normal way.
If you require further assistance please read NPG's online author reuse guidelines.
Note: *British Journal of Cancer* maintains copyright polices of its own that are different from the general NPG policies. Please consult this journal to learn more.
* Commissioned material is still subject to copyright transfer conditions

Dedication

This PhD thesis work is dedicated to

My dearest parents

My best friends

For their endless love and great support!

Acknowledgements

I would like to express my sincere appreciation to my mentor, Dr. Mien-Chie Hung for his full support and guidance on the course to pursue my Ph.D. degree. He provided the constructive training environment for integrating knowledge of biochemistry, molecular biology, cell biology and cancer biology in my research projects.

I also appreciate all my committee members, Drs. Di Hua Yu, Ann-Bin Shyu, Min Gyu Lee, Zhen Fan, Sharon Y.R. Dent, Mong-Hong Lee, Xiangwei Wu and Michael W. Van Dyke for their excellent questions and wonderful suggestions over the past years.

I would like to take this opportunity to thank all current and past members of Dr. Hung's laboratory, especially Dr. Weiya Xia, Ye Sun, Dr. Yan Wang, Dr. Dongping Liu, and Dr. Ming-chuan Hsu for their friendship and generous support. Also, I thank Su Zhang, Zhenbo Han, Jian Guan Shi, Jin-Fong Lee for daily assistance and Dr. Jennifer Hsu for manuscript editing.

In addition, I would like to thank all our collaborators, Drs. Dinshaw J. Patel, Kotaro Nakanishi, Wei-Chao Chang, Chung-Hsuan Chen, Brian P. James, Xiuping Liu and Chang-Gong Liu for their comments and technical supports.

Finally, I would like to thank my family. My parents give me all their love and care that make me strong enough to overcome the obstacles. Without their understanding and great support, I cannot achieve any accomplishments during the PhD study.

EGFR MODULATES MICRORNA MATURATION IN RESPONSE TO HYPOXIA THROUGH PHOSPHORYLATION OF ARGONAUTE2

Jia Shen, Ph.D.*

Advisory Professor: Mien-Chie Hung, Ph.D.

MicroRNAs (miRNAs) are generated by two-step processing to yield small RNAs that negatively regulate target gene expression at posttranscriptional level. Deregulation of miRNAs has been linked to diverse pathological processes, including cancer. Recent studies have also implicated miRNAs in regulatory roles to cope with a spectrum of stresses, such as hypoxia, which is frequently encountered in the poorly angiogenic core of a solid tumor. However, the upstream regulators of miRNA biogenesis machineries remain obscure, raising the question of how tumor cells efficiently coordinate and impose specificity on miRNA expression and function in response to stresses. Here, we show that EGFR, a well-characterized oncogene in human cancers, suppresses the maturation of specific tumor-suppressor-like miRNAs in response to hypoxic stress through phosphorylation of Argonaute2 (Ago2) at Tyr393. The association between EGFR and Ago2 is enhanced by hypoxia, leading to elevated Ago2-Y393 phosphorylation which in turn reduces the binding of Dicer to Ago2 and inhibits miRNA processing from precursor miRNAs (pre-miRNAs) to mature miRNAs. Interestingly, we also identify a long-loop structure in pre-miRNAs as a critical regulatory element in phospho-Y393-Ago2-mediated miRNA maturation. Furthermore, Ago2-Y393 phosphorylation mediates EGFR-enhanced cell survival and invasiveness under hypoxia, and correlates with poorer overall survival in breast cancer

patients. Our study reveals a previously unrecognized function of EGFR in miRNA maturation and demonstrates how EGFR is likely to function as a regulator of Ago2 through novel posttranslational modification. These findings suggest that modulation of miRNA biogenesis is important for stress response in tumor cells and has potential clinical implications (Shen et al., 2013).

Table of Content

Table of Figures

List of Tables

Chapter 1 Introduction

1.1 EGFR Activation and Endocytic Recycling

EGFR is a member of the ErbB family of receptor tyrosine kinases (RTK) with an extracellular ligand-binding domain, a single hydrophobic transmembrane domain and a cytoplasmic tyrosine kinase-containing domain (Olayioye et al., 2000). Binding of ligands, including EGF, HB-EGF, TGFα and amphiregulin (AR), to the extracellular domain induces the homo- or hetero-dimerization with other ErbB family members, and subsequent enhancement of the catalytic activity of the intrinsic tyrosine kinase, which is considered to be the "first-phase" activation (Koch et al., 1991). The "second-phase" activation takes place after trans-autophosphorylation of specific tyrosine (Y) residues within the cytoplasmic tail, creating mutiple docking sites to recruit signaling molecules containing Src homology 2 (SH2) domain or phosphortyrosine binding (PTB) domain, resulting in the activation of multiple signal transduction pathways near the plasma membrane (Grant and Donaldson, 2009). Ligands binding also results in rapid internalization of activated receptors, either through clathrin-dependent (CDE) or independent (CIE) pathway. Regardless of the mode of entry, internalized cargo is usually delivered to the early endosome and then further sorted to the late endosome and lysosome for degradation or routed to the trans-Golgi network (TGN) or transited to the recycling endosomal carriers that back to the plasma membrane as an equilibrium (Grant and Donaldson, 2009). All these events including dynamic network of molecular interactions and post-translational modifications ultimately lead to EGFR-mediated cell survival, proliferation, mobility and anti-apoptosis.

1.2 Sustained Signaling in Endosomes after Receptor Internalization

Numerous unique properties of endosomes, such as a relative small volume favoring ligand-receptor association and maintenance of receptor activity, an enrichment in PtdIns3P

(phosphatidylinositol 3-phosphate) allowing the assembly of complexes involving PX domain containing proteins, as well as the long residence time of activated receptors due to slow endosomal sorting, indicates these subcellular locations can serve as important signaling platforms after receptor internalization (Sorkin and von Zastrow, 2009). For example, EGFR after entry into the cell still remain ligand bound, phosphorylated and active in endosomes until the late stage of endosomal trafficking. Endocytosis has been proposed to be necessary for the duration of the EGFR signaling as supported by the detection of all the components of MAPK activation cascade in the endosomes (Sorkin and von Zastrow, 2009). Alternatively, distinct signaling may require receptor endocytosis and/or occur exclusively on endosomal membranes.

1.3 EGFR and Cancer

Amplification of EGFR expression or up-regulation of EGFR signaling pathway has been verified to be a common feature in a variety of human cancers including breast, glioma, ovarian, non-small-cell lung, prostate, pancreatic, renal, and head and neck cancers (Abd El-Rehim et al., 2004; Normanno et al., 2003). As a prognostic maker of advanced tumor stage, EGFR expression level/ activation is correlated with reduced patient survival and high risk of metastasis, therefore, it has been a central target for cancer therapy (Abd El-Rehim et al., 2004). However, the causes of EGFR over-expression in human cancers remain not very clear but at least involving gene amplification and mutation-induced constitutive activation. Only a few cancer types such as glioblastoma and non-small-cell lung cancer has been verified to display high incidence of EGFR mutation (20%-40%), while similar phenomena are rarely observed in other cancers (Halatsch et al., 2006; Paez et al., 2004; Sharma et al., 2007). Interestingly, recent studies found that the hypoxic tumor microenvironment can up-

regulate the translational level of EGFR (Franovic et al., 2007) and prolong its activation though deregulation of Rab5-mediated EGFR endocytosis pathway (Wang et al., 2009). Moreover, non-ligand stimulation, such as UV, IR, H2O2, and certain cytokines (like TNF-alpha) have been shown to activate EGFR directly or indirectly, thereby enhance cancer cell survival (Cao et al., 2008; Reynolds et al., 2003).

1.4 miRNA and Cancer

microRNAs (miRNAs) are abundant, short (20-25-nucleotide), single-stranded regulatory RNA molecules, that collectively play critical roles in diverse developmental and physiological processes in eukaryotes (Kim et al., 2009). The general defining features of miRNAs are the cleavage of their precursor transcripts by one or more RNase III enzymes, and the subsequent sorting of mature miRNAs into Argonaute proteins to form the RNA-induced silencing complex (RISC), a ribonucleoprotein complex mediating posttranscriptional gene silencing (Kim et al., 2009; Yang and Lai, 2011). As with other classes of Argonaute-bound small RNAs, miRNAs serve as antisense guides to identify and target messenger RNAs (mRNAs) via ~7 nt complementary base-pairing to the 5' ends of the mature miRNAs (preferentially nucleotides 2-8, the "Seed" of a miRNA). In consequence, the targeted mRNAs are degraded, destabilized or translationally suppressed by the Argonaute proteins (Kim et al., 2009; Meister, 2013). Computational and experimental studies have provided multilayer supporting evidence for the broad impact of a miRNA on hundreds of mRNA targets, such that a majority of the human transcripts are predicted and proven to carry conserved binding sites for multiple miRNAs (Kim et al., 2009). Not surprisingly, the deregulation of homeostatic control of miRNA biogenesis is associated with multiple pathological diseases, including cancer.

Global down-regulation of mature miRNA level as well as up-regulation of specific oncomiRs (miRNAs that are associated with oncogenic events) in certain tumor types has become an important feature in cancer development and progression (Leung and Sharp, 2007; Lu et al., 2005; Nicoloso et al., 2009). The steady level of a mature miRNA is determined by the rates of its transcription, biogenesis processing and turnover (Winter et al., 2009). Transcriptional regulation, either activation or silencing, accounts for significant portion of alterations in miRNA production (Choudhry and Catto, 2011), which however, fail to explain another striking observation in cancer that compared with normal tissues the primary transcripts of miRNAs (pri-miRNAs) are accumulated in tumors and the expression of mature miRNAs is inconsistent with the level of corresponding miRNA precursors (pre-miRNAs) (Blenkiron et al., 2007; Lu et al., 2005; van Kouwenhove et al., 2011; Ventura and Jacks, 2009). Indeed, miRNA maturation, as suggested by recent studies (Davis et al., 2008; Mori et al., 2014; Shen et al., 2013; Suzuki et al., 2009), is subject to complex regulation and defects during this process significantly contribute to tumorigenesis and cancer progression. In contrast to the universal model of linear miRNA processing (Kim et al., 2009; Winter et al., 2009), accumulating evidence, emerged in the past few years, leads to the recognition of signaling-mediated control of miRNA processing, which opens a plethora of new regulatory options to modulate individual or cluster of miRNAs differently. Such regulations mainly rely on the intensive interplay between miRNA core machineries, RNA-binding proteins (RBPs) and signaling transducers or executors in response to external or internal stimuli, and dynamically shape the extent of miRNA production to maintain the robust gene expression under specific pathophysiological conditions (Davis et al., 2008; Mori et al., 2014; Shen et al., 2013; Suzuki et al., 2009).

1.5 Classical Linear Processing of miRNAs

A canonical pathway driven by RNase III enzymes generates the majority of miRNAs in metazoan (Kim, 2005; Kim et al., 2009). The biogenesis of miRNA starts with RNA polymerase II-dependent (predominant) or RNA polymerase III-dependent transcription, generating a long primary transcript (pri-miRNA) that contains a typical hairpin structure. Like mRNAs, most pri-miRNAs are 5' 7-methyl-guanosine (m_7G) capped and 3' polyadenylated before further processing mediated by nuclear microprocessor Drosha/DGCR8 heterodimer (Kim et al., 2009). DGCR8 (DiGeorge syndrome critical region gene 8, also known as Pasha in invertebrates) functions as a molecular anchor that recognizes pri-miRNA at stem-ssRNA junction and positions RNase III endonuclease Drosha at correct catalytic sites to cleave ~11bp away from the junction, releasing a hairpin-shaped pre-miRNA (Kim et al., 2009). Alternatively, miRNAs can be generated from short intronic hairpins (named as mirtrons) which are excised by splicing and debranching to mimic a regular pre-miRNA, and consequently bypass the first-step cleavage mediated by Drosha/DGCR8 in the nucleus (Yang and Lai, 2011). The secondary structure (>14bp dsRNA stem along with a short 3' overhang) of the resulting miRNA precursor, ~55-70 nucleotide (nt) in length, is recognized by Exportin-5 (XPO5) in complex with Ran-GTP, enabling its subsequent shuttling to cytoplasm via GTP hydrolysis (Kim et al., 2009; van Kouwenhove et al., 2011). In the cytoplasm, the terminal loop of pre-miRNA is cleaved by another double-stranded RNA (dsRNA)-specific RNase III Dicer in collaboration with dsRNA-binding protein TRBP (TAR RNA-binding protein, also known as TARBP2, human immunodeficiency virus transactivation responsive RNA-binding protein 2) or PACT (also known as PRKRA, protein activator of PKR) (Kim et al., 2009; Winter et al., 2009). Both

5’-phosphorylated end and 3’ overhang of the pre-miRNA are anchored by the PAZ domain of Dicer, while the dsRNA stem is placed along the positively charged protein extension to reach the catalytic center of Dicer. This spatial arrangement determines the precise cleavage site in miRNA precursor that is a fixed distance, ~22nt, either from the 3’ end (3’ counting model) (Kim et al., 2009) or the 5’ end of the terminus (5’ counting rule) (Park et al., 2011). TRBP, as a cofactor, facilitates Dicer-mediated cleavage through direct binding with the pre-miRNA via its two dsRNA-binding domains (dsRBDs) and concomitantly enhances the stability of Dicer-RNA complex using its third dsRBD (Chendrimada et al., 2005; Daniels et al., 2009). Both TRBP and PACT, though not essential for miRNA maturation, participate in the recruitment of Argonaute2 (Ago2) to Dicer, forming the RISC loading complex (RLC) for efficient miRNA processing and subsequent RISC assembly (Winter et al., 2009). Notably, *in vitro* reconstitution of RISC loading and activation is achieved by Dicer, TRBP and Ago2 alone (Maniataki and Mourelatos, 2005). Exported miRNA precursors only join and fuel the RLC after the formation of this ternary complex, a process independent of ATP hydrolysis (Maniataki and Mourelatos, 2005). After cleavage, miRNA duplex is further unwound based on the rule of asymmetric separation (strand with less stable base pairs at its 5’ end in dsRNA intermediate is selected and loaded into RISC) (Kim et al., 2009). Although it remains unclear how the RLC precisely coordinates the sequential events such as precursor loading, cleavage, duplex unwinding, and the subsequent cargo loading into RISC, evidence suggests that the stable end of the Dicer-cleaved RNA duplex is bound to TRBP in RLC, whereas the other end interacts with Ago2 (Kim et al., 2009; Meister, 2013), resulting in the functional guide strand (mature miRNA) that is complementary to its mRNA targets and the passenger strand which is frequently fast degraded. After dsRNA unwinding,

Ago2 (and possibly other AGO proteins) loaded with mature miRNA dissociates with Dicer and TRBP to form the active RISC for target gene silencing (Meister, 2013). Argonautes are highly specialized binding modules that function as regulators in miRNA maturation and also executors in small RNA-mediated gene silencing (Hutvagner and Simard, 2008; Winter et al., 2009). All the AGO proteins are characterized by evolutionarily conserved MID and PAZ domains involved in RNA binding and an RNase H-like PIWI domain for endonuclease activity (Hutvagner and Simard, 2008; Meister, 2013). In mammals, there are four AGO proteins (Ago1-4) but only Ago2 is catalytically active and could function as an endonuclease (Hutvagner and Simard, 2008). Structural studies suggest that the 3' end of a mature miRNA is stably bound by the PAZ domain while the 5' phosphate group of the small RNA is anchored by the MID domain (Meister, 2013). Proper small RNA loading and duplex unwinding are further assisted by the N-terminal domain in Argonautes (Kwak and Tomari, 2012). In some occasions, a processing intermediate is generated by Ago2-dependent cleavage of pre-miRNA to facilitate miRNA maturation and removal of the passenger strand. Additionally, AGO proteins are capable to stabilize mature miRNAs via direct binding and post-transcriptionally regulate miRNA abundance independent of endonuclease activity (Diederichs and Haber, 2007). Recently, a Dicer-independent miRNA biogenesis pathway (as exemplified by pre-miR-451) that utilizes Ago2 slicer catalytic activity for processing was identified (Cheloufi et al., 2010; Cifuentes et al., 2010). The short stem region of pre-miR-451 cannot be recognized by Dicer but is trimmed by Ago2 to generate the corresponding mature miRNA (Cheloufi et al., 2010). However, the extent to which such phenomena (processing that completely depends on Ago2) occur is still unclear and need further investigations.

1.6 Signaling-Mediated Regulation of miRNA Processing

miRNAs are often deregulated in cancer (Leung and Sharp, 2007; Lu et al., 2005; Nicoloso et al., 2009). In contrast to the defined oncogene or tumor suppressor, miRNA alteration is rarely caused by gene amplification or disruption (Yang and Lai, 2011). Instead, impairment of crucial steps in the process of miRNA maturation, either in the nucleus or in the cytoplasm, could be the underlying main causes that significantly contribute to the development of malignancies. Notably, recent studies (Cheng et al., 2014; Davis et al., 2008; Mori et al., 2014; Shen et al., 2013; Suzuki et al., 2009; Yamagata et al., 2009) demonstrate the intensive crosstalk between signaling pathways and miRNA processing, suggesting that the biogenesis of miRNA is under tight signaling control and has become an important part of the large regulatory networks.

1.6.1 Regulation of miRNA Processing in the Nucleus

The stability of the nuclear microprocessor is self-controlled by the cross-regulation between Drosha and DGCR8 (Kim, 2005; Kim et al., 2009), while the processing efficacy of pri-miRNA is further tuned by other accessory RNA-binding proteins, such as DDX5 (also known as p68) and DDX17 (also known as p72) (Kim et al., 2009; van Kouwenhove et al., 2011). Both DDX5 and DDX17 directly interact with Drosha/DGCR8 to form a larger nuclear processing complex and function as restricted promoting factors that are specifically required for efficient processing of a subset of pri-miRNAs (Fuller-Pace and Moore, 2011; Slezak-Prochazka et al., 2010; van Kouwenhove et al., 2011). Intriguingly, DDX5 and DDX17 also serve as signal mediators that bridge the nuclear microprocessor activity with other signaling pathways under varying circumstances. In response to estrogen (E2), activated estrogen receptor (ERα) together with E2 attenuates the processing of subclass pri-

miRNAs into precursors through direct interaction with DDX5 and DDX17. In consequence, the RNA-binding subunits in Drosha complex is competitively blocked by the cognate nuclear receptor of steroid hormones, resulting in the suppression of miRNA processing and subsequently the stabilization of ERα target genes (Yamagata et al., 2009). In the context of DNA damage, tumor suppressor p53 binds with DDX5 to enhance Drosha/DGCR8-mediated processing of a cluster of miRNAs which exert growth suppressive functions. Transcriptionally inactive p53 mutants, frequently identified in human tumors, interfere with the functional assembly between Drosha complex and DDX5, which in consequence hinder the nuclear processing of those miRNAs (Suzuki et al., 2009). Similar case is also illustrated by the SMAD signal transducers in response to transforming growth factor-β (TGFβ) and bone morphogenetic protein (BMP) growth factor (Davis et al., 2008). The SMADs, in complex with the microprocessor component DDX5, promote the nuclear processing of miRNA (specifically, miR-21, a well-characterized oncomiR in cancer) via a consensus binding sequence (similar to the known SMAD-response element in gene promoters) in dsRNA stem of the pri-miRNA. More recently, cell-density-dependent control of miRNA biogenesis was uncovered and tightly linked to tumor-suppressive Hippo signaling pathway via its downstream target YAP (*Yes-associated protein* 1, oncogene, inactivated by Hippo signaling) (Mori et al., 2014). At low cell density, DDX17 (p72) is bound and sequestered by nuclear YAP, which in turn dissociates DDX17 from the nuclear microprocessor complex and hence decreases the processing efficacy of a group of miRNAs in the nucleus. When reach high cell density, YAP is restricted in cytoplasm by activated Hippo signaling. DDX17, in that scenario, associates with Drosha/DGCR8 complex and enhances miRNA processing through binding to a specific sequence motif in the 3' flanking region of a pri-

miRNA. Notably, DDX5 and DDX17 are also known to function as transcription regulators (Fuller-Pace and Moore, 2011), either coactivators (predominant) or corepressors. For instance, both DDX5 and DDX17 serve as coactivators of ERα, β-catenin and MyoD through facilitating the recruitment of other components of transcriptional machinery to the target gene promoters (Caretti et al., 2006; Endoh et al., 1999; Metivier et al., 2003; Yang et al., 2006). More specifically, DDX5 is a coactivator of p53, AR, RunX2 and the p50 subunit of NF-kB via direct interaction with those important transcription factors (Bates et al., 2005; Clark et al., 2008; Jensen et al., 2008; Wang et al., 2012), while DDX17 coactivates MDM2 transcription, in both p53-dependent and independent manor (Fuller-Pace and Moore, 2011). The precise roles of DDX5 and DDX17 in cancer development remain controversial. *Ddx5*-deficient and *Ddx17*-deficient mouse embryonic fibroblasts (MEFs) are characterized by reduced cell growth and enhanced apoptosis (Fukuda et al., 2007). Consistently, silencing both *DDX5* and *DDX17* inhibits cell proliferation (Jalal et al., 2007), whereas overexpression of DDX5 facilitates cell growth and promotes epithelial-to-mesenchymal (EMT) transition upon growth factor stimulation (Yang et al., 2006). However, higher expression of DDX17 in breast tumors associates with a favorable prognosis with significantly increased disease-free and overall survival (Wortham et al., 2009). DDX5, in contrast, is often overexpressed and frequently gene-amplified, with rare mutations, in breast invasive carcinomas (8.6% amplification vs. 0.3% mutations, from the Cancer Genome Atlas). Different roles of DDX5 and DDX17, in terms of prognosis, are also reported in other cancer types, including head and neck, prostate and colorectal cancers (Causevic et al., 2001; Clark et al., 2008; Haines et al., 1993). Possibly, their biological functions, as tumor promoter or suppressor, are cell-type-dependent or restricted by certain genetic background.

One thing interesting is that the binding partners of DDX5/DDX17, involved in transcriptional modulation or miRNA processing, are largely overlapped, suggesting an intimate collaboration in gene expression between transcriptional and posttranscriptional regulations. Nonetheless, the specific function of DDX5 and DDX17, as components of Drosha/DGCR8 complex, in cancer development is still unclear and need to be further elucidated by systemic investigation of their target miRNAs.

Drosha/DGCR8-mediated miRNA processing is also subject to other regulation mechanisms, including additional binding partners with microprocessor and multiple RNA-binding proteins that can recognize and directly interact with subclass pri-miRNAs (van Kouwenhove et al., 2011). DGCR8 is a heme-binding protein. Heme promotes DGCR8 dimer to trimerize upon loading pri-miRNAs and subsequently facilitates pri-miRNA cleavage via blocking the auto-inhibition domain in DGCR8 (Faller et al., 2007). MeCP2 (methyl-CpG binding protein2), a transcriptional repressor that is critical for proper development and function in central nerve system, is another direct interaction partner with DGCR8 (Cheng et al., 2014). MeCP2 binds to DGCR8 via its C-terminal domain and interferes with the assembly of Drosha/DGCR8 complex. Interestingly, the association between MeCP2 and DGCR8 is tightly regulated by the phosphorylation status of MeCP2 at Ser80, which is constantly phosphorylated under resting stage but rapidly dephosphorylated upon neuronal activity. As a protein-binding switch, phosphorylation of Ser80 in MeCP2 “opens” its conformation to interact with DGCR8 and thus inhibits miRNA maturation through dissembling the microprocessor complex (Cheng et al., 2014). Another essential regulatory module in nuclear miRNA processing belongs to the huge family of RNA-binding proteins (RBPs). RBPs, including DDX5 and DDX17, are key players in miRNA

biogenesis as they control multistep processing as well as the localization, degradation and functional activity of miRNAs. Most RBPs recognize specific sequence motifs or secondary structures via their RNA-binding domains. For instance, mRNA splicing factor SRSF1 (also known as SF2/ASF) binds to the stem region of specific pri-miRNAs (Wu et al., 2010), while hnRNP A1 (heterogeneous nuclear ribonucleoprotein A1) and KSRP (KH-type splicing regulatory protein, also known as KHSRP) recognize the terminal loop of subclass pri-miRNAs (Guil and Caceres, 2007; Trabucchi et al., 2009). Regardless of that, all of the three facilitate the cleavage by Drosha/DGCR8 upon anchoring the pri-miRNAs (except for pri-let-7 which is inhibited by hnRNP A1) (Michlewski and Caceres, 2010). In contrast, Lin28, an RBP exclusively expressed in undifferentiated stage, specifically binds to the terminal loop of pri-let-7, thereby inhibits its processing in the nucleus (Rybak et al., 2008). Similarly, NF90 and NF45, two known components of the larger Drosha/DGCR8 complex, suppress Drosha-mediated cleavage via competitive loading with certain pri-miRNAs (Sakamoto et al., 2009). The RNA targets of those RBPs are unavoidably overlapped, raising the question that how upstream signals efficiently coordinate their RNA-interactomes, either spatially or temporally, to influence the process of specific miRNA maturation in the nucleus. Rarely, DNA-binding protein, as exemplified by BRCA1 (the tumor suppressor breast cancer1), also promotes the processing of subclass miRNAs via direct interaction with their primary transcripts (Kawai and Amano, 2012). BRCA1 associates with super microprocessor complex as well as other additional processing modulators, including Smad3, p53 and DHX9. The DNA-binding domain is required for BRCA1 anchoring to the branched structure at the root of a hairpin in the pri-miRNAs, similar to its DNA-binding preference (Kawai and Amano, 2012). Nonetheless, the

regulatory function of BRCA1 in miRNA processing was examined in the absence of DNA damage. It remains unknown whether BRCA1 functions the same in response to DNA damage, and if so, how important those BRCA1-regulated miRNAs are in the process of DNA repair.

1.6.2 Regulation of miRNA Shuttling

Genetic mutations in Exportin-5 were identified both in colon cancer cell lines and in human colorectal tumors (Melo et al., 2010). A frame-shift mutation in XPO5 creates a premature termination codon, resulting in a truncated protein that lacks a small region in the C-terminus. Interestingly, the Exportin-5 mutant fails to form a proper XPO5/Ran-GTP/pre-miRNA ternary complex due to its reduced binding and/or recognition capability with the cargo, pre-miRNA. In consequence, miRNA precursors after the first-step processing are trapped in nucleus, leading to the reduced expression of mature miRNAs (Melo et al., 2010). However, genetic alterations of XPO5 are heterogeneous in human cancers, and in general, low-frequency events. XPO5 is amplified without mutations in ovarian serous cystadenocarcinoma and glioblastoma (with 2.8%, and 1.5% incidence respectively, from the Cancer Genome Atlas), while gene amplification and mutations of XPO5 coexist in other cancer types, including breast, prostate and colon cancers (1.4% amplification *vs.* 0.5% mutation in colorectal carcinomas, from the Cancer Genome Atlas). Notably, XPO5 frame-shift mutations are present in 22.8% of human primary colorectal tumors with microsatellite instability (Melo et al., 2010), suggesting that the genetic control of miRNA exportation is critically important in this subpopulation of patients. The upstream signaling regulators for miRNA exportation, either via Exportin-5 or Ran-GTP, are not yet identified so far.

1.6.3 Regulation of miRNA processing in the cytoplasm

As a haploinsufficient tumor suppressor, mutations and heterozygous deletion of *DICER1* are frequently observed in various human tumors (Hill et al., 2009; Kumar et al., 2009; Lambertz et al., 2010). The steady level of Dicer is positively regulated by TRBP as a complex (Chendrimada et al., 2005), while the expression of Dicer is further controlled by multiple miRNAs via its super long 3'UTR. Both Let-7 and miR-103/107 reduce Dicer protein level through direct interaction with multiple binding sequences existing in 3'UTR or the coding region of DICER mRNA (Martello et al., 2010; Tokumaru et al., 2008). High expression of miR-103/107 attenuates Dicer-mediated miRNA processing, resulting in general down-regulation of mature miRNAs. Subsequently, blocked biogenesis, specifically the miR-200 family, promotes the epithelial-to-mesenchymal transition (EMT) in breast cancer cell lines (Martello et al., 2010). More recently, Dicer was found to be SUMOylated after short-exposure to cigarette smoke in alveolar macrophages (Gross et al., 2014). However, the detailed mechanistic nature as well as the potential functional importance of this modification is still unclear.

TRBP, a key component of the RISC-loading complex, is also susceptible to genetic disruptions. Frame-shift mutants of TRBP, with reduced binding affinity with Dicer, were identified in human colorectal tumors with microsatellite instability (Garre et al., 2010; Melo et al., 2009). In general, the mutation rate of TRBP is very low (for instance, less than 1.5% in colorectal adenocarcinoma, from the Cancer Genome Atlas), except for adenoid cystic carcinoma from which TRBP is deleted in 15% of the patients (from the Cancer Genome Atlas). The underlining mechanisms of genetic deletion as well as the corresponding functional consequences in those tumors remain unknown and need to be

investigated. Interestingly, TRBP is rapidly phosphorylated by Erk (mitogen-activated protein kinase 1) at S142, S152, S283 and S286 in response to growth factor stimulation (Paroo et al., 2009). Phosphorylation of TRBP stabilizes both TRBP and Dicer, resulting in enhanced miRNA processing in the cytoplasm. Of note, the expression of let-7 tumor suppressor family is down-regulated in the context of TRBP phosphorylation (Paroo et al., 2009), raising the question that how phosphorylated TRBP specifically inhibits the maturation of let-7 miRNAs.

Not surprisingly, the biogenesis control of let-7 family is concomitantly targeted by multiple pathways. In the cytoplasm, pre-let-7 bound by Lin28 is frequently uridylated by TUT4 (also known as ZCCHC11) at the 3' terminus, which consequently inhibits Dicer cleavage for maturation and tags the precursor RNA for rapid degradation by nucleases (Heo et al., 2009). In contrast, KSRP anchors to the conserved region of let-7 terminal loop and that of the other miRNAs, thereby facilitates their maturation through interaction with Dicer in the cytoplasm (Trabucchi et al., 2009). The loop structure of pre-miRNA is also recognized by the endo-RNase MCPIP1 (monocyte chemoattractant protein induced protein 1, also known as ZC3H12A), which antagonizes Dicer to bind and cleave the loop from the target miRNA precursors for degradation (Suzuki et al., 2011). Notably, both Lin28 and MCPIP1 are up-regulated in response to inflammation (Iliopoulos et al., 2010; Suzuki et al., 2011), while KSRP is phosphorylated and functionally inhibited by p38 MAP kinase and the PI3K-AKT pathway (Briata et al., 2005; Gherzi et al., 2006), suggesting that most regulators in miRNA biogenesis are under intensive control of signaling networks.

Another essential regulatory module in miRNA biogenesis belongs to the Argonautes. Particularly, Ago2, a regulator in miRNA maturation and an executer in miRNA-mediated

gene silencing, is under tight regulation in response to varies signals. Ago2 is stabilized and functionally potentiated by hydroxylation at proline 700 mediated by type I collagen propyl-4-hydroxylase (C-P4H(I)) (Qi et al., 2008; Wu et al., 2011). During the undifferentiated cell stage (such as embryonic stem cells and embryocarcinoma cell lines), Ago2 is polyubiquitylated by the E3 ligase mLin-41 (mouse homologue of Lin-41, also known as TRIM71), and subsequently undergoes proteasome-mediated degradation (Rybak et al., 2009). Of note, Lin-41, similar to Lin-28, is targeted and suppressed by let-7, thereby is silenced in differentiated cells. So far, the specific E3 ligase that responsible for Ago2 ubiquitination in somatic cells has not been identified yet. Nonetheless, miRNA-loading-free Dicer and Ago2 are marked by polyubiquitination which serves as a sign for degradation through recruiting the selective autophagy receptor NDP52 (Gibbings et al., 2012). In the context of cellular stress, Ago2 is modified by pADPr (poly ADP-ribosylation) and in consequence relieves miRNA-mediated gene silencing (Leung et al., 2011). The level of mature miRNAs under that condition was not examined in the study; therefore, it remains unknown whether miRNA processing is similarly affected by this modification. Besides that, the functionality of Ago2 in miRNA maturation is also modulated by its binding partner HSP90 (heat shock protein 90) which hydrolyses ATP to facilitate the loading of RNA duplex from Dicer into Ago2 (Iki et al., 2010; Iwasaki et al., 2010; Johnston et al., 2010).

Like most signaling mediators, Ago2 receives signals (phosphorylations) in response to external or internal stimuli and transmits new signals (functional changes) to orchestrate gene expression programs via miRNA regulation. Human Ago2 is phosphorylated at Ser387 by both p38 MAP kinase and the proto-oncogene Akt3 (Horman et al., 2013; Zeng et al., 2008). S387-phosphorylation of Ago2 facilitates its localization to the cytoplasmic

processing bodies (P bodies, intracellular places for mRNA turnover and translational repression) and enhances its binding with GW182, a key component of RISC. As a net result, Ago2-mediated translational repression is strengthened while its cleavage activity towards mRNAs is controversially reduced (Horman et al., 2013). Mass spectrometry analysis indicates that Ago2 is tyrosine phosphorylated at both Y393 and Y529. Phosphorylation of Ago2 at Y529 reduces its small RNA binding capability *in vitro (Rudel et al., 2011)*. However, neither the kinases that are responsible for Ago2 tyrosine phosphorylation nor the functional relevance of Y393 phosphorylation had been demonstrated until our recent work was published in Nature.

Chapter 2 Material and Methods

2.1 Cell Culture and Treatment

Human lung cancer cell line (A-549), human hepatoma cell line (Hep3B), human embryonic kidney cell line (293T), human cervical cancer cell line (HeLa), human mammary epithelial cell lines (MCF-10A and MCF-12A), and human breast cancer cell line (BT-549) were obtained from ATCC. Breast cancer cell line (MDA-MB-231) was gift from Dr. Patricia S. Steeg (National Cancer Institute). RCC4 cell line was kindly given by Dr. Thai Huu Ho from MD Anderson Cancer Center. MCF-10A and MCF-12A cells were grown(Debnath et al., 2003) in DMEM-F12 medium supplemented with 5% horse serum, epidermal growth factor (EGF, 20 ng/ml), insulin (10 μg/ml), cholera toxin (100 ng/ml) and hydrocortisone (0.5 μg/ml). Other cells were grown in DMEM-F12 medium supplemented with 10% fetal bovine serum (FBS). HeLa TetOff-inducible advanced cell line were purchased from Clontech and maintained in DMEM-F12 medium supplemented with 10% Tet-System Approved FBS (Clontech) with both G418 (500 μg/ml) and doxycycline (100 ng/ml). For HeLa TetOff-inducible EGFR and Ago2 stable clones (Plvx-Tight-Vector Control; WT and KD EGFR; WT and Y393F Ago2), cells were maintained in DMEM-F12 medium supplemented with 10% Tet-System Approved FBS (Clontech) with G418 (500 μg/ml), Puromycin (1 μg/ml) and doxycycline (500 ng/ml). The expression of GOI (EGFR or Ago2) was induced after doxycycline removal in accordance with manufacturer's instructions. For hypoxia treatment, cells were seeded at same density in DMEM-F12 medium supplemented with 10% FBS and allowed 4 to 6 hours for adherence in regular cell culture incubator before moving into the hypoxia chamber (INVIV O_2 400, setting as 1% O_2 and 5% CO_2, RUSKINN). HeLa TetOff-inducible stable clones after doxycycline removal were seeded at same density and cultured in regular cell incubator for O/N before moving

into the hypoxia chamber. All cell samples were lysed inside of the hypoxia chamber for both IP-WB and RNA extraction. For induction of oxidative stress, cells cultured in DMEM-F12 supplemented with 10% FBS were treated with 500 μM H_2O_2 (Sigma) or 500 μM sodium arsenite (Sigma) for indicated time before collection. Epidermal growth factor (EGF) and Transforming Growth Factor-α (human TGF-α, Sigma) were prepared according to the manufacturers' instructions. Cells were serum-starved and then treated with EGF (20 ng/ml) or TGF-α (10 ng/ml) for indicated time before collection. To induce DNA damage, cells cultured in normal medium were treated with Cisplatin (50 μM) or Etoposide (50 μM) for indicated time before collection. 50 nM AG1478 (Calbiochem) and 1 μM Iressa (Gefitinib) were used to inhibit EGFR kinase activity. 1 μM FM19G11 (Sigma) and 6 μM CAY10585 (Cayman Chemicals) were used to inhibit the transcriptional activity of HIF1/2α.

2.2 Antibodies and Peptides

For WB: Flag epitope tag M2 (1: 2,000, Sigma); Flag tag antibody #2368 (1:1,000, Cell Signaling); Anti-HA, 12CA5, (1:2000, Roche Molecular Biochemicals); c-myc antibody 9E10 (1:2,000, Roche Molecular Biochemicals); HIF1α, clone54 (1:500, BD Biosciences); HIF2α, D9E3 #7096 (1:500, Cell Signaling); VHL, PA5-17477, (1:500, Thermo Scientific Pierce Antibodies); antibody against phosphotyrosine, 4G10 (1:3,000, Millipore); Dcp1a, ab47811 (1:1,000, Abcam); Ago2/EIF2C2, ab32381 (1:1,000, Abcam); Argonaute2, C34C6 (1:1,000, Cell Signaling); Anti-AGO2, 11A9 (1:1,000, Sigma); Dicer, H-212 (1:200, Santa Cruz Biotechnology); Dicer, #3363 (1:500, Cell Signaling); Anti-LAMP1, CD107a (1:1,000, Millipore); GW182, A302-329A (1:1,000, Bethyl Laboratories); Alix, 3A9 (1:1,000, Cell Signaling); TRBP, 46D1 (1:1,1000, Abnova); EEA1, clone14 (1:1,000, BD Biosciences); Hrs, ab56468 (1:1,1000, Abcam); EGFR, sc-03 (1:1,1000, Santa

Cruz Biotechnology); LOX, NB100-2527 (1: 1000, Novus Biologicals); p-Y1086-EGFR, #2220, (1:1,000, Cell Signaling); Grb2, 610112, (1:1000, BD Biosciences); p-Y393-AGO2 (1:1,500, homemade); α-tubulin (1:5,000, Sigma); β-actin, AC-74 (1:2,000, Sigma); LaminB1, 4B10, (1:500, Novus Biologicals). For IP: Flag epitope tag M2 (Sigma); EGFR, ab-13 (Thermo Scientific). For IF: GW182, 4B6 (1:50, Abcam); Anti-AGO2, 11A9 (1:200, Sigma); Dcp1a, ab47811 (1:200, Abcam); EGFR, sc-03 (1:150, Santa Cruz Biotechnology); EGFR, ab-13 (1:250, Thermo Scientific); EGFR, ICR10 (1:50, Abcam); Anti-HIF1α, clone EP1215Y (1:200, Millipore); p-Y393-AGO2 (1:2,000, homemade). For IHC: Anti-HIF1α, clone EP1215Y (1:400, Millipore); Anti-HIF2α, NB100-122, (1:300, Novus Biologicals); EGF Receptor, D38B1, (1:100, Cell Signaling); p-Y393-AGO2 (1:3,200, homemade). The following peptides were chemically synthesized for antibody production in mice (Lifetein Conc.), Elisa verification (Lifetein Conc.) and peptide competition assay in immunohistochemistry (IHC). Phospho-Y393-Ago2-peptide: NTDP-pY-VREFG; Non-phospho-Y393-Ago2-peptide: NTDP-Y-VREFG. Random chosen phospho-tyrosine peptides (EGFR-pY1068-Peptide and STAT3-pY705-Peptide) were purchased from Cell Signaling for peptide competition assay in IHC.

2.3 Construcs and shRNAs

pcDNA6.A-EGFR, expressing full-length human EGFR with a carboxyl-terminal myc-6×His tag, was constructed and described previously(Hsu et al., 2009). EGFR extracellular domain plus transmembrane region (EC, amino acids 1-644), EGFR intracellular domain (IC, amino acids 645-1186), EGFR deletion of C-terminal (ΔCD, amino acids 1-955) were subcloned into pcDNA6.A/myc-His vector (Invitrogen). Kinase-dead $EGFR^{K721R}$ (KD EGFR) was generated using the Quick-Change Site-Directed Mutagenesis

Kit according to the manufacturer's instruction (Stratagene). Full-length human Ago2 was amplified from the cDNA of HeLa cells and subcloned into a modified pCMV5 vector containing an N-terminal FLAG tag. Functional domains of Ago2 (FDM1: 1-372 aa; FDM2: 1-517 aa; FDM3: 227-860 aa; FDM4: 373-860 aa; FDM5: 518-860 aa) were subcloned into the same pCMV5 vector for mapping protein regions binding with EGFR. For *in vitro* pull-down and kinase assays, full-length Ago2, Ago2-FDM2 and Ago2-FDM4 were subcloned into pGEX6P1-GST vector. For generating YFP-interaction system, full-length EGFR and Ago2 were subcloned into pBABE-CMV-DEST-Neo (fused with YFPn, generated by Dr. S. Zhou) and pBABE-CMV-DEST-Puro (fused with YFPc, generated by Dr. S. Zhou) respectively. For generating HeLa TetOff-inducible stable clones, full-length WT EGFR, KD EGFR and WT Ago2 (with fused C-terminal FLAG tag) were subcloned into Plvx-Tight-Puro vector (Clontech). For generating Ago2 stable clones, full-length Ago2 (with fused C-terminal FLAG tag) were subcloned into pCDH-CMV-MCS-EF1-Puro (CD510B-1) and pCDH-CMV-MCS-EF1-copGFP (CD511B-1, System Biosciences) vectors. All mutant constructs of Ago2 (Y393F, Y393D, Y393E) were generated using the Quick-Change Site-Directed mutagenesis kit (Stratagene) and confirmed by DNA sequencing. For live-cell imaging, WT-EGFR fused with C-terminal GFP was constructed and described previously(Hsu et al., 2009). Full-length human Ago2 was subcloned into pTagBFP-C vector (with N-terminal BFP tag). Human pre-microRNA Expression Constructs Lenti-miR-192-WT (MI0000234) and Lenti-miR-21-WT (MI0000077) were purchased from System Biosciences. Lenti-miR-192-3M and Lenti-miR-21-3M were generated using the Quick-Change Site-Directed mutagenesis kit (Stratagene) and confirmed by DNA sequencing. The pre-miRNA sequence of miR-192-3M is:

GCCGAGACCGAGUGCACAGGGCUCUGACCUAUGAAUUGACAGCCAGUGGUGU
GGUCUCCCCUCUGGCUGCCAAUUCCAUAGGUCACAGGUAUGUUCGCCUCAAU
GCCAGC; the pre-miRNA sequence of miR-21-3M is:
UGUCGGGUAGCUUAUCAGACUGAUGUUGACUUAUUAAUCUCAUGGCAACACC
AGUCGAUGGGCUGUCUGACA (red color highlights the nucleotides that were mutated). RNA interference was performed using lentiviral short hairpin RNAs (shRNAs) from MISSION™ TRC-Hs (human) shRNA Library according to the instructed protocol. Lentiviral packaging system, pCMV-dR8.2 dvpr (#8455) and pCMV-VSVG (#8454), pBabe-puro-WT-VHL (#19234) were bought from Addgene. The oligo sequences of shRNAs are listed below and confirmed by DNA sequencing. ON-TARGETplus Non-Targeting Pool (D-001810-10) and ON-TARGETplus DICER1 siRNA SMARTpool (targeting CDS of Dicer) were purchased from Dharmacon, Thermo Scientific.

Scrambled Control (#1864, Addgene):
CCTAAGGTTAAGTCGCCCTCGCTCGAGCGAGGGCGACTTAACCTTAGG;

EGFR shRNA-E1 (TRCN0000121067):
CCGGGCTGCTCTGAAATCTCCTTTACTCGAGTAAAGGAGATTTCAGAGCAGCTT
TTTG (targeting 3' UTR of EGFR);

EGFR shRNA-E2 (TRCN0000121068):
CCGGGCCACAAAGCAGTGAATTTATCTCGAGATAAATTCACTGCTTTGTGGCTTT
TTG (targeting CDS of EGFR);

Grb2 shRNA-1 (TRCN0000029372):

CCGGGATCTACATCTGTCTCCAGAACTCGAGTTCTGGAGACAGATGTAGATCTT

TTT (targeting CDS of Grb2);

Grb2 shRNA-2 (TRCN0000029373):

CCGGCAGATATTCCTGCGGGACATACTCGAGTATGTCCCGCAGGAATATCTGTT

TTT (targeting CDS of Grb2);

HIF1α shRNA#1 (TRCN0000003810):

CCGGGTGATGAAAGAATTACCGAATCTCGAGATTCGGTAATTCTTTCATCACTTT

TT (targeting CDS of HIF1α);

HIF1α shRNA#2 (TRCN0000010819):

CCGGTGCTCTTTGTGGTTGGATCTACTCGAGTAGATCCAACCACAAAGAGCATT

TTT (targeting 3' UTR of HIF1α);

EPAS1/HIF2α shRNA#1 (TRCN0000003806):

CCGGCAGTACCCAGACGGATTTCAACTCGAGTTGAAATCCGTCTGGGTACTGTT

TTT (targeting CDS of HIF2α);

EPAS1/HIF2α shRNA#2 (TRCN0000003805):

CCGGGCGCAAATGTACCCAATGATACTCGAGTATCATTGGGTACATTTGCGCTT

TTT (targeting CDS of HIF2α).

2.4 Mass Spectrometry

Mass spectrometric analysis was performed as previously described(Lee et al., 2008). Briefly, endogenous EGFR was purified by immunoprecipitation with anti-EGFR antibody

(Ab-13) and analyzed by SDS-PAGE. All the protein bands co-immunoprecipitated with EGFR was excised and analyzed by nanoelectrospray mass spectrometry for protein ID identification. To identify phosphorylation sites of Ago2, we purified FLAG-tagged Ago2 that co-expressed with EGFR in 293T cells and analyzed the results by SDS-PAGE and Western-Blot. The protein band corresponding to Ago2 was excised and subjected to in-gel digestion with trypsin. After being isolated from the gel, samples were analyzed by nanoelectrospray mass spectrometry, using an Ultimate capillary LC system (LC Packings) coupled to a QSTARXL quadrupole time-of-flight mass spectrometer (Applied Biosystem/MDS Sciex). All the identified phospho-residues were further confirmed by manual interpretation of the spectra.

2.5 RNA Deep Sequencing and Hierarchical Clustering Analysis

Customized Next-Generation RNA deep sequencing, including both small RNA application and whole transcriptome analysis, was performed according to the standard procedure instructed by Applied Biosystems. All the RNA sequencing data were deposited to GEO with accession number GSE44804. Briefly, total RNA was extracted from HeLa stable clones expressing scrambled control (S) or EGFR shRNA-E1 (E1) that were seeded at same density and cultured under normoxia or hypoxia (1% Oxygen) for 24 hours. All RNA samples passed quality test with RIN-values greater than 8 as measured by Agilent Technologies Bioanalyzer, were subjected to RNA deep sequencing. *For whole transcriptome analysis*, SOLiD fragment colorspace transcriptome reads (50nt) were mapped to the human genome (hg19) and assigned to ensemble transcripts using Bioscope 1.3.1 (Life Technologies). The values of reads per kilobase per million reads (RPKM) were determined by Bioscope 1.3.1 CountTags tool using default parameters. Primary alignments

with a minimum mapping quality of 10 and minimum alignment score of 10 were counted. *For small RNA analysis,* library inserts were size selected between 18 and 40nts and analyzed using CLC Genomics Workbench 4.7.1. 35nt colorspace reads were trimmed of adaptor sequence and mapped against human pre-miR sequences (miRBase version 16.0). Values of reads per million mapped reads (RPM) were based on mapped reads with no more than 2 mismatches total. A read was considered to come from a mature miRNA if it mapped to pre-miRNA sequences with no more than three upstream or downstream bases, and missing no more than two upstream or downstream bases from predicted mature or mature* sequences as defined in miRBase version 16.0. All the other pre-miRNA mapped reads were assigned as pre-miRNA signal. *For Hierarchical Clustering Analysis,* Data files from small RNA or whole transcriptome analysis were first filtered based on the normalized expression value RPM (cutoff genes with all mapped reads ≤100 counts) or RPKM (filtered with count value ≥0.5 RPKM). Gene expression profiles were then transformed into Log2 data for comparing expression differences. For miRNA maturation analysis, we transformed the original expression data (Log2 transformed) into relative expression of pre- and mature miRNA levels that affected by EGFR knockdown (as calculated by expression change-fold). We define relative expression of pre- or mature miRNA＝Log2 (pre- or mature miRNA in HeLa scrambled control)-Log2 (pre- or mature miRNA in HeLa EGFR shRNA-E1 stable clone). For identifying the mRNAs that regulated by EGFR and likely targeted by top-scoring mHESM, mRNAs modulated by EGFR knockdown (with Log2 fold-change affected by EGFR ≥ 0.4 or ≤ -0.4) were sorted and over-lapped with the predicted mRNAs (based on published data and TargetScan prediction with total context score ≤ -0.20) that targeted by top-scoring mHESM. For all the other analysis, Log-transformed gene expression files were

further normalized by mean centering to correct average gene expression from all the samples as log2-ratio of 0. Centroid Linkage Clustering was performed and the interactive graphical results from Cluster were further analyzed by TreeView for displaying heatmaps.

2.6 qRT-PCR assays and Northern-Blot analysis

qRT–PCR assays as described previously[26] were performed to measure the expression of mRNA, pri-, pre- and mature miRNAs with some adaptations. Briefly, cells were washed twice with PBS and immediately lysed in QIAzol. For mRNA, pri- and mature miRNA detection, half of the lysed sample was subjected to total RNA extraction using miRNeasy Mini Kit (Qiagen). For pre-miRNA detection, the other half of the lysed sample was subjected to small RNA fraction purification using the miRvana miRNA isolation kit (Ambion). To measure the expression of mRNA or pri- or pre-miRNAs, cDNA was synthesized from 1ug purified total RNA or 500ng purified small RNA (size-fractioned) by SuperScript III First-Strand cDNA synthesis system using random hexamers (Invitrogen) according to the manufacturer's instructions. qPCR was performed using real-time PCR machine (iQ5, BioRad). For detection of mature miRNAs, TaqMan MicroRNA assay kit (Applied Biosystems) was used in accordance with the manufacturer's protocol. qPCR was performed using 7500 Fast Real-Time PCR System (Applied Biosystems). All the data analysis was performed using the comparative Ct method. Results were first normalized to internal control β-actin mRNA or U6 snRNA, which were almost not affected by hypoxia or EGFR knockdown, and then the relative expression of pri-, pre- or mature miRNAs in response to hypoxia was given by normalized expression level under hypoxia relative to the corresponding normalized expression under normoxia. Each RNA sample (except for RIP

experiment) was analyzed in duplicate and presented as an average of two independent RNA preparations. The sequences of qPCR primers are given in the Supplementary Information.

Northern-Blot analysis was performed as described previously(Varallyay et al., 2008). miRCURY LNA probes (targeting hsa-miR-21 or hsa-miR-192, Exiqon) and DNA oligonucleotide (5'-GGGGCCATGCTAATCTTCTCTGTATCGTTCCAATTTTAGT ATATGTG-3'; Sigma) targeting U6 (internal control) were end-labeled with [γ-32P] ATP and used as probes for Northern Blot analysis.

2.7 Immunoprecipitation and immunoblotting

Immunoprecipitation and immunoblotting were performed as previously described(Lee et al., 2008). Briefly, cells were washed twice with cold PBS and scraped into lysis buffer containing complete protease inhibitors (all the above steps were done inside of the hypoxia chamber). After brief sonication, cell lysates were centrifuged at 14,000*g* for 20 min at 4°C to remove insoluble cell debris and then subjected to IP-WB.

2.8 Iodixanol continous density gradient

Optiprep iodixanol density media was obtained from Sigma-Aldrich. Continuous density gradients were performed as described previously with some adaptations(Gibbings et al., 2009). Briefly, HeLa cells seeded at the same density were either cultured under normoxia or hypoxia (1% Oxygen) for 24 hr before collection. Cells were then washed twice in PBS and re-suspended with PBS. 10% of the suspended cells were lysed by RIPA buffer as the whole cell lysate input for later on protein analysis. The rest of the cells were re-suspended in 500 µl 0.25 M sucrose, 4 mM $MgCl_2$, 8.4 mM $CaCl_2$, 10 mM EGTA, 50 mM Hepes-NaOH at pH 7.0 with complete protease inhibitors. Cells were lysed by 40 strokes of

dounce homogenizer and 10 passages through a 26-gauge needle, and centrifuged at 1,000*g* for 5 min twice to remove cellular debris and nuclei. Continuous 0–30% optiprep gradients were prepared in 78 mM KCl, 4 mM $MgCl_2$, 8.4 mM $CaCl_2$, 10 mM EGTA and 50 mM Hepes-NaOH at pH 7.0 using a gradient mixer (gradient station, Biocomp Instruments). Postnuclear supernatant was added to the top of 13 ml gradients and centrifuged at 90,000*g* for 20 h. Fractions (0.5 ml per fraction) were collected from the bottom of the gradient using a fraction collector (BioFrac, BioRad) that measures conductivity to verify continuity of gradients. For analysis, 30 μl whole cell lysate input (with total volume 500 μl) was loaded along with 30 μl protein samples from each fraction (500 μl per fraction) in SDS-PAGE, and subjected for WB and quantified by Odyssey Infrared Imaging System.

2.9 Generation of stable clones expressing GOI and shRNAs

YFP-interaction system (in HTC-1080 and HeLa cells) and RCC4 stable transfectants expressing vector control or WT-VHL were generated by retroviral infection. All the other stable clones expressing GOI or shRNAs were generated by Lentiviral infection. For retroviral infection, packaging plasmids (gag/pol and VSV-G) were co-transfected with pBABE-Neo-EGFR-YFPn or pBABE-Puro-Ago2-YFPc into 293T cells, and viral particles were harvested at 48 hr post-transfection. HTC-1080 and HeLa cells were infected with one or co-infected with both viruses for 24 hr in the presence of polybrene (10 μg/ml) and subsequently selected by G418 (1,000 μg/ml) or puromycin (1 μg/ml) or G418 (500 μg/ml) together with puromycin (0.5 μg/ml). For RCC4 stable transfectants, pBabe-puro-vector or pBabe-puro-HA-WT-VHL together with pCL-Ampho (optional) was transfected into phoenix cells, and viral particles were harvested at 48 hr post-transfection. The other steps were the same as described above. HeLa TetOff-inducible stable clones were generated

following the protocol instructed by Clontech. Briefly, 293T cells were seeded in DMEM-F12 medium supplemented with 10% Tet-System Approved FBS (Clontech) for 24 hr before transfection. Lentiviral packaging plasmids (generation II), pCMV-dR8.2-dvpr and pCMV-VSVG, were co-transfected with lentiviral constructs expressing GOI (plvx-tight-vector; WT or KD EGFR; WT or Y393F Ago2) into Tet-Free 293T cells. Viral particles were harvested at 48 hr post-transfection and further infected into Tet-Free targeting cells (HeLa TetOff Advanced Cell Line) for 24 hr in the presence of polybrene (10 μg/ml). At 48 hr post-infection, cells were selected by both G418 (500 μg/ml) and puromycin (1 μg/ml) in DMEM-F12 medium supplemented with 10% FBS and doxycycline (500 ng/ml) for generating stable clones without induction of GOI. For generating EGFR shRNA, Grb2 shRNA, HIF1α shRNA, HIF2α shRNA and other Ago2 stable clones (including knocking down endogenous EGFR in HeLa CMV Ago2 stable clones and stable expression of miR-192-WT, miR-192-3M, miR-21-WT and miR-21-3M in HeLa TetOff Ago2 stable clones), similar lentiviral infection procedure (with no restriction of Tet-Free) was performed. Stable clones were generated either by puromycin (2 μg/ml in HeLa; 1 μg/ml in MDA-MB-231) selection or sorted twice by flow cytometry based on the expression of GFP.

2.10 miRNA-Reporter Assay

Oligonucleotides complementary to the sequences of mature miR-21, miR-31, miR-192, miR-193a-5p or all of the later three seeding sequences were ligated into pMIR-Reporter (Ambion) and verified by DNA sequencing. HeLa TetOff Ago2 stable clones were co-transfected with each miR-Reporter (firefly luciferase) together with internal control (pRL-Renilla luciferase control reporter) and cultured under normoxia or hypoxia for 36-48 hr after doxycycline removal. The luciferase activity of miR-Reporter was determimed by

the ratio of firefly to renilla luciferase as measured by the Dual-Luciferase Reporter Assay System (Promega) and further normalized to the one of vector control cultured under normoxia. The oligonucleotide sequences for each pMIR-Reporter are listed in the Supplementary Information.

2.11 RNA-Binding Protein Immunoprecipitation (RIP-Assay)

RNA-Binding Protein Immunoprecipitation Kit (Magna RIP, Millipore) was used for RIP-Assay, according to the manufacturer's instruction. Briefly, HeLa TetOff Ago2 stable clones were cultured under hypoxia for 24 hr after doxcycline removal and then treated with MOCK (DMSO) or TKI (Iressa, 1 μM) for 8 hr before collection. Cells were lysed in RIP Lysis Buffer with both protease inhibitor and RNase inhibitor, and 5% of the total cell lysates were used for Western-Blot analysis as experimental control. FLAG antibody was bound to the magnetic beads and added into each RIP reaction (RIP lysate in RIP immunoprecipitation buffer with RNase inhibitor) for incubation O/N at 4 °C. Beads were washed 6 times in cold RIP washing buffer and 10% of the beads were kept as RIP-input to show the precipitated protein quantity of WT or Y393F Ago2. Proteins were digested in Protease K buffer at 55 °C for 30 min, and total RNA was extracted using miRNeasy Mini Kit (Qiagen). A 15-μl elution of RNA (with total volume 30 μl) was used for cDNA systhesis and further analyzed by qPCR. Except for first-strand synthesis, the procedure for RIP-Assay using HeLa TetOff Ago2 stable clones expressing ON-TARGET control siRNA pool or ON-TARGET Dicer1 siRNA SMART pool is similar. After RNA purification from anti-FLAG immunoprecipitates, 15-μl elution of RNA (with total volume 30 μl) was synthesized into cDNA using SuperScript III with random hexamers (Invitrogen) for

detection of miRNA precursors, while another 15-ul elution of RNA was reversely transcribed into cDNA using TaqMan MicroRNA assay kit for detection of mature miRNAs.

2.12 In vitro Pull-Down Assay

Recombinant GST-Ago2 (full-length), GST-Ago2-FDM2, GST-Ago2-FDM4 and GST were expressed in *E. coli* (BL-21) and purified by glutathione-sepharose beads. Similar quantity of protein samples were incubated with *in vitro* transcription and translation lysates of myc-tagged full-length EGFR (pCDNA6.a-WT-EGFR), produced by TNT coupled reticulocyte lysate system (Promega), in binding buffer (25 mM Tris-HCl, pH 7.5, 125 mM NaCl, 1 mM phenylmethylsulfonyl fluoride, 1 μg of leupeptin/ml, 1 μg of aprotinin/ml, and 1 μg of pepstatin/ml) for O/N at 4 °C. Beads were washed five times with Tris-buffered saline and subjected to SDS-PAGE for autoradiography.

2.13 In vitro Kinase Assay

Recombinant GST-WT-Ago2 and GST-Y393F-Ago2 were incubated with or without (negative controls) purified human EGFR (E2645, Sigma) in HTScan 1× tyrosine kinase buffer (Cell Signaling) supplemented with 200 μM cold ATP and 2.5 mM DTT for 40 min at 30 °C. The reaction of purified EGFR without substrate was carried out under the same condition as another negative control. Kinase Assay was stopped by 8.5% phosphoric acid, subjected to SDS-PAGE and analyzed by Western-Blot using 4G10 antibody.

2.14 Confocal Microscopy Analysis

Confocal Microscopy analysis was performed as described previously(Hsu et al., 2011). Briefly, cells after treatment were washed three times with cold PBS, fixed in 4% paraformaldehyde for 20 min at RT. For experiments under hypoxia, cells were washed with

cold PBS and then added with 4% paraformaldehyde before moving out of the hypoxia chamber. Cells were then permeabilized with 0.5% Triton X-100 for 10 min, and incubated with 5% bovine serum albumin for 1 hr. After that, cells were incubated with primary antibodies overnight at 4°C, and then washed with PBS, and further incubated with the appropriate secondary antibody diluted at 1:300 and tagged with Alexa 488, Alexa 568 or Alexa 647 (Molecular Probes) for 1 hr at room temperature. Nuclei were stained with 4,6-diamidino-2-phenylindole (DAPI) before mounting. Confocal fluorescence images were captured using a Zeiss LSM710 laser microscope. In all cases, optical sections through the middle planes of the nuclei, as determined using nuclear counterstaining, were obtained. For Live-Cell imaging, HeLa cells were co-transfected with EGFR-GFP and BFP-Ago2, and then cultured under normoxia or hypoxia for 24 hr. 50 nM Lyso-Tracker (Red DND-99, Invitrogen) was added into cells right before confocal analysis. Alternatively, HeLa cells co-expressing EGFR-GFP and BFP-Ago2 was further transduced with CellLight Rab7-RFP (CellLight late endosome-RFP, Invitrogen) according to the manufactory's instruction for 24 hr, and after that, cells were cultured under normoxia or hypoxia for 24 hr before confocal analysis.

2.15 Duolink Assay (in situ Proximity Ligation Assay)

In situ Proximity Ligation Assay was performed according to manufacturer's instructions (OLINK BIOSCIENCE). Briefly, HeLa stable transfectants expressing scrambled control or shRNAs (targeting Grb2 or HIF1α or HIF2α) were seed on 8-well chamber slides and cultured under normoxia or hypoxia for 24 hr. Cells were then washed (inside of the hypoxia chamber), fixed, permeablized and blocked before primary antibody (against endogenous EGFR and Ago2) incubation at 4°C overnight. After washing,

secondary antibodies conjugated with oligonucleotides (Minus and Plus) were added into each reaction and incubated for 1 hr at 37°C. Cells were washed before adding ligation solution and further incubated at 37°C for 30 min. Finally fluorescently labeled oligonucleotides (FITC in our case) together with Polymerase were added into each reaction for amplification of the original ligated nucleotide circles. The positive signal is visualized as distinct fluorescence spot and each spot represents one cluster of protein-protein interaction.

2.16 Cell Apoptosis Analysis

Evaluation of apoptosis by the annexin V-propidium iodide (PI) binding assay was performed according to the standard protocol. APC-Annexin V and propidium iodide (PI) (BD Biosciences) were prepared according to the manufacturer's instructions. The extent of apoptosis was quantified as percentage of annexin V-positive cells.

2.17 Cell Proliferation Assay

Cell proliferation was measured by BrdU Cell Proliferation Assay Kit (#6813, Cell Signaling) according to the manufacturer's instructions.

2.18 Soft Agar Assay

HeLa Ago2 stable clones (1×10^4cells) and MDA-MB-231 Ago2 stable clones (5×10^3cells) were resuspended in DMEM containing 10% FBS with 0.5% agarose and layered on top of 1.0% agarose in DMEM on 24-well plates. A 500-μl normal culture medium containing 1 μg/ml puromycin was added to the top of each well and changed every five days. Cultures were maintained for 15 days. Colonies that grew beyond 50 μm in diameter were scored as positive. Each experiment was done in triplicate.

2.19 Cell Migration Assay

Cell migration assays were performed in Biocoat transwell filter inserts (8um, 24-well plates, BD Biosciences) as described previously with some adaptations. Briefly, Cells were pre-treated with MOCK (DMSO) or TKI (Iressa, 1 μM) for 6 hr before trypsinization. DMEM-F12 containing 10% FBS with MOCK or TKI was added to the bottom chamber. Cell suspensions (2×10^4 HeLa Ago2 stable clones or 1×10^4 MDA-MB-231 Ago2 stable clones) in serum-free DMEM-F12 with MOCK or TKI were added to the upper chamber. After migration for 18 hr under normoxia or hypoxia, cells on the top surface of the membrane were removed and the remaining cells, which migrated through the inserts, were fixed and stained with crystal violet. The average number of migrated cells per field (counted visually under a light microscope at original magnification ×200) was calculated based on five randomly selected fields per membrane in triplicate.

2.20 Three-Dimensional Invasion Assay

The 3-D Oris™ cell invasion assay was performed according to the manufacturer's instructions (Platypus Technologies). Briefly, 100ul of the BME coating solution was added into the wells (96-well-black plate, Platypus Technologies) and incubated in a humidified cell culture chamber for 15-30 min for solidification. Oris™ cell seeding stoppers were inserted perpendicular to each well bottom and fully engaged with the bottom of each well. HeLa Ago2 stable clones (5×10^4 cells) were resuspended in 100ul DMEM-F12 medium supplemented with 10% FBS and puromycin (1 μg/ml) with Mock (DMSO) or Iressa (1 μM). Cell suspensions were added into each well through one of the side ports of the Oris™ cell seeding stopper and allowed O/N for complete cell attachment. Stoppers were removed by the Oris™ stopper tool. The top medium of each well was removed and any unattached cells

were cleared by gently washing with PBS. 40ul Oris^{TM} BME stock reagent mixed with Mock or Iressa (1 μM) was added into each well to create a 3-D BME overlay. Then, the plate was incubated in a humidified cell culture chamber for 30 min for polymerization of the 3-D BME overlay. Finally, 100 μl of serum-free cell culture medium with Mock or Iressa (1 μM) was added on the top of the 3-D BME overlay. We recorded full-images of the well center (with no cells at T_0) at different time points (T=0, T_{24}=24 hr and T_{48}=48 hr) using a Zeiss LSM710 laser microscope. Invasion capacity was reported as the average number of cells (5 different wells per experimental group) that invaded into the center of wells in 48 hr.

2.21 Orthotopic xenograft breast cancer model

Orthotopic breast cancer mouse model was performed as previously described(Hsu et al., 2011). Briefly, MDA-MB-231 cells (1×10^6 cells) were injected into the mammary fat pads of nude mice (at Day 0). Two hours before sacrifice, mice were intraperitoneally injected with Hypoxy-probe (pimonidazole hydrochloride, HPI, Inc.) at a dosage of 60 mg/kg body weight according to the manufacturer's instructions. Five series of tumor samples (2 mice per group) were collected every 4 days (started from Day 8 to Day 24) and analyzed by IHC staining. All animal procedures were conducted under the guidelines approved by the Institutional Animal Care and Use Committee (IACUC) at MD Anderson Cancer Center (Protocol Number 06-87-06139).

2.22 Immunohistochemical Staining

Immunohistochemical staining was performed as previously described(Xia et al., 2009). To validate the specificity of p-Y393-Ago2 antibody in IHC, we performed peptide

competition assay by staining human breast tumor sample with p-Y393-Ago2 antibody blocked with Mock or phospho-Y393-Ago2-peptide or non-phospho-Y393-Ago2-peptide, or two randomly chosen phospho-tyrosine peptides, EGFR-pY1068-Peptide and STAT3-pY705-Peptide (Cell Signaling), at the same concentration (1 μg/ml). The procedure for IHC staining in orthotopic xenograft model was similar. The hypoxy-probe was stained using the Hypoxyprobe™-1 Plus Kit (HPI, Inc.). Universal LSAB™+ Kit/HRP (Dako) was used for detection of p-Y393-Ago2 in mouse xenograft tumor samples. Human breast tumor tissues samples were obtained under the guidelines approved by the Institutional Review Board at MD Anderson Cancer Center.

2.23 Primer Information for qPCR

Primers for qPCR	5' to 3'	Notes
U 6-Forward:	CTCGCTTCGGCAGCACA	Internal Control
U 6-Reverse:	AACGCTTCACGAATTTGCGT	Internal Control
Pre-mir15b-Forward:	AGCACATCATGGTTTACATGC	*
Pre-mir15b-Reverse:	CTAGAGCAGCAAATAATGATTCG	*
Pre-mir16-1-Forward:	GCAGCACGTAAATATTGGCGT	*
Pre-mir16-1-Reverse:	CAGCAGCACAGTTAATACTGGAGA	*
Pre-mir16-2-Forward:	GCACGTAAATATTGGCGTAGT	*
Pre-mir16-2-Reverse:	AAGCAGCACAGTAATATTGGTG	*
Pre-mir24-1,2-Forward:	CTCCCGTGCCTACTGAGCT	*
Pre-mir24-1,2-Reverse:	CCCTGTTCCTGCTGAACTGAG	*
Pre-mir26a-1,2-Forward:	TTCAAGTAATCCAGGATAGGCTGT	*

Pre-mir26a-1,2-Reverse:	TGCAAGTAACCAAGAATAGGCC	*
Pre-mir26b-Forward:	TTCAAGTAATCCAGGATAGGCTGT	*
Pre-mir26b-Reverse:	CAAGTAATGGAGAACAGGCTG	*
Pre-mir27a,b-Forward:	GCAGGGCTTAGCTGCTTG	*
Pre-mir27a,b-Reverse:	GGCGGAACTTAGCCACTGT	*
Pre-mir29a,c-Forward:	ATGACTGATTTCTTTTGGTG	*
Pre-mir29a,c-Reverse:	ATAACCGATTTCAGATGGTG	*
Pre-mir34a-Forward:	TGGCAGTGTCTTAGCTGGTTG	*
Pre-mir34a-Reverse:	GGCAGTATACTTGCTGATTGCTT	*
Pre-mir100-Forward:	AACCCGTAGATCCGAACTTG	*
Pre-mir100-Reverse:	TACCTATAGATACAAGCTTGTGCG	*
Pre-mir103-1,2-Forward:	GCTTCTTTACAGTGCTGCCT	*
Pre-mir103-1,2-Reverse:	TTCATAGCCCTGTACAATGCT	*
Pre-mir107-Forward:	CAGCTTCTTTACAGTGTTGCCT	*
Pre-mir107-Reverse:	GATAGCCCTGTACAATGCTGC	*
Pre-mir125b-1-Forward:	GTCCCTGAGACCCTAACTTG	*
Pre-mir125b-1-Reverse:	AGCCTAACCCGTGGATTT	*
Pre-mir125b-2-Forward:	GTCCCTGAGACCCTAACTTG	*
Pre-mir125b-2-Reverse:	AAGAGCCTGACTTGTGATGT	*
Pre-mir138-1,2-Forward:	CAGCTGGTGTTGTGAATCAG	*
Pre-mir138-1,2-Reverse:	ACCCTGGTGTCGTGAAATAG	*
Pre-mir145-Forward:	GTCCAGTTTTCCCAGGAATC	★
Pre-mir145-Reverse:	AGAACAGTATTTCCAGGAAT	★

Pre-mir191-Forward:	GCAACGGAATCCCAAAAG	*
Pre-mir191-Reverse:	GACGAAATCCAAGCGCA	*
Pre-mir192-Forward:	CTGACCTATGAATTGACAGCC	*
Pre-mir192-Reverse:	TGACCTATGGAATTGGCAG	*
Pre-miR193-Forward:	GTCTTTGCGGGCGAGAT	*
Pre-miR193-Reverse:	AACTGGGACTTTGTAGGCCA	*
Pri-mir21-Forward:	TTTTGTTTTGCTTGGGAGGA	
Pri-mir21-Reverse:	AGCAGACAGTCAGGCAGGAT	
Pri-mir31-Forward:	TGAGTGTGTTTTCCCTCCCT	*
Pri-mir31-Reverse:	GCCATGGCTGCTGTCAG	*
Pri-miR-192-Forward:	TGGTGGCGGGTAGTGGA	
Pri-miR-192-Reverse:	TGGCATTGAGGCGAACAT	
Pri-miR-193a-Forward:	ACCCCGAACTCCGAGGAT	
Pri-miR-193a-Reverse:	TGGGACTTTGTAGGCCAGTT	
EIF2C2-Q-Forward:	CACCATGTACTCGGGAGCC	
EIF2C2-Q-Reverse:	CAAAGTCGGGTCTAGGTGGA	
Dicer1-Q-Forward:	GAGCTGTCCTATCAGATCAGGG	
Dicer1-Q-Reverse:	ACTTGTTGAGCAACCTGGTTT	
ACTB-Q-Forward:	GCACAGAGCCTCGCCTT	Internal Control
ACTB-Q-Reverse:	GTTGTCGACGACGAGCG	Internal Control

Notes:

(1) For detection of mature miRNAs, TaqMan MicroRNA assay kits (Applied Biosystems) were used in accordance with the manufacturer's protocol.

(2) For pre-miR-31 detection, we used Hs_mir-31_1_PR miScript Precursor Assay (Qiagen) in accordance with the manufacturer's protocol.

(3) The primer sequences marked with "*" were from Jiang *et al*(Jiang et al., 2005).

(4) The primer sequences marked with "★" were from Suzuki *et al*[26].

2.24 Oligonucleotide sequences for pMIR-Reporter

Oligonucleotide	5' to 3'
miR-21-binding-F:	CTAGTTCAACATCAGTCTGATAAGCTAA
miR-21-binding-R:	AGCTTTAGCTTATCAGACTGATGTTGAA
miR-31-binding-F:	CTAGTAGCTATGCCAGCATCTTGCCTA
miR-31-binding-R:	AGCTTAGGCAAGATGCTGGCATAGCTA
miR-192-binding-F:	CTAGTGGCTGTCAATTCATAGGTCAGA
miR-192-binding-R:	AGCTTCTGACCTATGAATTGACAGCCA
miR-193a-5p-binding-F:	CTAGTTCATCTCGCCCGCAAAGACCCAA
miR-193a-5p-binding-R:	AGCTTTGGGTCTTTGCGGGCGAGATGAA
miR-31-192-193a-binding-F:	CTAGTCATCTTGCCTCATAGGTCAGCAAAGACCCAA
miR-31-192-193a-binding-R:	AGCTTTGGGTCTTTGCTGACCTATGAGGCAAGATGA

Chapter 3 EGFR Modulates microRNA Maturation in Response to Hypoxia through Phosphorylation of Argonaute2

Most of this work has been published in:

Shen J, Xia W, Khotskaya YB, Huo L, Nakanishi K, Lim SO, Du Y, Wang Y, Chang WC, Chen CH, Hsu JL, Wu Y, Lam YC, James BP, Liu X, Liu CG, Patel DJ, Hung MC. ***EGFR modulates microRNA maturation in response to hypoxia through phosphorylation of AGO2. Nature.*** *2013 May 16;497(7449):383-7.*

3.1 EGFR interacts with Ago2 in response to hypoxia

3.1.1 Ago2 is a novel EGFR-interacting protein

Activated epidermal growth factor receptor (EGFR) encompassed in intracellular vesicles is capable of activating intracellular signaling pathways before lysosomal degradation (Gould and Lippincott-Schwartz, 2009). Importantly, proteins associating with internalized EGFR likely differ from those transducing signaling at plasma membrane (Mosesson et al., 2008), suggesting a higher degree of signaling complexity that is not well characterized. By mass spectrometric analysis, we identified Ago2 as a novel EGFR-interacting protein (Fig. 3-1), and validated their association by co-immunoprecipitation (Co-IP) and pull-down assays (Fig. 3-2). The Juxt/Kinase domain of EGFR is essential for binding with Ago2 at the N-terminal region.

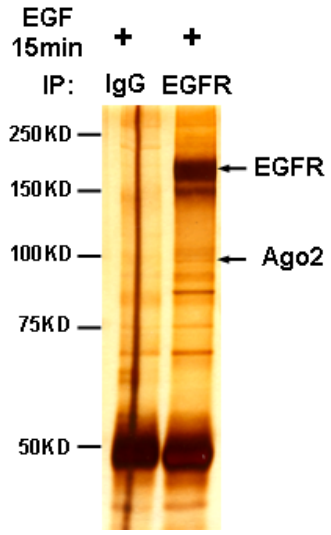

Figure 3-1 Ago2 is a novel EGFR-interacting protein, in addition to those previously reported (Huo et al., 2011).

Immunoprecipitation was performed in serum-starved EGF treated HeLa cells (with moderate expression of EGFR) with IgG control or anti-EGFR antibody Ab-13. Unique peptides of Argonarute2 were identified by mass spectrometric analysis in EGFR-immunoprecipitated protein sample, as shown by silver staining of the representative purification of endogenous EGFR.

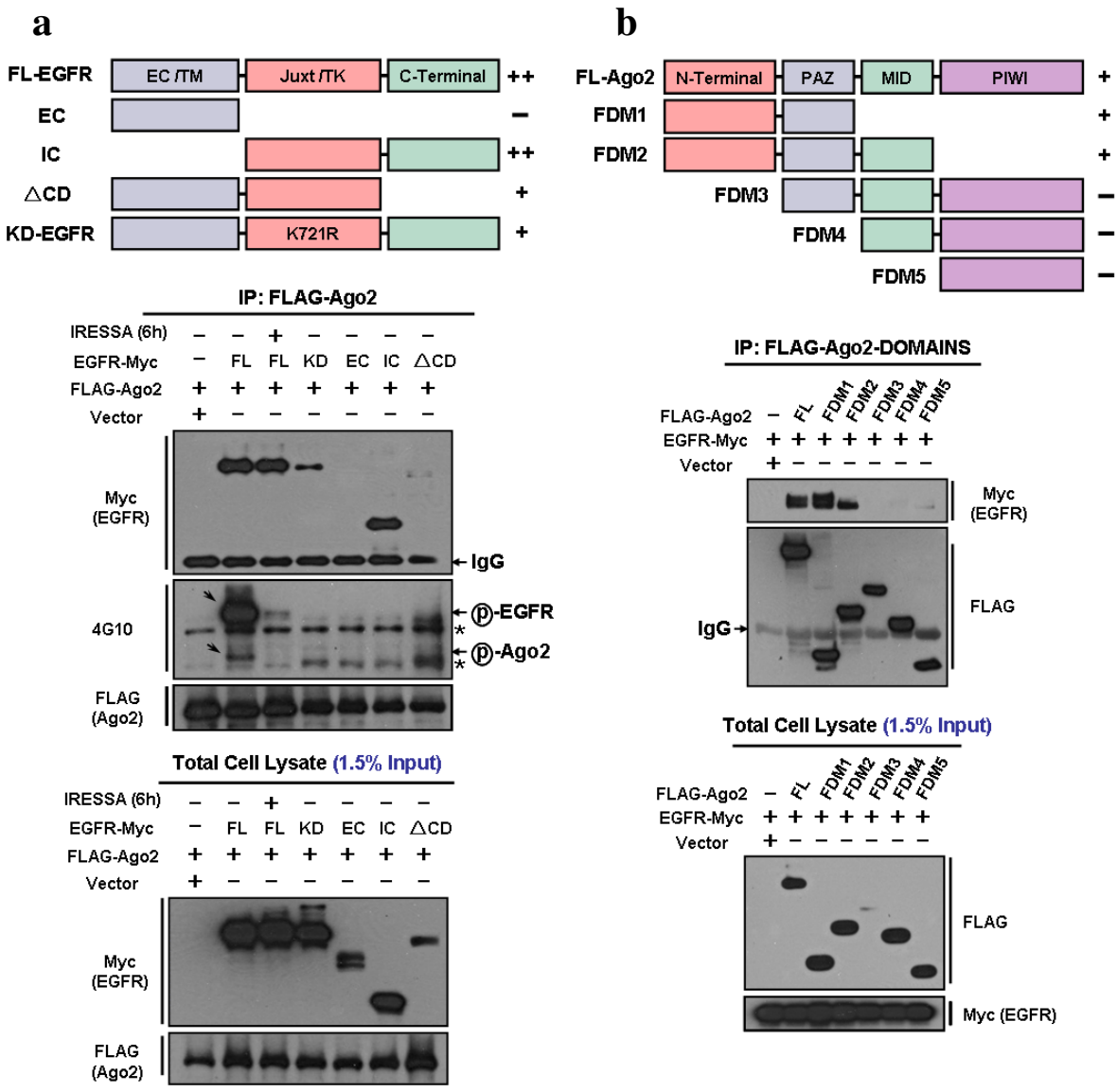

Figure 3-2 EGFR Juxt/Kinase domain and the N-terminal region of Ago2 are required for direct protein-protein association.

a, FLAG-tagged Ago2 was co-expressed with vector-control, full-length EGFR (with or without Iressa treatment), Kinase-Dead EGFR^{K721R} or different functional domains in 293T cells. Anti-FLAG immunoprecipitates were blotted with myc antibody to show the interaction between EGFR and Ago2. The efficacy of Iressa (tyrosine kinase inhibitor targeting EGFR) treatment was verified by the reduced tyrosine phosphorylation of EGFR. * indicates the non-specific signal recognized by FLAG antibody. **b,** Myc-tagged WT-EGFR was co-expressed with vector-control, FLAG-tagged full-length Ago2 or different domains in 293T cells. Anti-FLAG immunoprecipitates were blotted with myc antibody to show the interaction between EGFR and Ago2.

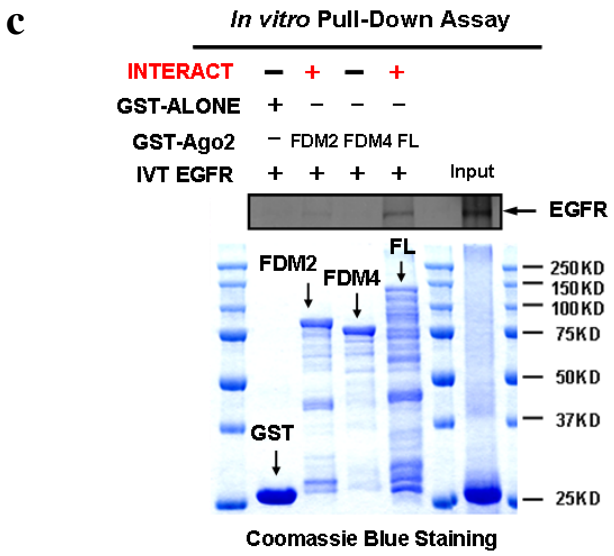

Figure 3-2 EGFR Juxt/Kinase domain and the N-terminal region of Ago2 are required for direct protein-protein association.

c, Pull-down assay was performed by incubating *in vitro* translated full-length EGFR with purified GST-control, GST-Ago2-FDM2, GST-Ago2-FDM4, or GST-full-length-Ago2. Protein samples were precipitated with Glutathione-sepharose beads and subjected to SDS-PAGE, which was visualized by S-35 radioisotopic detection. The quantity of precipitated GST-fusing protein is shown by Coomassie blue staining.

3.1.2 Hypoxia enhances the interaction between Ago2 and EGFR

Human Ago2 was initially reported as a membrane-associated cytoplasmic protein (Cikaluk et al., 1999) and is the catalytic center of RNA-induced silencing complex (RISC) (Eulalio et al., 2008). Ago2 also associates Dicer and TRBP (HIV-1 transactivating response RNA-binding protein) to form the RISC loading complex, which is involved in the second step of miRNA processing from pre- to mature miRNAs (Chendrimada et al., 2005; Diederichs and Haber, 2007). To investigate the physiological role of EGFR-Ago2 interaction, we screened different upstream EGFR-activating stimuli, including ligands and stresses (Franovic et al., 2007; Lemmon and Schlessinger, 2010; Reynolds et al., 2003; Wang et al., 2009), in HTC-1080 stable clone expressing split-half-YFP-fused EGFR and Ago2 (Fig. 3-3), in which the YFP fluorescence can only be reconstituted upon protein-protein association (Lee et al., 2010) (Fig. 3-4a). Of the four different types of stimuli, hypoxic stress induced the strongest level of YFP fluorescence (Figs. 3-3, 3-5) with distinct foci formed in cytoplasm (Fig. 3-4b), suggesting that internalized EGFR interacts with Ago2 in aggregates. Dynamic EGFR-Ago2 association was further validated in HeLa cells and various cancer cell lines by Co-IP (Figs. 3-4c, 3-6) and co-localization assays (Figs. 3-7, 3-8), and was found to be RNase-resistant (Fig. 3-9), supporting that EGFR and Ago2 are direct physical interacting partners *in vivo*.

a

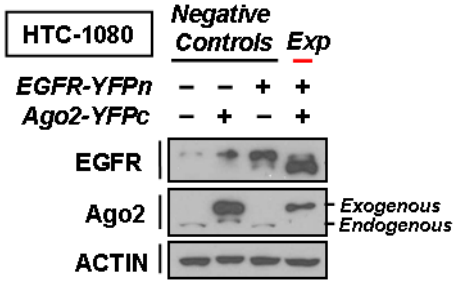

b

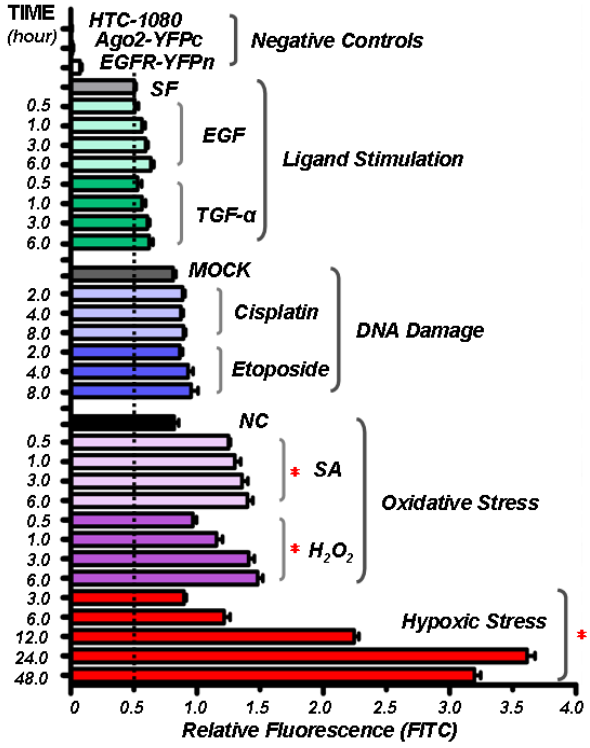

Figure 3-3 EGFR interacts with Ago2 in response to hypoxia and oxidative stress.

To be continued in next page.

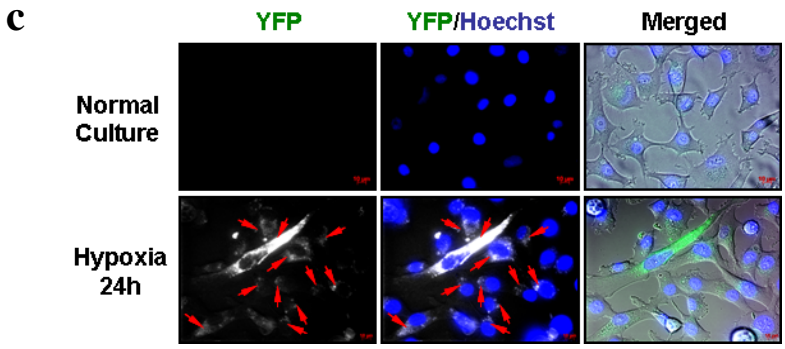

Figure 3-3 EGFR interacts with Ago2 in response to hypoxia and oxidative stress.

a, Western blot analysis of total cell lysates from HTC-1080 parental and HTC-1080 stable transfectants expressing Ago2-YFPc, EGFR-YFPn or both EGFR-YFPn and Ago2-YFPc, as indicated. **b,** YFP fluorescence (detected by Flow Cytometry in FITC channel) was induced upon co-expression of EGFR and Ago2, and was further enhanced when cells were cultured under hypoxia or oxidative stress. SF: Serum-Free O/N; EGF: 20 ng/ml; TGF-α: 10 ng/ml; Cisplatin: 50 μM; Etoposide: 50 μM; SA: Sodium Arsenite (500 μM); H_2O_2: 500 μM; Hypoxia: 1% O_2. Dashed line indicates the basal level of fluorescence detected in serum-starved HTC-1080 stable transfectant co-expressing EGFR and Ago2. All data were normalized to the one of HTC-1080 parental cells (Relative YFP Fluorescence = YFP Fluorescence − Auto-Fluorescence detected in HTC-1080 parental cells) with default setting Auto-Fluorescence =0. Statistical analysis was carried out using student's *t* test. The group of treatment was compared to its corresponding experimental control (ligands vs. SF; Cisplatin and Etoposide vs. MOCK; SA, H_2O_2 and hypoxia vs. NC). Data are shown as mean ± s.d., *n*=3. *indicates $P<0.05$. **c,** Representative live-cell images showing Hypoxia induced YFP fluorescence in HTC-1080 stable transfectant co-expressing split-half-YFP-tagged EGFR and Ago2. Living cells were stained with Hoechst (marker for nuclear) to show the cytoplasmic localization of the YFP foci as marked by red arrows.

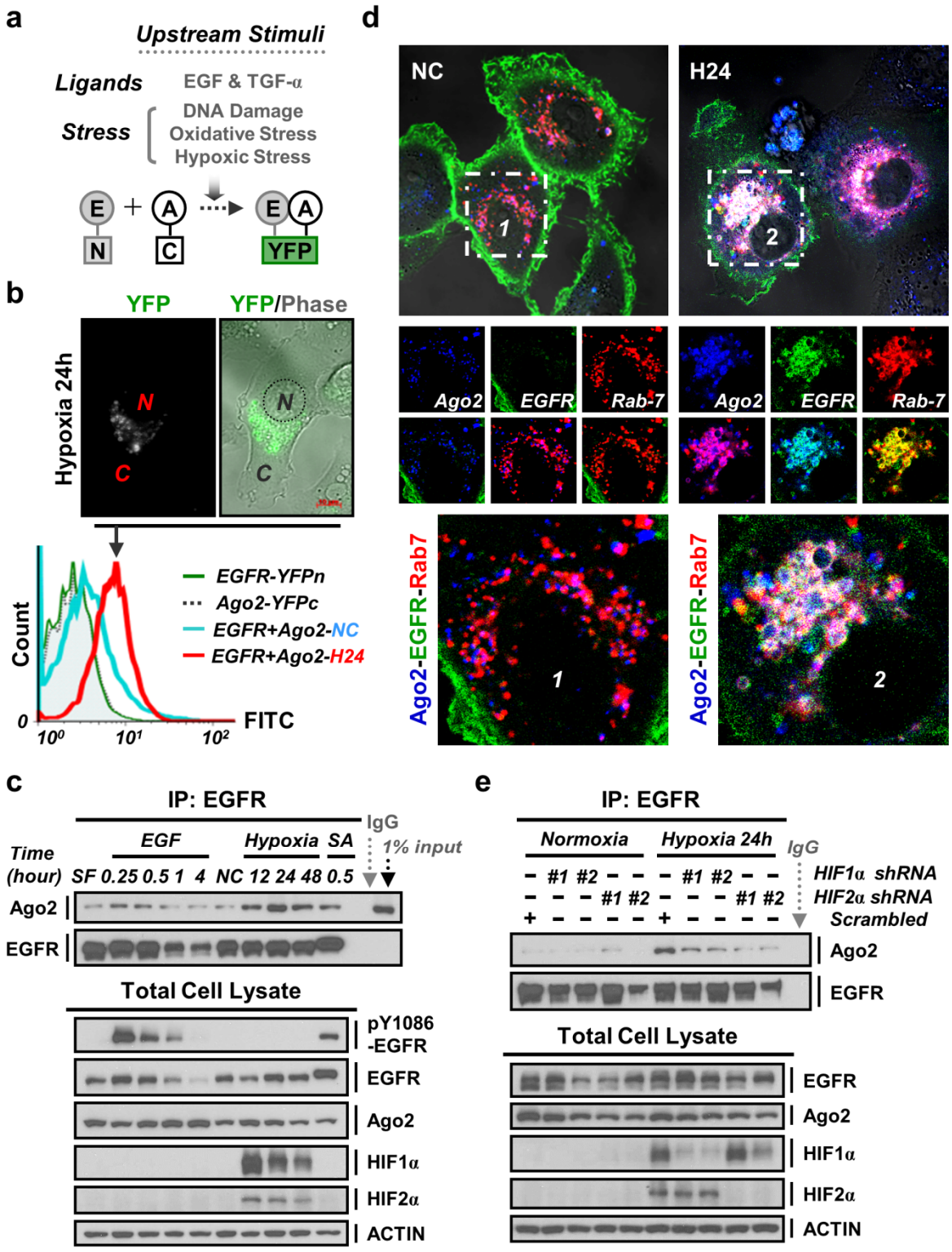

Figure 3-4 EGFR interacts with Ago2 in response to hypoxia.

Figure 3-4. EGFR interacts with Ago2 in response to hypoxia.

a, Split-half-YFP-fused EGFR and Ago2 were stably expressed in HTC-1080 cells to screen for upstream stimuli that might trigger EGFR-Ago2 interaction. E, EGFR; A, Ago2. **b,** Top, representative live-cell image. N, nuclear; C, cytoplasmic. Bottom, FACS analysis of HTC-1080 stable transfectants as indicated. **c,** IP-Western blot analysis of HeLa cells in response to different stimuli. EGF, 20 ng/ml; SA, 500 μM; hypoxia, 1% O_2. **d,** Confocal microscopy analysis of live HeLa cells as indicated. Rab7, a marker for late endosomes/MVBs. NC, normoxia; H24, hypoxia 24 hr. **e,** IP-Western blot analysis of HeLa stable transfectants expressing HIF1/2α shRNAs.

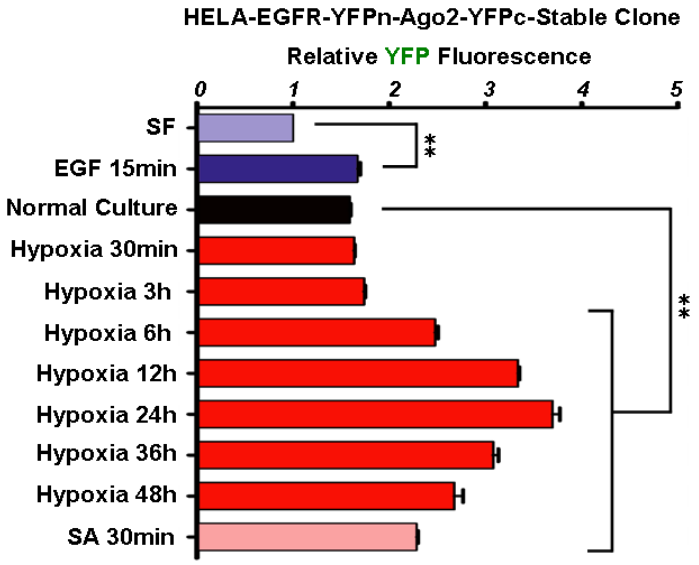

Figure 3-5 EGFR interacts with Ago2 in response to hypoxia and oxidative stress.

Similar YFP-interaction system was generated in HeLa cell line. The YFP fluorescence (detected in FITC channel) of HeLa stable transfectant (expressing both EGFR-YFPn and Ago2-YFPc) in response to ligand stimulation (EGF, 20 ng/ml), SA treatment (500 μM) or hypoxia (1% O_2) was analyzed by flow cytometry. All the data were normalized to the basal level of fluorescence in SF (serum-free O/N) group. Statistical analysis was carried out using student's *t* test. Data are shown as mean ± s.d., *n*=3. **indicates P<0.01.

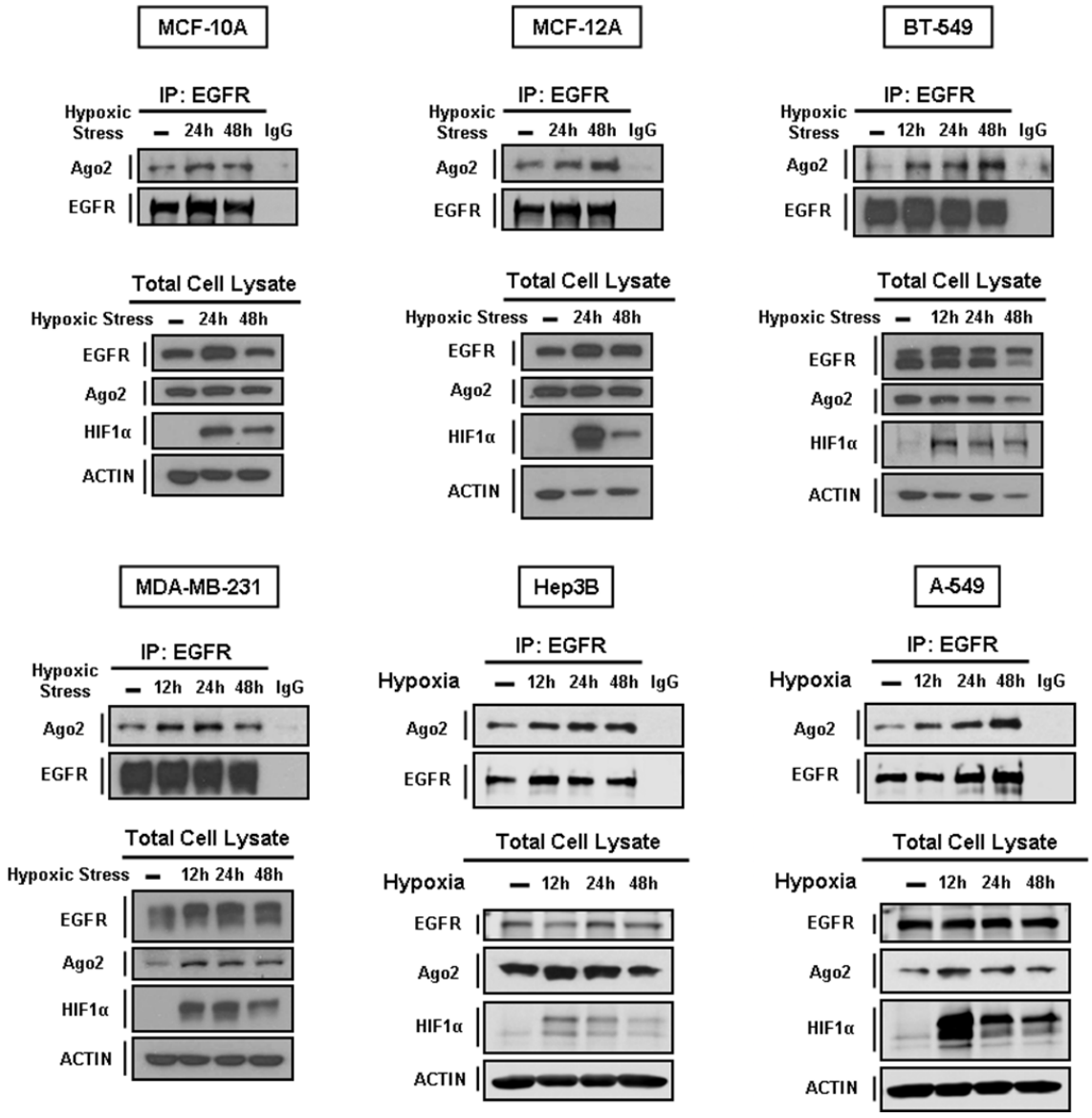

Figure 3-6 EGFR-Ago2 interaction was enhanced by hypoxia in multiple cell lines.

Western blot analysis of endogenous EGFR immunoprecipitated from MCF-10A (breast); MCF-12A (breast); BT-549 (breast); MDA-MB-231 (breast); Hep3B (liver) and A-549 (lung) cells cultured under normoxia or hypoxia, as indicated. HIF1α was used as a positive control for cell hypoxic response. β-actin was used as protein loading control.

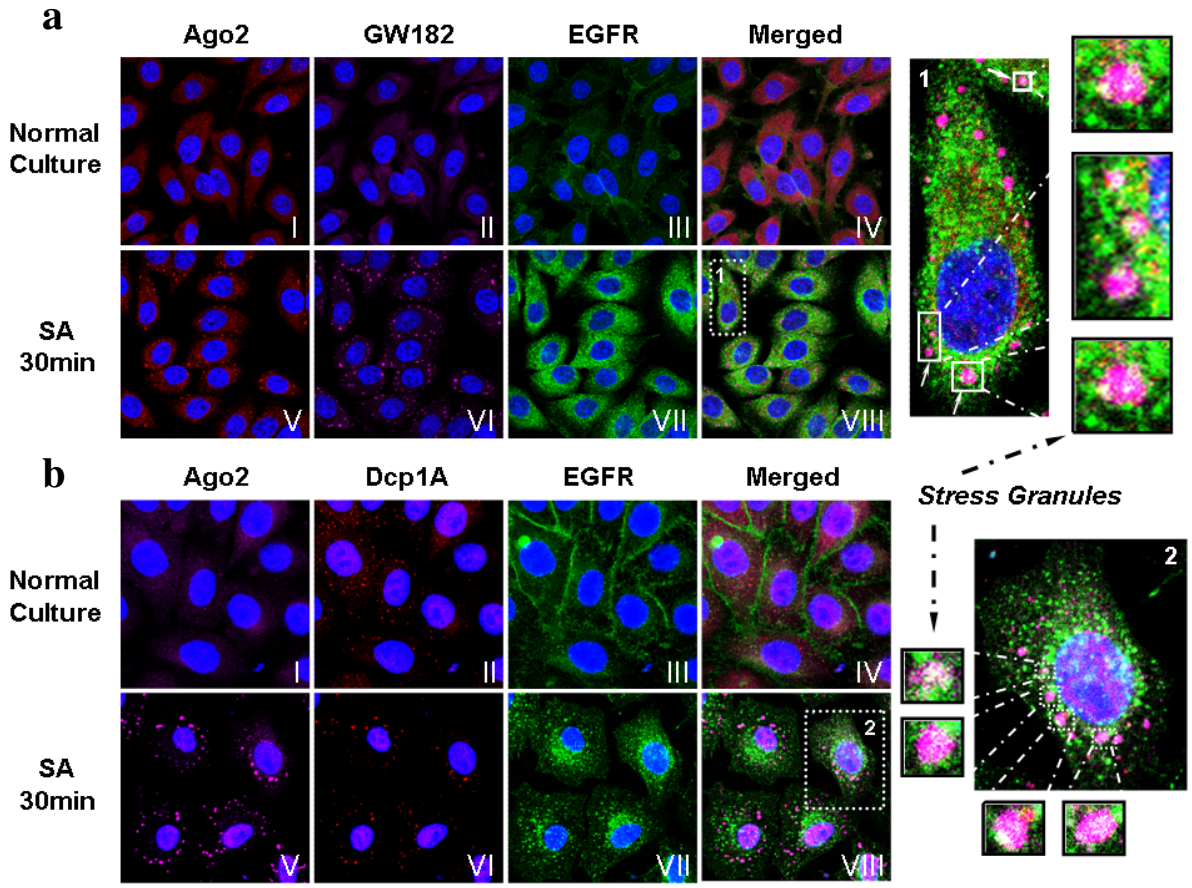

Figure 3-7 EGFR colocalizes with Ago2 in a sub-population of SA-induced stress granules (as marked by GW182, Dcp1A and Ago2)

a, HeLa cells were cultured in normal medium or treated with 500 μM sodium arsenite (SA, classical stress granule inducer) for 30 min. Cells were fixed and stained against endogenous Ago2 (red), GW182 (magenta), EGFR (green) and DAPI (blue). Stress granules are indicated by the SA-induced colocalization of Ago2 and GW182(Parker and Sheth, 2007). Right: magnification of image insets. **b,** Left, HeLa cells with same treatments as panel **a** were fixed and stained against endogenous Ago2 (magenta), Dcp1A (red), EGFR (green) and DAPI (blue). Stress granules are indicated by the SA-induced colocalization of Ago2 and Dcp1A (Parker and Sheth, 2007). Right, enlargement of the insets.

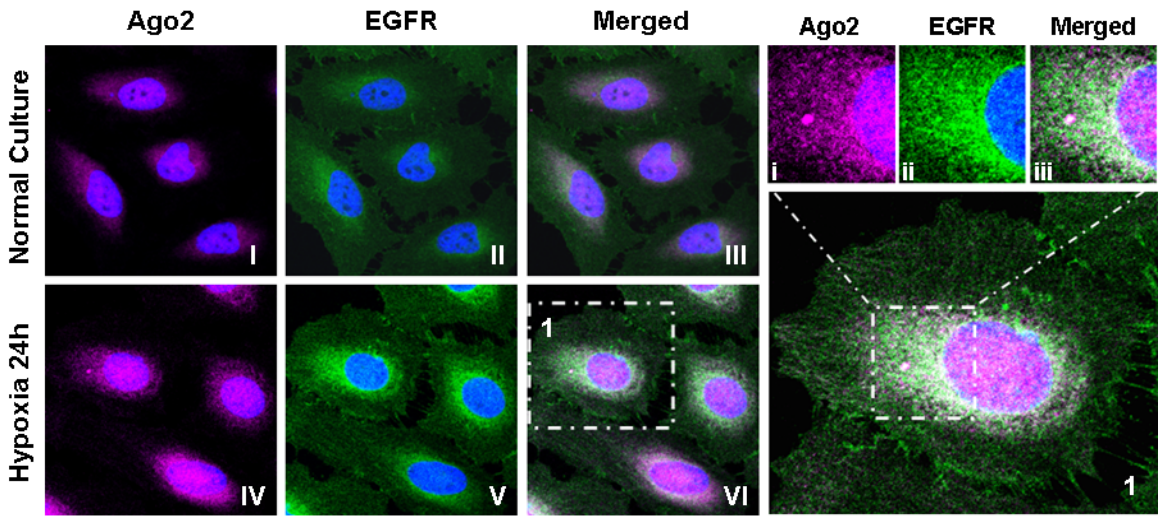

Figure 3-8 EGFR colocalizes with Ago2 in response to hypoxic stress.

HeLa cells were cultured under normoxia or hypoxia (1% O_2) for 24 hr. Cells were then fixed and stained against endogenous Ago2 (magenta), EGFR (green) and DAPI (blue). Right: magnification of image insets.

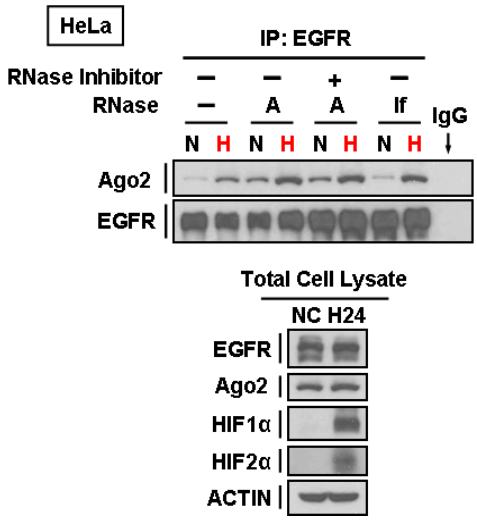

Figure 3-9 Hypoxia-enhanced EGFR-Ago2 interaction is resistant to RNase treatments.

Western blot analysis of total cell lysates and EGFR immunoprecipitates from HeLa cells that were cultured under normoxia or hypoxia for 24 hr, as indicated. Cell lysates were treated with 2 μg RNase A (cleaving single-stranded RNA, Sigma) with or without 500 units of ribonuclease inhibitor RNase-Out (Life Technologies) or 100 unites of RNase I_f (single strand specific RNA endonuclease, NEB) as indicated at 4 ℃ overnight before performing immunoprecipitation. N, normoxia; H, hypoxia for 24 hr.

3.1.3 EGFR interacts with Ago2 at MVBs in response to hypoxia

Hypoxia is known to upregulate EGFR (Franovic et al., 2007) and prolong its activation through retention in endocytic trafficking (Wang et al., 2009). Indeed, hypoxia enhanced EGFR expression in late endosomes/multivesicular bodies (MVBs; F2-F4, Fig. 3-10), where it co-localized with Ago2 (Figs. 3-4d, 3-11) and co-fractionated (Fig. 3-10) with RISC components (Ago2, Dcp1A, and GW182) as well as the RISC loading complex (Dicer, TRBP, and Ago2). Silencing Grb2, a key modulator of EGFR endocytosis (Jiang et al., 2003), diminished EGFR-Ago2 interaction (Fig. 3-12), highlighting the importance of internalization. Furthermore, inhibition or silencing of hypoxia-inducible transcriptional factors (HIF1/2α) (Bertout et al., 2008) reduced EGFR-Ago2 association (Figs. 3-4e, 3-13a) and colocalization (Figs. 3-13b, 3-14) under hypoxia while stabilization of HIF1/2α triggered their interaction under normoxia (Fig. 3-15). Nonetheless, EGFR-Ago2 association in RCC4 cells (endogenous VHL null with constitutively expressed HIF1/2α) was further strengthened by hypoxia regardless of the exogenous expression of WT-VHL (Fig. 3-16). These results indicate that stable expression of HIF1/2α is sufficient to trigger EGFR-Ago2 interaction that is further enhanced by hypoxia likely through a HIF1/2α-independent mechanism.

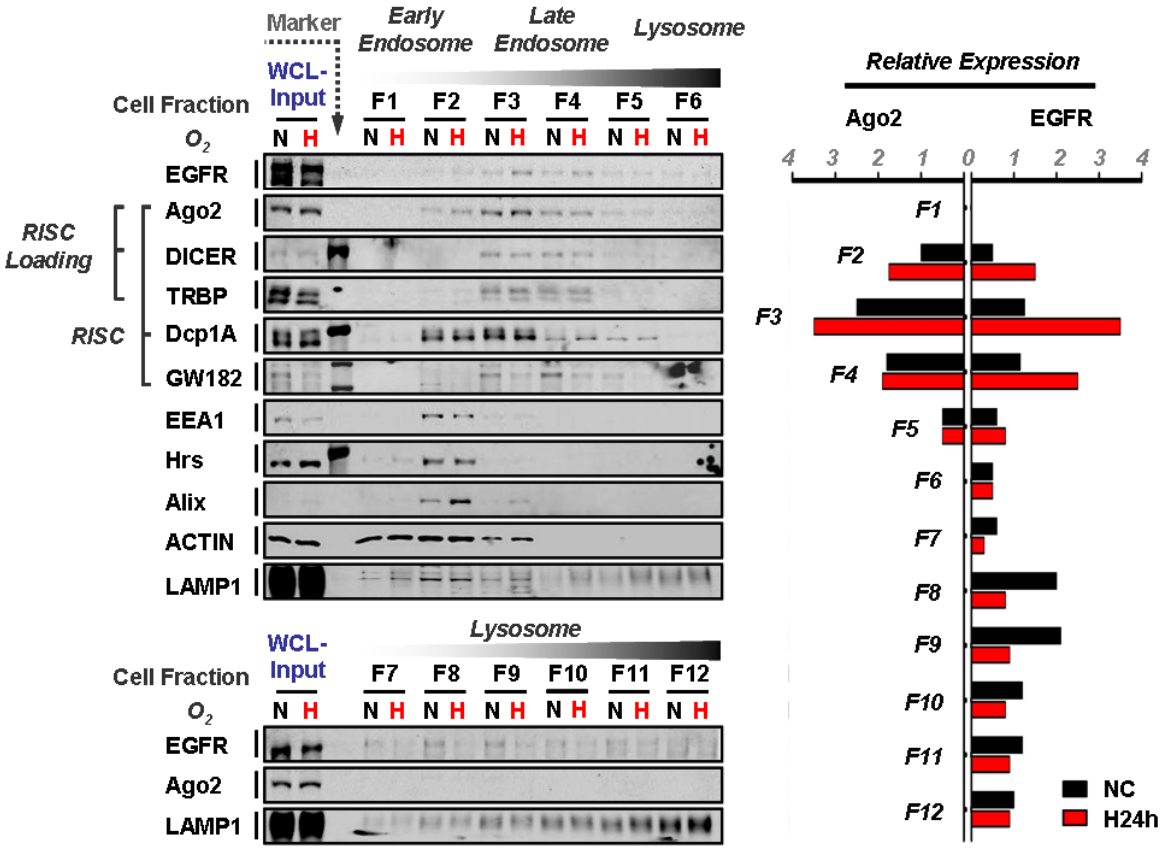

Figure 3-10 EGFR is co-fractionated with RISC loading complex and RISC complex at late endosome/MVB (multivesicular body).

Left, Western blot analysis of endogenous EGFR, Ago2, and other known components of RISC (Eulalio et al., 2008) and RISC loading complex (Diederichs and Haber, 2007), as indicated, in cell fractions from early endosomes (F1-2, indicated by Actin, EEA1 and Hrs), late endosomes/MVB (F2-4, indicated by Hrs, Alix, Actin and Lamp1), to lysosomes (F4-12, indicated by Lamp1). Ago2 was enriched in late endosomes/multivesicular bodies (MVBs), consistent with previous reports (Gibbings et al., 2009; Lee et al., 2009). N, cultured under normoxia; H, cultured under hypoxia for 24 hr. Right, relative expression (each fraction signal was normalized according to its corresponding WCL-input) of EGFR and Ago2 in each fraction as indicated.

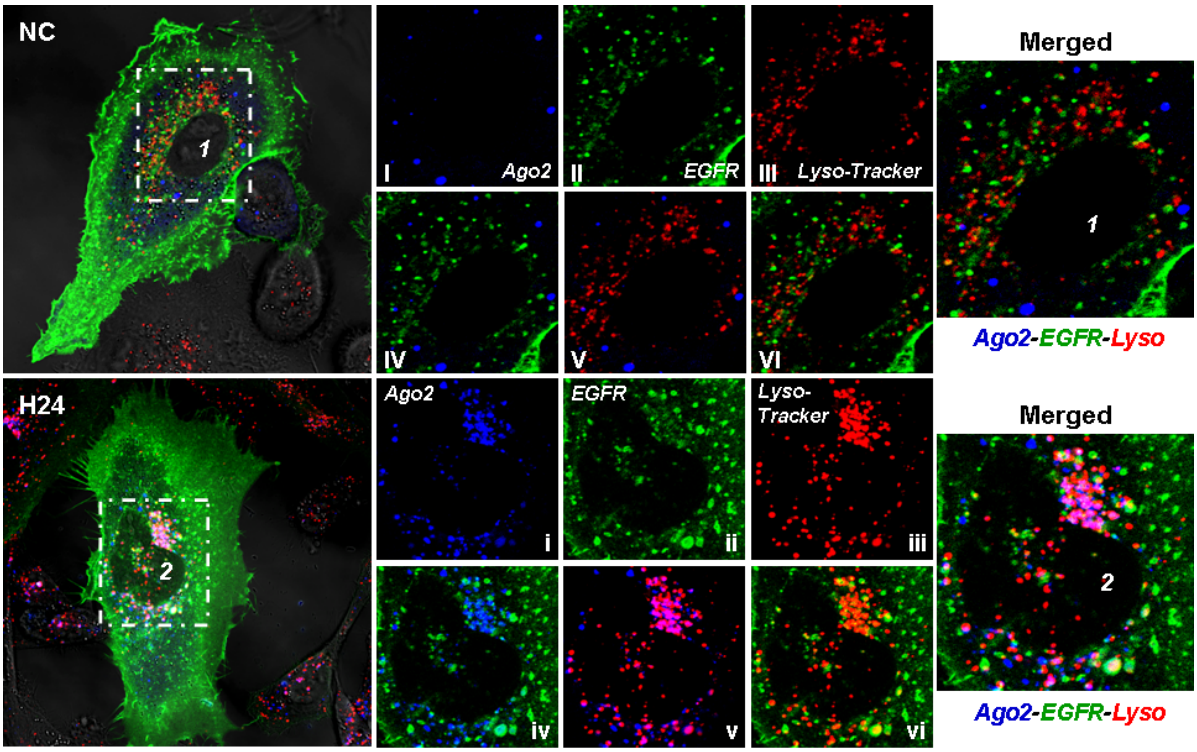

Figure 3-11 EGFR colocalizes with Ago2 at late endosomes/MVBs or lysosomes in response to hypoxia.

HeLa cells co-transfected with EGFR-GFP (green) and BFP-Ago2 (blue) were cultured under normoxia or hypoxia (1% O_2) for 24hr. Cells were stained with 50 nM Lyso-Tracker (red color, accumulated in low internal PH compartments(Knodler and Steele-Mortimer, 2005)) right before live-cell confocal imaging. Hypoxia enhanced colocalization of EGFR and Ago2 at late endosomes/MVBs/lysosomes is indicated by the positive staining of Lyso-Tracker. Right: magnification of image insets.

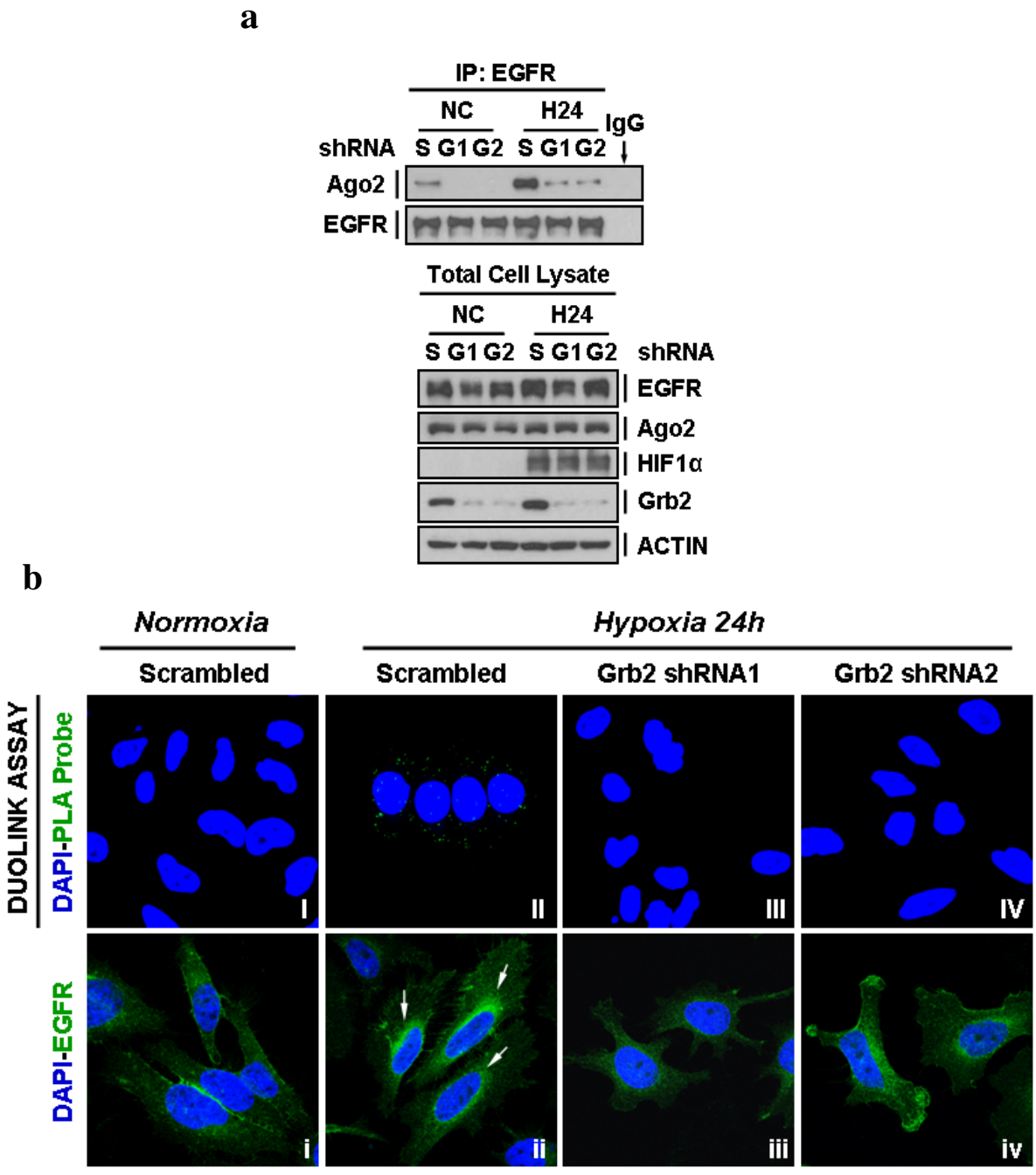

Figure 3-12 Grb2-mediated internalization is critical for the interaction between EGFR and Ago2.

Figure 3-12. Grb2-mediated internalization is critical for the interaction between EGFR and Ago2.

a, Western blot analysis of total cell lysates and EGFR immunoprecipitates from HeLa stable transfectants expressing scrambled control or shRNAs targeting Grb2 that were cultured under normoxia or hypoxia for 24 hr as indicated. S, scrambled control; G1, Grb2 shRNA1; G2, Grb2 shRNA2. HIF1α was used as positive control for cell hypoxic response. β-actin was used as protein loading control. **b,** Upper panel, in situ proximity ligation assay was performed in HeLa stable transfectants expressing scrambled control or shRNAs targeting Grb2 that were cultured under normoxia or hypoxia for 24 hr as indicated. Each GFP foci indicated one cluster of EGFR-Ago2 colocalization. Lower panel, HeLa stable transfectants treated the same as upper panel were fixed and stained against endogenous EGFR (green) and DAPI (blue). Hypoxia enhanced EGFR internalization as marked by the arrows in image ii. Grb2 knockdown blocked EGFR endocytosis as expected.

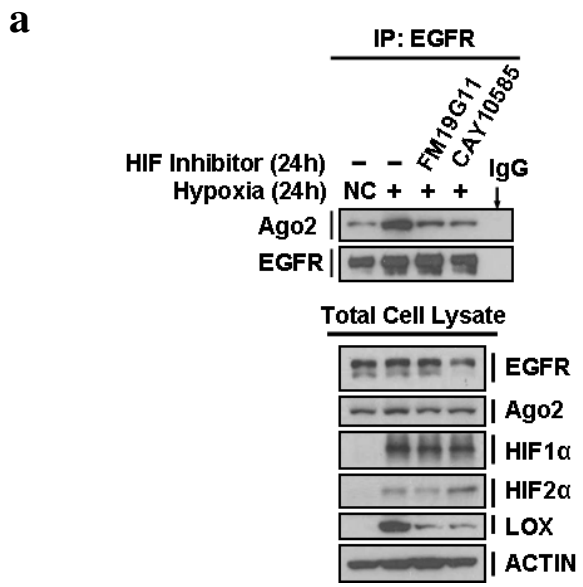

Figure 3-13 The transcriptional activity of HIF1/2α is important for hypoxia-enhanced EGFR-Ago2 interaction.

a, Western blot analysis of total cell lysates and EGFR immunoprecipitates from HeLa cells that were cultured under normoxia or hypoxia with or without HIF1/2α inhibitors for 24 hr as indicated. The efficacy of HIF1/2α inhibitors was reflected by the reduced expression of LOX, a well-known target of HIF1/2α (Erler et al., 2006). HIF1/2α as used as positive control for cell hypoxic response. β-actin was used as protein loading control.

b

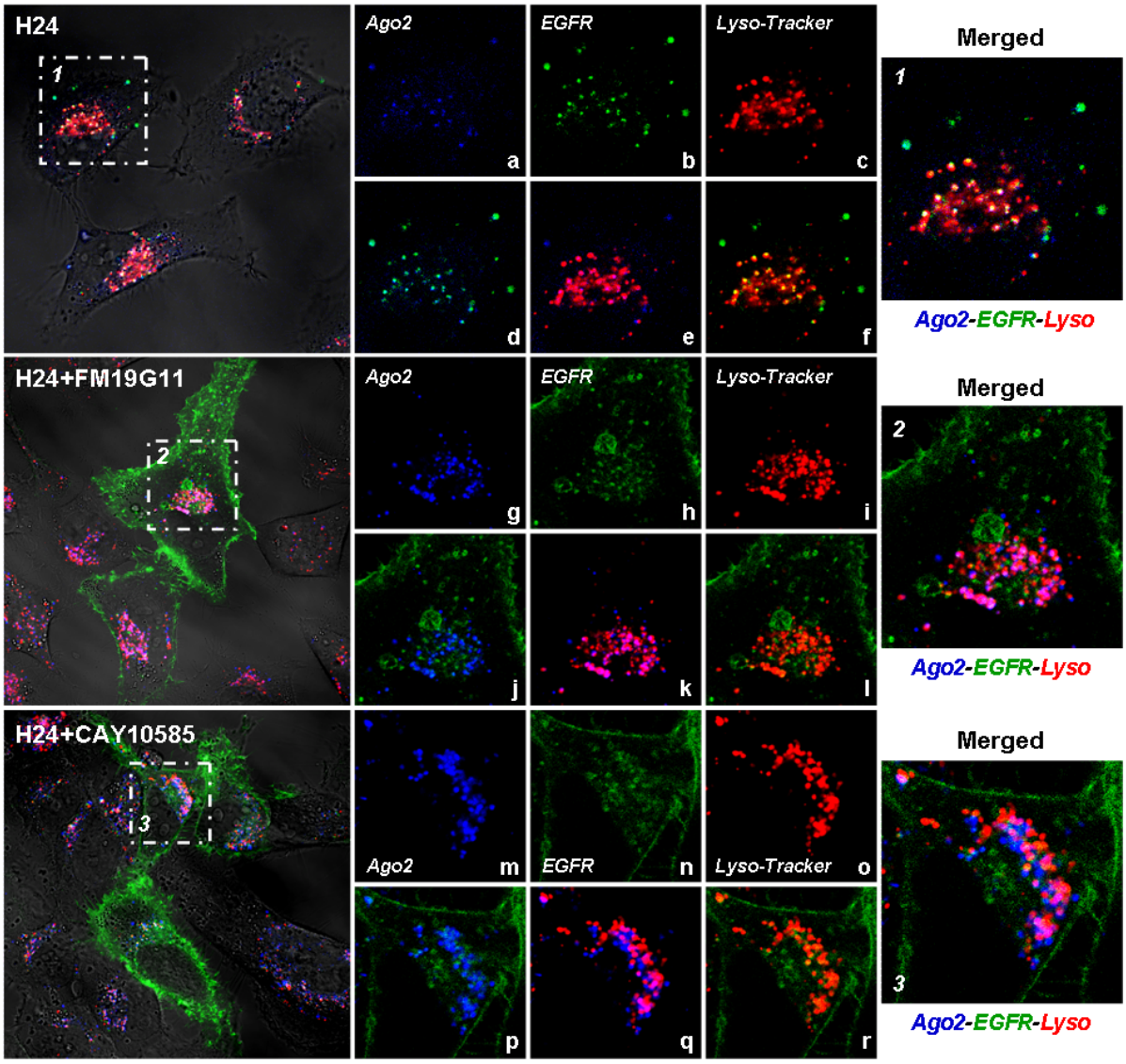

Figure 3-13. The transcriptional activity of HIF1/2α is important for hypoxia-enhanced EGFR-Ago2 interaction.

b, HeLa cells co-transfected with EGFR-GFP (green) and BFP-Ago2 (blue) were cultured under hypoxia (1% O_2) with or without HIF1/2α inhibitors (FM19G11 inhibits the transcriptional activity of HIF1/2α (Moreno-Manzano et al., 2010); CAY10585 blocks HIF1α accumulation and reduces its transcriptional activity (Basu et al., 2011) for 24hr. Cells were stained with 50 nM Lyso-Tracker (red color, accumulated in low internal PH compartments) right before live-cell confocal imaging. Right: magnification of image insets.

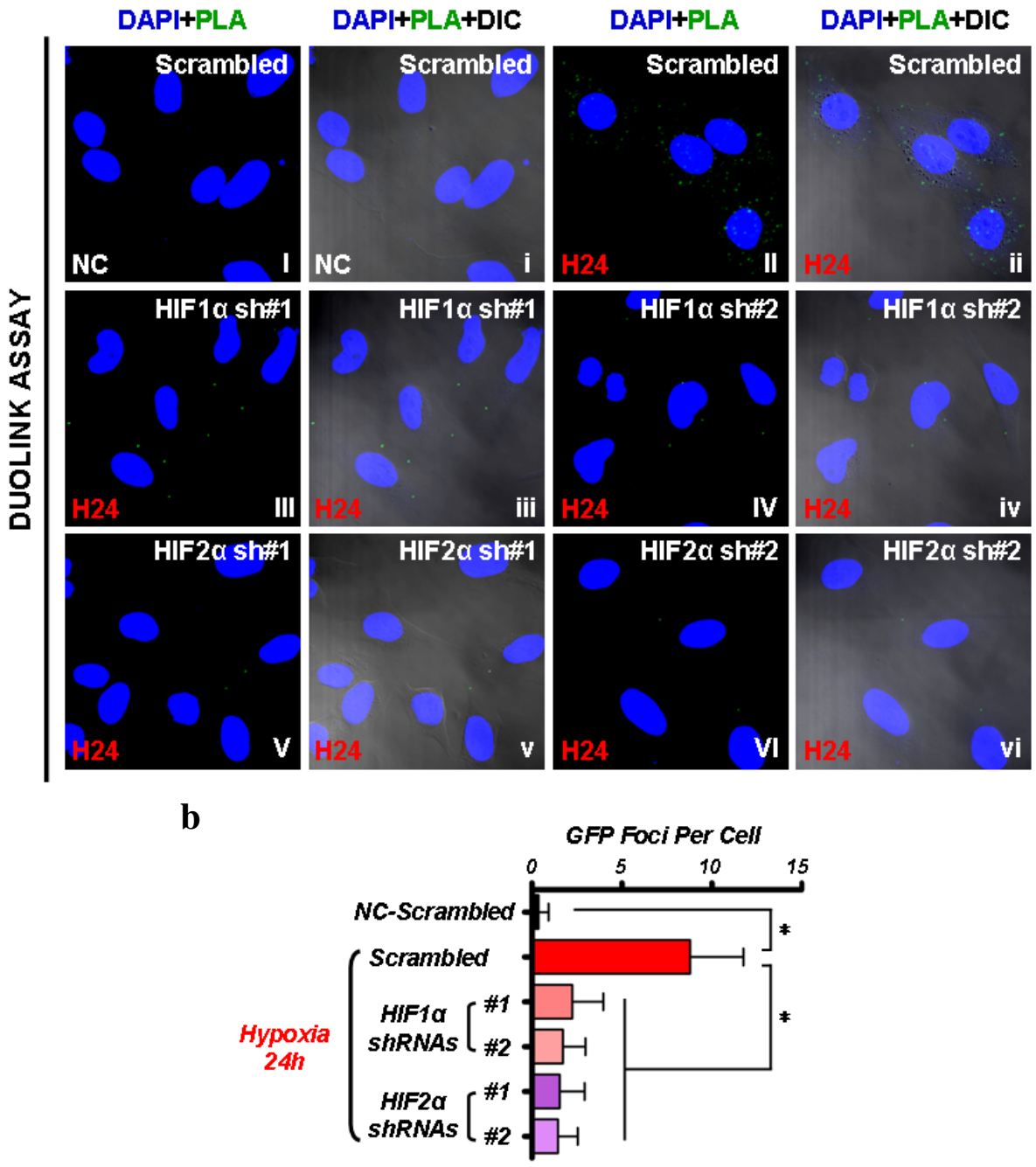

Figure 3-14 Both HIF1α and HIF2α are important for EGFR-Ago2 interaction in response to hypoxia.

Figure 3-14. Both HIF1α and HIF2α are important for EGFR-Ago2 interaction in response to hypoxia.

a, *In situ* proximity ligation assay was performed in HeLa stable transfectants expressing scrambled control or shRNAs targeting HIF1α or HIF2α as indicated that were cultured under normoxia or hypoxia for 24 hr. Each GFP foci indicated one cluster of EGFR-Ago2 colocalization/interaction. **b,** Quantitative result for panel **a**. Fifty cells in each experimental group were counted for the number of GFP foci per cell. Statistical analysis was carried out using student's *t* test. HIF1/2α knockdown cells were treated as one group to compare with the scrambled control. Data are shown as mean ± s.d., *n*=50. *indicates P<0.05.

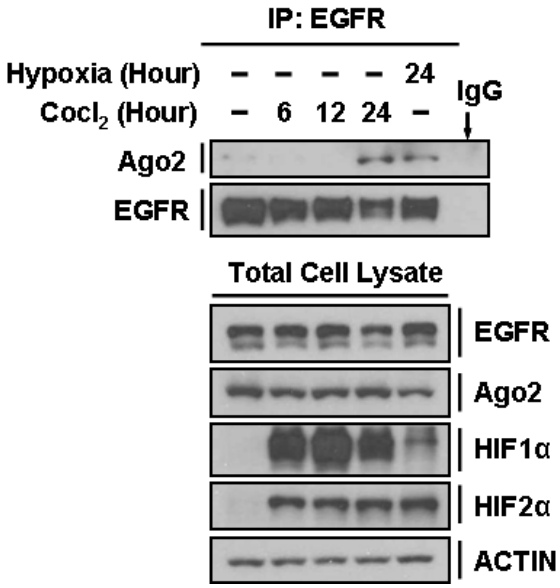

Figure 3-15 Stabilization of HIF1/2α by $CoCl_2$ treatment finally enhanced EGFR-Ago2 interaction under normoxia.

Western blot analysis of the total cell lysates and EGFR immunoprecipitates from HeLa cells that were treated with $CoCl_2$ (100 μM) or cultured under hypoxia for 24 hr as indicated. The expression of HIF1/2α was stabilized right after $CoCl_2$ treatment for 6 hr (consistent with previous report (Slomiany and Rosenzweig, 2006), whereas the interaction between EGFR and Ago2 was not induced until 24 hr later (similar to what we found in EGFR-Ago2 association in response to hypoxia), suggesting that downstream events of HIF1/2α stabilization may also play a role in EGFR-Ago2 interaction.

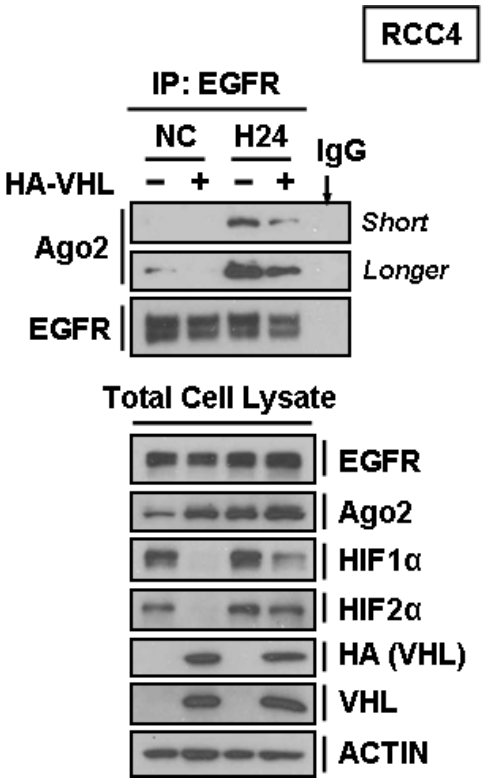

Figure 3-16 EGFR-Ago2 interaction was induced by hypoxia through HIF1/2α dependent and independent mechanisms.

Western blot analysis of the total cell lysates and EGFR immunoprecipitates from RCC4 (endogenous VHL null with constitutively expressed HIF1/2α) stable transfectants expressing vector control or WT-VHL that were cultured under normoxia or hypoxia for 24 hr. Re-expression of WT-VHL in RCC4 cells reduced the expression of HIF1/2α as previously reported (Ivan et al., 2001) and decreased the association between EGFR and Ago2. However, EGFR-Ago2 interaction in RCC4 vector control and WT-VHL stable clones was further induced by hypoxia regardless of the constitutively expressed HIF1/2α.

3.2 EGFR modulates miRNA maturation in response to hypoxia

To assess the functional importance of EGFR-Ago2 interaction in miRNA regulation, we profiled RNA expression in HeLa stable clones expressing scrambled control or EGFR shRNA-E1 under normoxia or hypoxia by RNA deep sequencing (Figs. 3-17a, 3-18). Hierarchical clustering analysis of relative expression of pre- and mature miRNAs (Scrambled vs. EGFR shRNA-E1, Fig. 3-17b) identified one distinct cluster of miRNAs under hypoxia (dashed box, Fig. 3-19a). In the presence of EGFR, the level of pre-miRNAs increased with a concomitant decrease in the expression of mature miRNAs. However, the maturation of this cluster of miRNAs was not significantly altered by EGFR under normoxia (Fig. 3-19a), implying that their processing from pre- to mature miRNAs was negatively regulated by EGFR specifically in response to hypoxia. We defined this sub-cluster of miRNAs as mHESM (miRNAs regulated by Hypoxia-dependent EGFR-Suppressed Maturation). We then pooled mHESM and narrowed down the candidates based on their absolute mature miRNA expression affected by EGFR knockdown. A majority of the top-scoring mHESM turned out to be tumor suppressor-like (Leung and Sharp, 2007, 2010; Lu et al., 2005; Nicoloso et al., 2009; Ventura and Jacks, 2009) (Fig. 3-20). To determine the functional relevance of mHESM, mRNAs regulated by EGFR were sorted and overlapped with the predicted mRNA targets of top-scoring mHESM, revealing 439 mRNAs that are regulated by EGFR and also targeted by top-scoring mHESM (Fig. 3-19b). In response to hypoxia, EGFR reduced the production of mHESM but enhanced the expression of corresponding mRNA targets (Fig. 3-19b), supporting the importance of EGFR-modulated miRNA maturation. The inhibitory role of EGFR in miRNA maturation in response to hypoxia was further validated in HeLa stable transfectants expressing scrambled control or

shRNAs targeting EGFR (Fig. 3-21) by quantitative PCR (qPCR). Moreover, induction of WT but not kinase-dead (KD) EGFR in HeLa TetOff-inducible stable clones (Fig. 3-22a) inhibited the maturation of top-scoring mHESM in response to hypoxia (Figs. 3-22b,c), suggesting that EGFR kinase activity is important for EGFR-suppressed miRNA maturation.

a

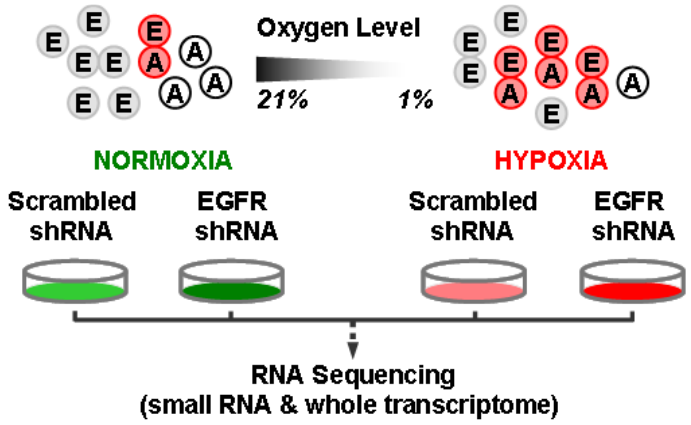

b

Define R-Pre and R-Mature:
Relative Expression Affected by EGFR

R-Pre = Log_2 Pre-miR (Scrambled) - Log_2 Pre-miR (EGFR shRNA-E1)
R-Mature = Log_2 Mature-miR (Scrambled) - Log_2 Mature-miR (EGFR shRNA-E1)

Figure 3-17 Experimental design for RNA deep sequencing analysis.

a, Total RNA extracted from HeLa stable clones expressing scrambled control or EGFR shRNA (shRNA-E1) that cultured under normoxia or hypoxia for 24 hr was analyzed by RNA deep sequencing for both small RNA application and whole transcriptome analysis. E, EGFR; A, Ago2. Red circles indicate the interaction between EGFR and Ago2. **b,** Definition of R-Pre and R-Mature for Hierarchical Clustering Analysis.

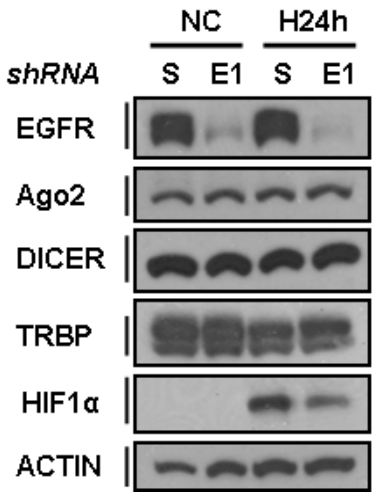

Figure 3-18 Verification of EGFR knockdown efficacy in HeLa stable transfectants for RNA deep sequencing.

Western blot analysis of total cell lysates from HeLa stable clones expressing scrambled control or EGFR shRNA-E1 that were cultured under normoxia or hypoxia for 24 hr. HIF1α was used as a positive control for cell hypoxic response. β-actin was used as protein loading control. S, scrambled control; E1, EGFR shRNA-E1.

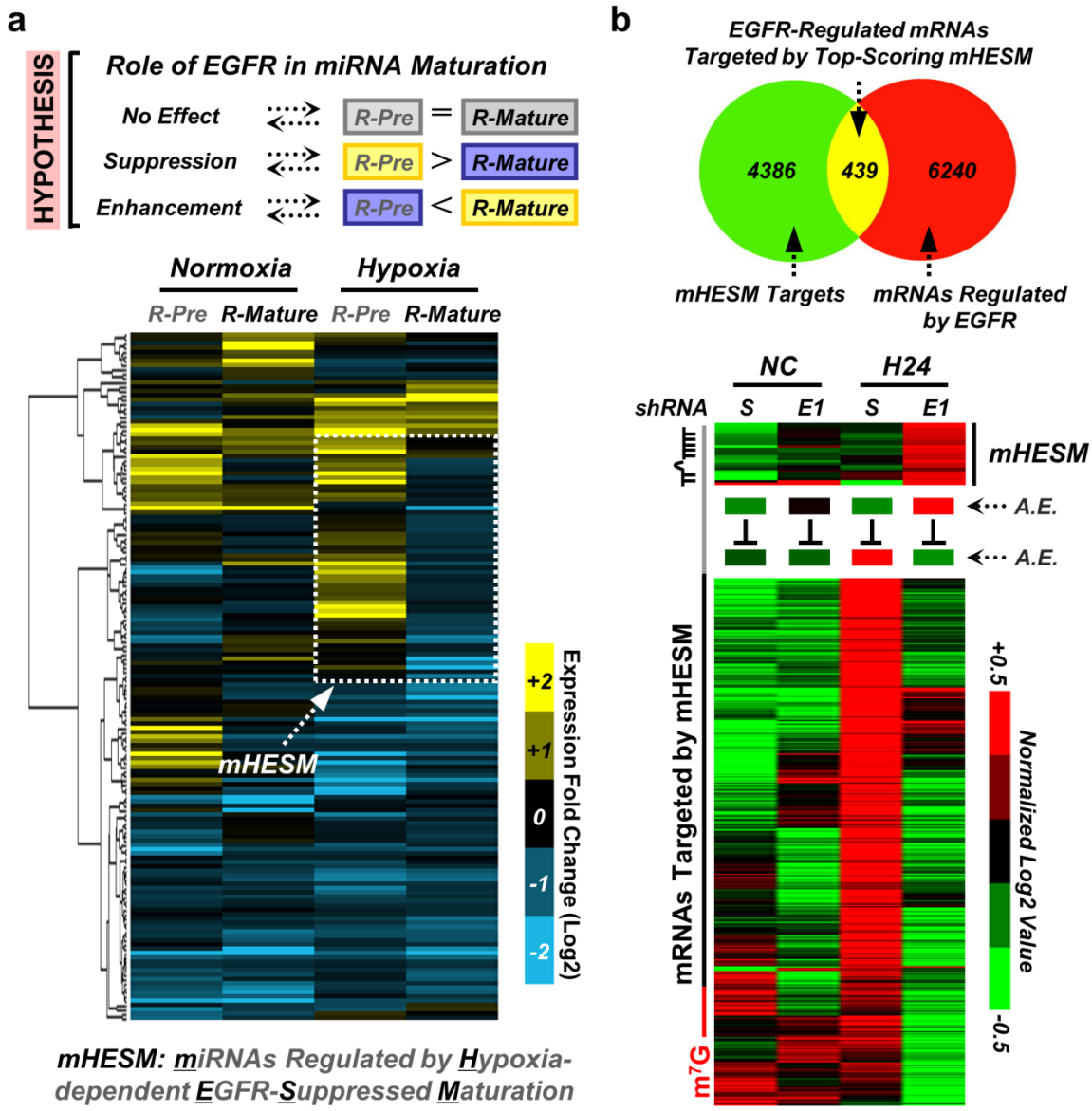

Figure 3-19 EGFR modulates miRNA maturation in response to hypoxia.

a, Top, hypothesized role of EGFR in miRNA maturation; Bottom, Hierarchical Clustering Analysis of R-Pre and R-Mature identified one distinct cluster of miRNAs whose maturation was suppressed by EGFR under hypoxia. We define this sub-cluster as mHESM. **b,** Top, Venn diagram highlighting the mRNAs that are regulated by EGFR and likely to be targeted by top-scoring mHESM. Bottom, EGFR-mediated suppression of top-scoring mHESM concurrent with the up-regulation of targeting mRNAs in response to hypoxia. A.E., average expression.

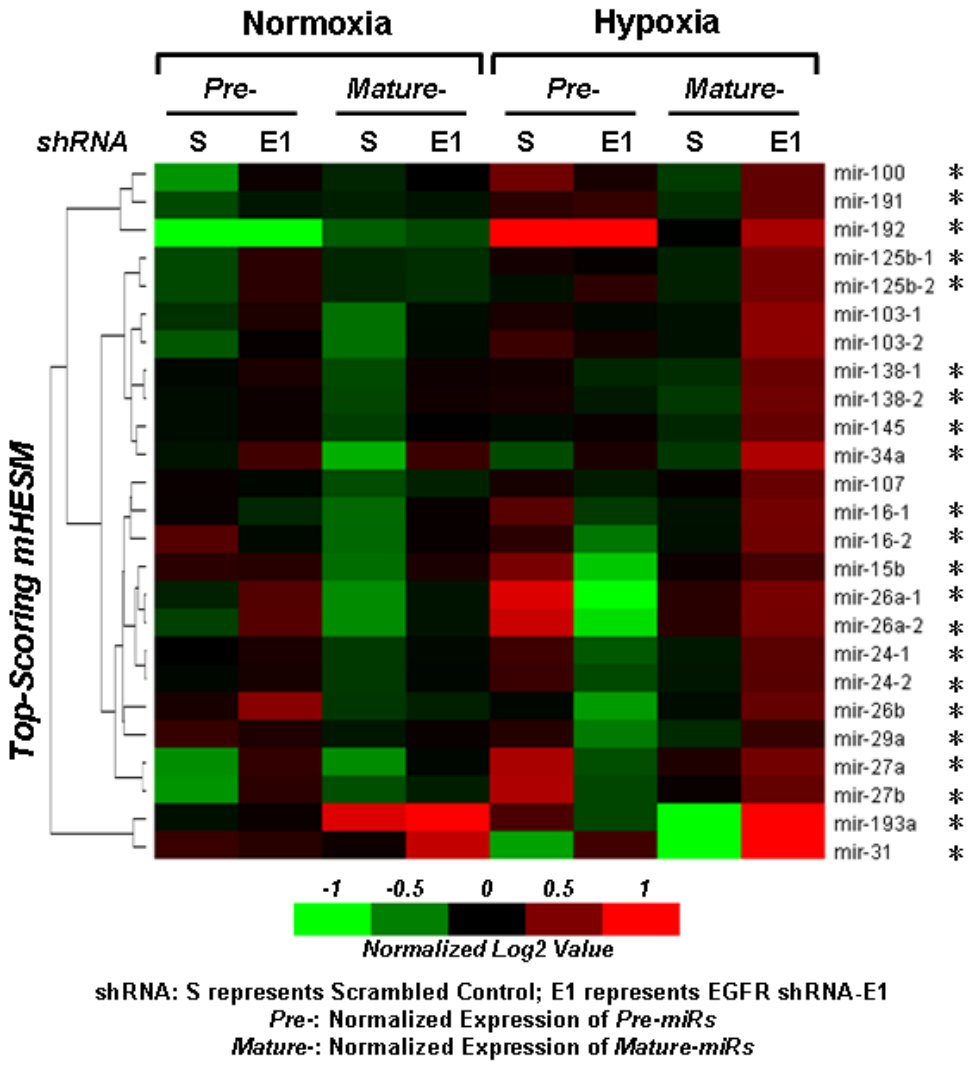

Figure 3-20 Hierarchical Clustering Analysis of top-scoring mHESM.

mHESMs were sorted based on their absolute mature miRNA expression affected by EGFR knockdown. 20 top-scoring mHESM were selected (note: miR-193a includes miR-193a-5p and miR-193a-3p) and tumor-suppressor-like miRNAs were marked with an asterisk (*). Expression of pre- or mature miRNAs was log2 transformed and further normalized by mean centering to correct average gene expression from all the samples as log2-ratio of 0. Centroid Linkage Clustering was performed and the interactive graphical result from Cluster was analyzed by TreeView to display the heatmap.

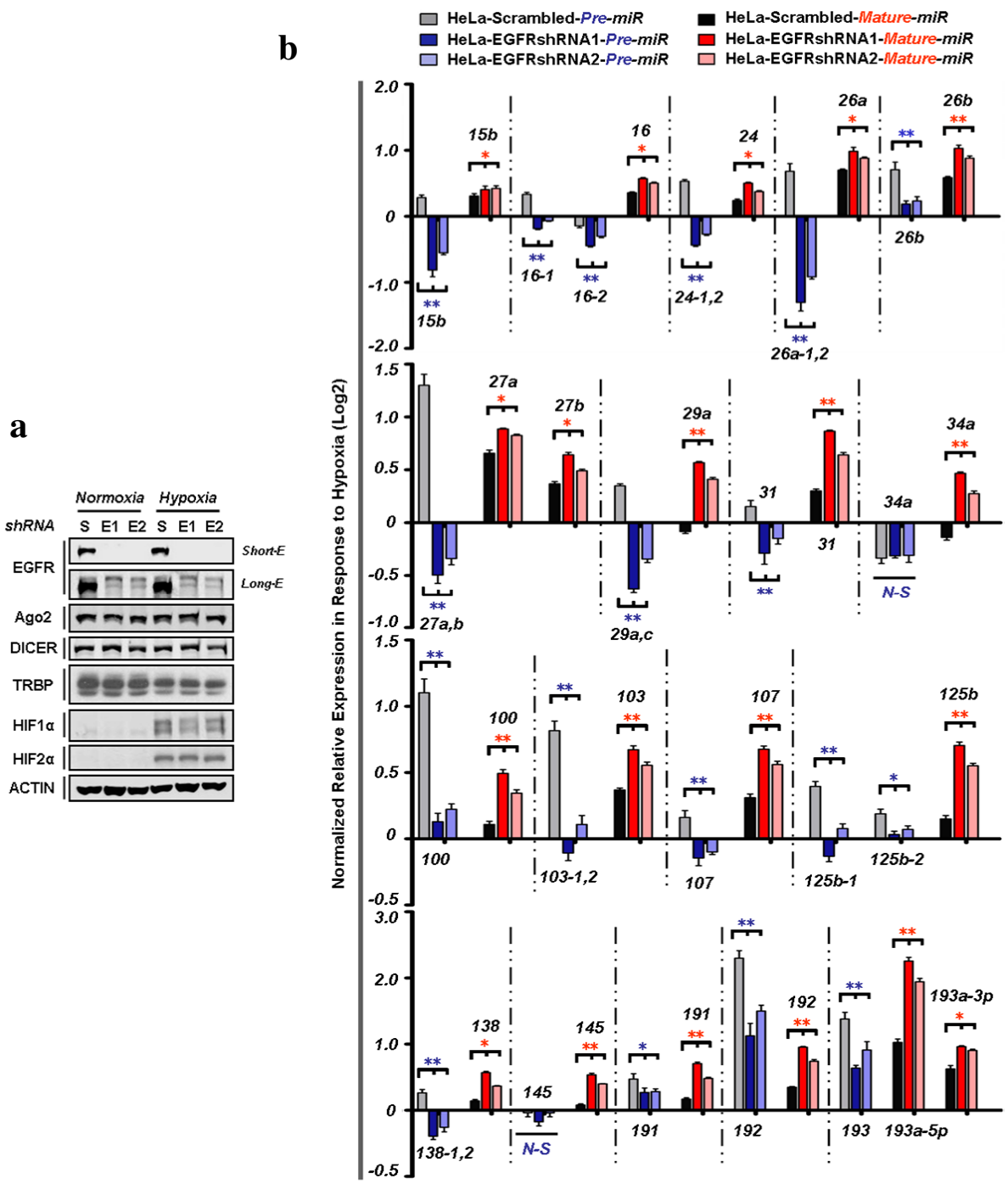

Figure 3-21 EGFR suppresses the maturation of mHESM in response to hypoxia.

Figure 3-21 EGFR suppresses the maturation of mHESM in response to hypoxia.

a, Western blot analysis of HeLa stable clones expressing scrambled control or EGFR shRNAs (E1, E2) that cultured under normoxia or hypoxia for 24 hr, as indicated. S, scrambled control; E1, EGFR shRNA-E1; E2, EGFR shRNA-E2. HIF1α and HIF2α were used as positive control for cell hypoxic response. β-actin was used as protein loading control. **b,** Normalized relative expression (Log2) of pre- and mature miRNAs in HeLa stable clones (verified in panel **a**) in response to hypoxia. Statistical analysis was carried out using Student's *t* test. EGFR knockdown cells (E1 and E2) were considered as one group to compare with the scrambled control. Data are shown as mean ± s.d., n=4, *N-S* indicates $P>0.05$, * indicates $P<0.05$, **indicates $P<0.01$.

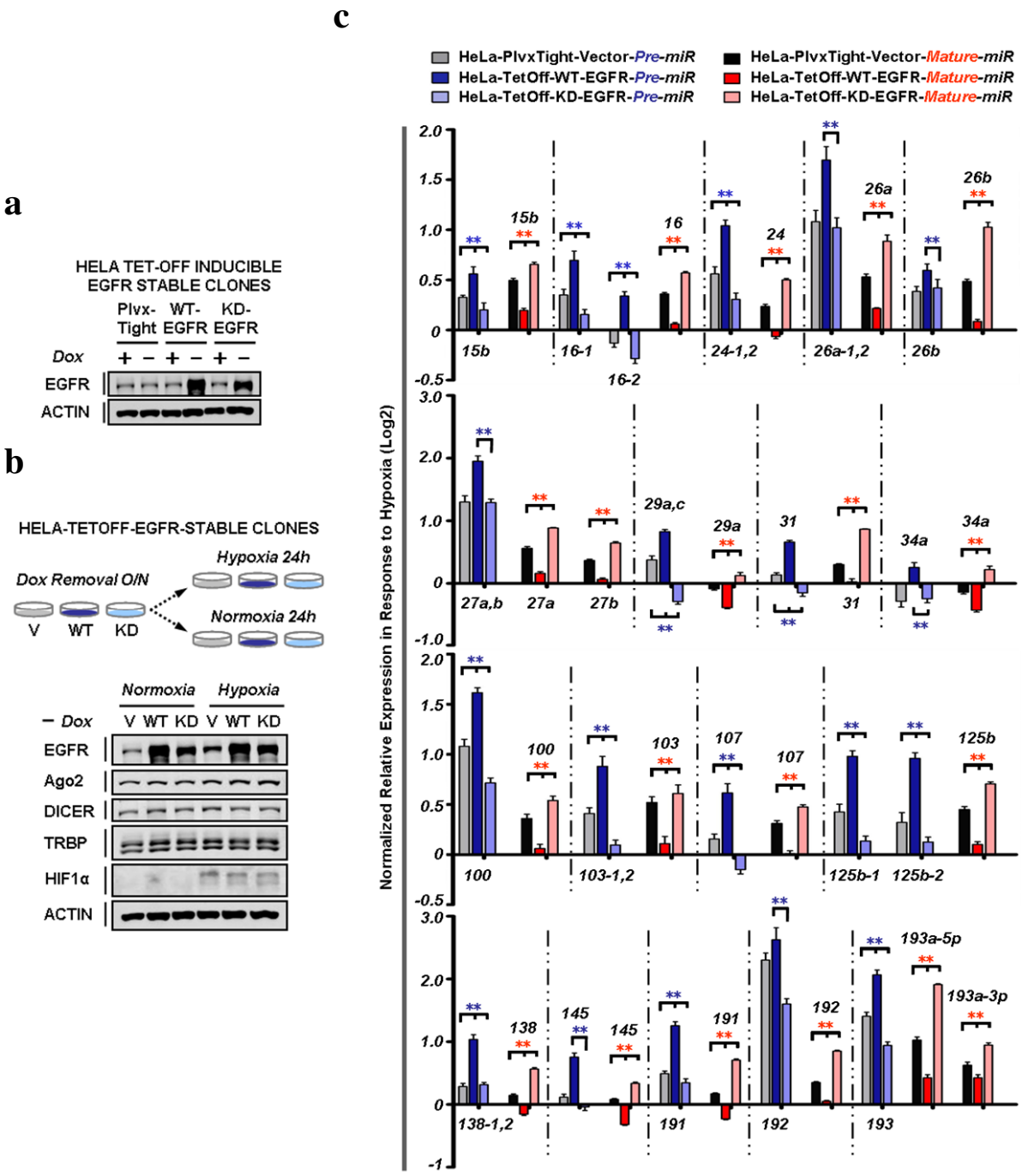

Figure 3-22 EGFR kinase activity is essential for EGFR-suppressed miRNA maturation.

Figure 3-22. EGFR kinase activity is essential for EGFR-suppressed miRNA maturation.

a, HeLa TetOff-inducible stable clones expressing vector control, wild-type (WT) or kinase-dead (KD) EGFR were generated and validated by Western blot. **b,** Western blot analysis of HeLa TetOff-inducible EGFR stable clones that cultured under normoxia or hypoxia for 24 hr after doxycycline removal O/N. HIF1α was used as positive control for cell hypoxic response. β-actin was used as protein loading control. **c,** Normalized relative expression (Log2) of pre- and mature miRNAs in HeLa TetOff-inducible EGFR stable clones (verified in panel **b**) in response to hypoxia. Statistical analysis was carried out using ANOVA or student's *t* test (comparing WT and KD EGFR). Data are shown as mean ± s.d., *n*=4. **indicates P<0.01.

3.3 EGFR phosphorylates Ago2 at Y393 to suppress the maturation of long-loop mHESM in response to hypoxia

3.3.1 Ago2 is tyrosine phosphorylated by EGFR at Y393 in response to hypoxia

To investigate whether Ago2 is a phosphorylation substrate of EGFR, we purified FLAG-tagged Ago2 co-expressed with EGFR and identified one tyrosine phosphorylation site (Fig. 3-23) at a highly conserved residue Y393 (Fig. 3-24) in Ago2. Results from in vitro kinase assay (Fig. 3-25a) further demonstrated Ago2-Y393 as a direct phosphorylation site targeted by EGFR. Mutational analysis suggested that phospho-Y393-Ago2 exists in vivo (Figs. 3-26, 3-27), which was then validated in HeLa TetOff-inducible Ago2 stable clones (Figs. 3-25b, 3-28a) using the polyclonal antibody (p-Y393-Ago2) we generated (Fig. 3-29). Interestingly, hypoxia enhanced Ago2-Y393 phosphorylation (Fig. 3-25b) which in turn reduced Ago2-Dicer/TRBP association (Figs. 3-25b, 3-26, 3-27), suggesting that EGFR is a novel upstream regulator of RISC loading complex.

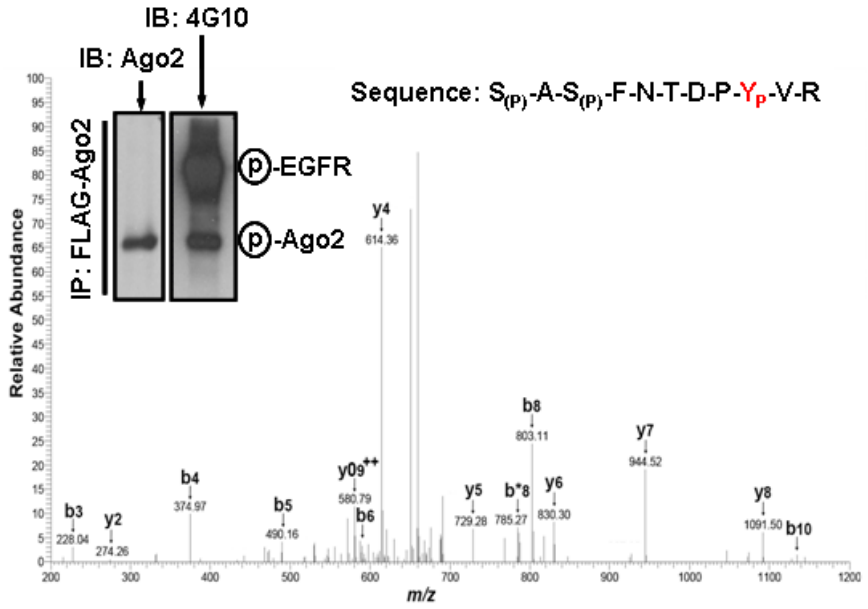

Figure 3-23 Ago2 is tyrosine phosphorylated at residue 393 as identified by mass spectrometric analysis.

Top left, Western blot verification showing the tyrosine phosphorylation of purified Ago2 that co-expressed with EGFR in 293T cells. Tyrosine phosphorylation was detected by 4G10 antibody. Bottom, mass spectrometric analysis of Ago2 identified Tyr393 as the single tyrosine residue that been phosphorylated *in vivo*. This phospho-tyrosine residue has previously been reported (Rudel et al., 2011), but neither the enzyme required for this phosphorylation nor the biological outcomes of Ago2-Y393 phosphorylation has been studied so far.

a

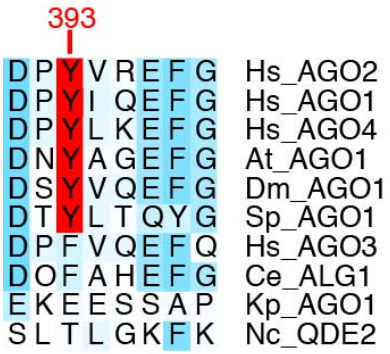

b

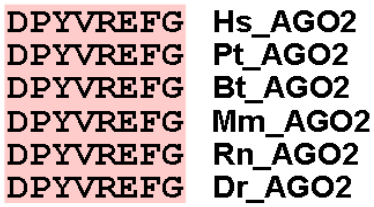

Figure 3-24 Tyr393 of hAgo2 is highly conserved among vertebrates and coexists in hAgo1, hAgo4 but not hAgo3.

a, Sequence alignment of the AGO family around Y393 of hAgo2. Highlighted with blue are well-conserved amino acids (intensity indicates degree of conservation). Hs, *Homo sapiens*; At, *Arabidopsis thaliana*; Dm, *Drosophila melanogaster*; Sp, *Saccharomyces pombe*; Ce, *Caenorhabditis elegans*; Kp, *Kluyveromyces polysporus*; Nc, *Neurospora crassa*. **b,** The adjacent amino acid sequence of hAgo2-Y393 (DPYVREFG) is identical among vertebrates. Hs, *Homo sapiens*; Pt, *Pan troglodytes; Bt, Bos taurus; Mm, Mus musculus; Rn, Rattus norvegicus; Dr, Danio rerio.*

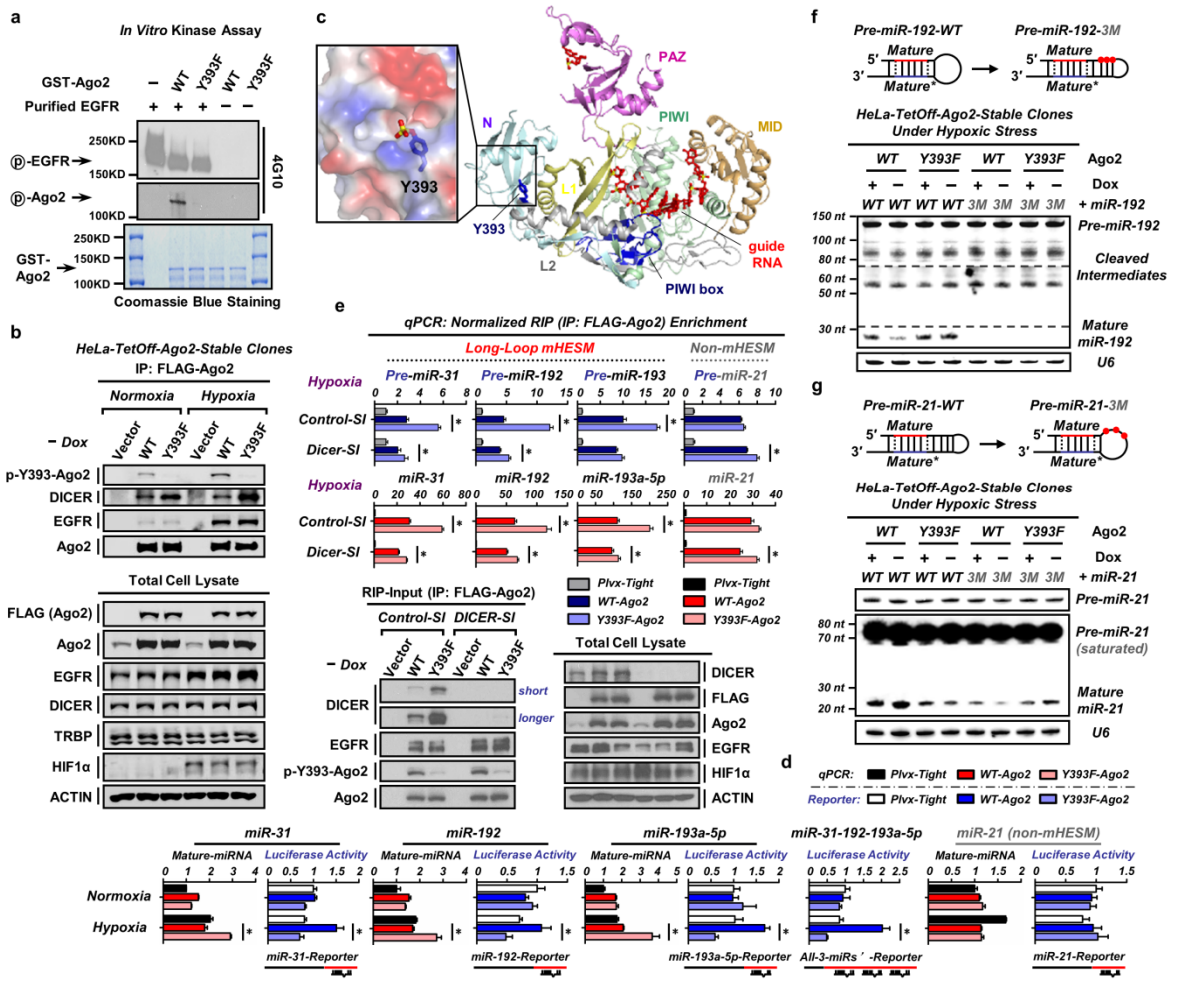

Figure 3-25 EGFR phosphorylates Ago2 at Y393 to suppress the maturation of long-loop mHESM in response to hypoxia.

a, *in vitro* kinase assay detected by 4G10 antibody. **b,** Relative position of Y393 in the structure of hAgo2 with bound guide RNA (Schirle and MacRae, 2012). **c,** IP-Western blot analysis of HeLa TetOff-inducible Ago2 stable clones. **d,** Normalized expression of miRNA and corresponding luciferase activity of miR-reporters, *n*=4. **e,** RIP enrichment of pre- and mature miRNAs, *n*=3. **f** and **g,** Northern blot analysis as indicated. Dashed lines indicate different exposure time. Whole panel data are shown in Figs. 3-35, 3-36. Data represent mean ± s.d.; * indicates P<0.05, *t* test.

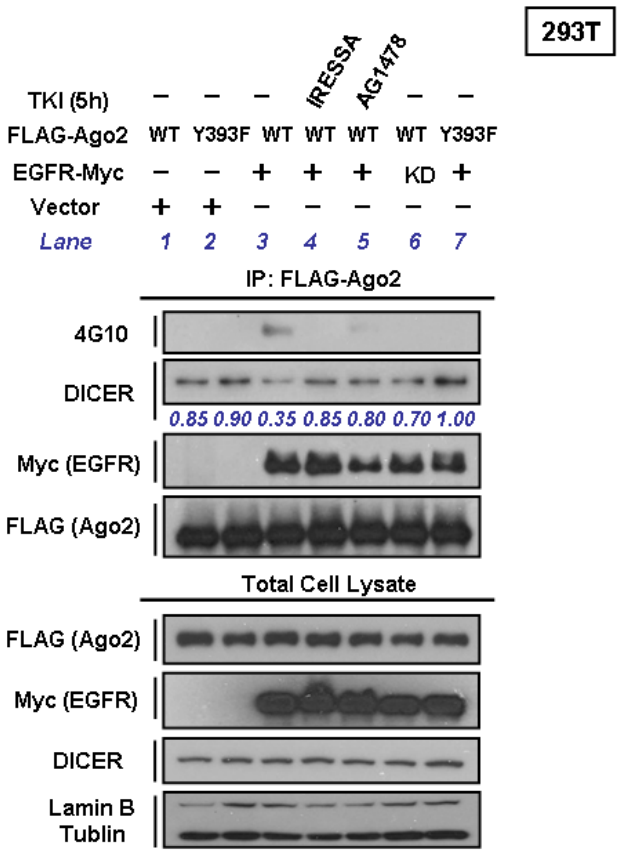

Figure 3-26 Tyr393 of Ago2 is the major phosphorylation site targeted by EGFR *in vivo* and the phosphorylation of this residue reduces Ago2 binding to Dicer.

IP-Western analysis of WT and Y393F Ago2 in 293T cells, as indicated. Expression of Y393F mutant Ago2 or treatment with tyrosine kinase inhibitor (TKI) of EGFR abolished EGFR-mediated tyrosine phosphorylation of Ago2 (Lanes 4, 5, 6, 7 vs. Lane 3), supporting this residue as a target of EGFR. Interestingly, phosphorylation of Ago2 at Y393 reduced its interaction with Dicer, which can be restored by either TKI treatment (Iressa or AG1478) or by expressing the Y393F mutant Ago2 (Lane 3 vs. the other lanes). The quantitation of Dicer that interacts with Ago2 is shown below. Iressa (1 μM), tyrosine kinase inhibitor (also known as gefitinib) used in clinic for targeting EGFR; AG1478 (50 nM), specific EGFR inhibitor (Levitzki and Gazit, 1995) (IC_{50} for selective inhibition of EGFR = 3 nM *in vitro* vs. IC_{50} for targeting HER2-neu and PDGFR >100 μM).

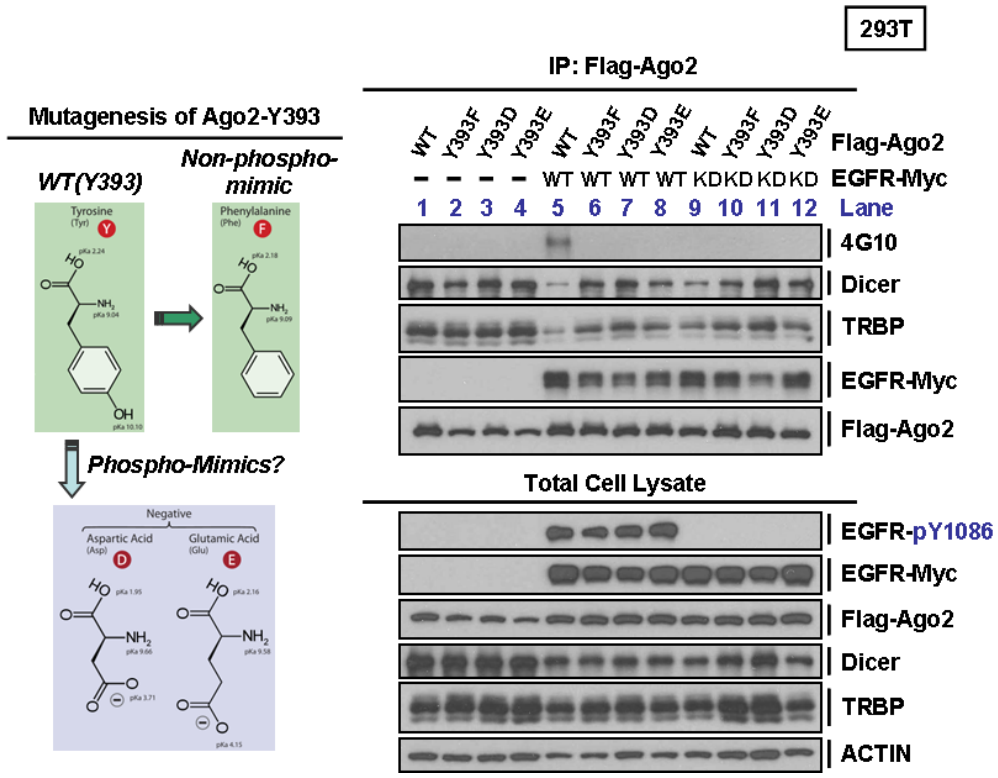

Figure 3-27 Ago2-Y393 phosphorylation reduces Ago2-Dicer/TRBP interaction, which however cannot be imitated by Y393D or Y393E mutant Ago2.

Left, Ago2 Y393 was mutated to phospho- and non-phospho-mimics. Right, IP-Western analysis of WT, Y393F, Y393D and Y393E Ago2 in 293T cells, as indicated. WT Ago2 was tyrosine phosphorylated by WT but not KD EGFR (Lane 5 vs. Lane 9). Mutating Tyr393 into phenylalanine (F) or aspartic acid (Y393D) or glutamic acid (Y393E) abolished EGFR mediated tyrosine phosphorylation of Ago2 (Lanes 6, 7, 8 vs. Lane 5). Ago2-Y393 phosphorylation reduced its binding with Dicer and TRBP (Lane 5 vs. Lanes 1, 2, 6, 9, 10). Y393D and Y393E mutants showed similar property as Y393F mutant, suggesting that both aspartic acid and glutamic acid cannot fully imitate phosphorylated Y393 in Ago2. The phenomenon that phospho-tyrosine cannot be mimicked by aspartic acid and glutamic acid was also reported previously (Anthis et al., 2009).

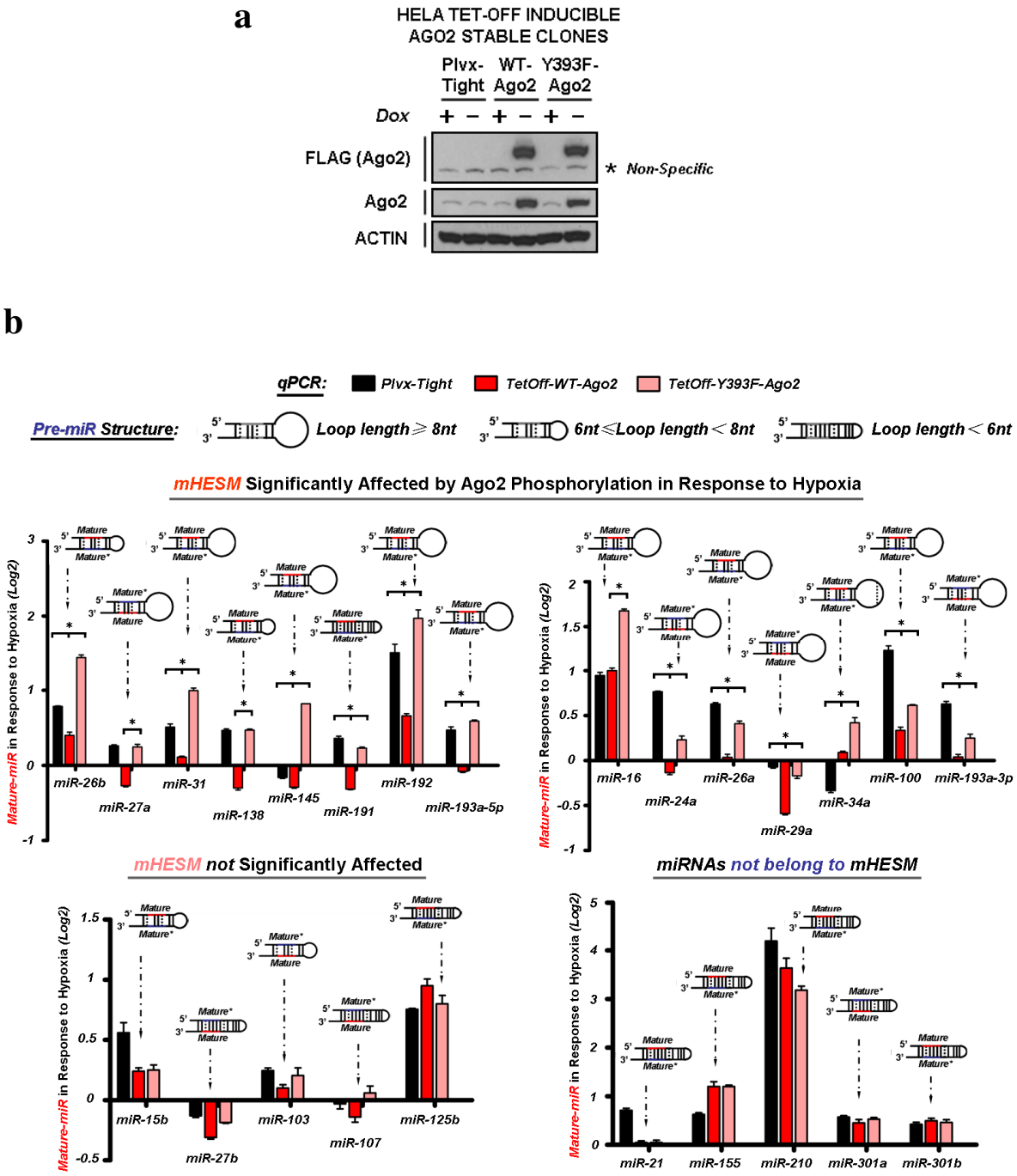

Figure 3-28 Most mHESM regulated by Ago2-Y393 phosphorylation in response to hypoxia contain long-loop structure in their precursors.

Figure 3-28. Most mHESM regulated by Ago2-Y393 phosphorylation in response to hypoxia contain long-loop structure in their precursors.

a, HeLa TetOff-inducible stable clones expressing vector control, WT or Y393F Ago2 were generated and verified by Western blot, as indicated. * indicates the non-specific signal recognized by FLAG antibody. **b,** Normalized relative expression (Log2) of mature miRNAs in HeLa TetOff-inducible Ago2 stable clones (as verified in Fig. 3-25b) in response to hypoxia. The structures of corresponding miRNA precursors were shown in the diagram. Statistical analysis was carried out using student's *t* test (comparing WT Ago2 or vector control to Y393F Ago2). Data are shown as mean ± s.d., *n*=4, *indicates P<0.05.

a

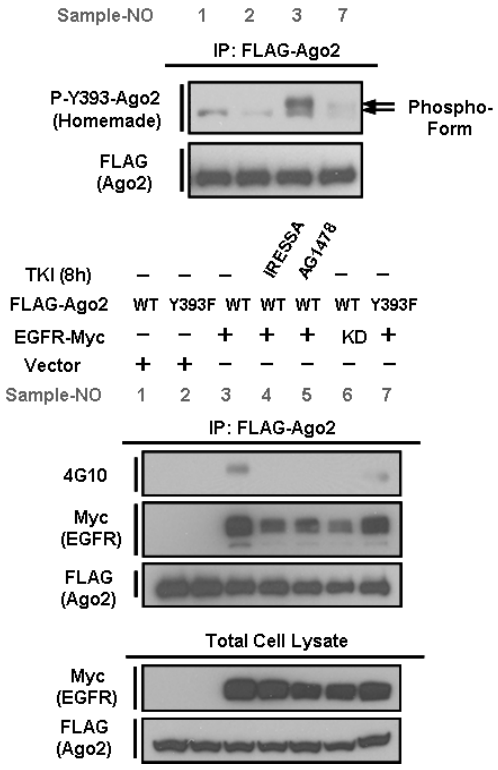

Figure 3-29 Characterization of mouse polyclonal antibody against phospho-Y393-Ago2 (homemade).

a, Top, anti-FLAG immunoprecipitates (Sample-NO.1, 2, 3, 7) were blotted with homemade antibody against p-Y393-Ago2. Bottom, Western blot analysis of corresponding anti-FLAG immunoprecipitates and total cell lysates from 293T cells.

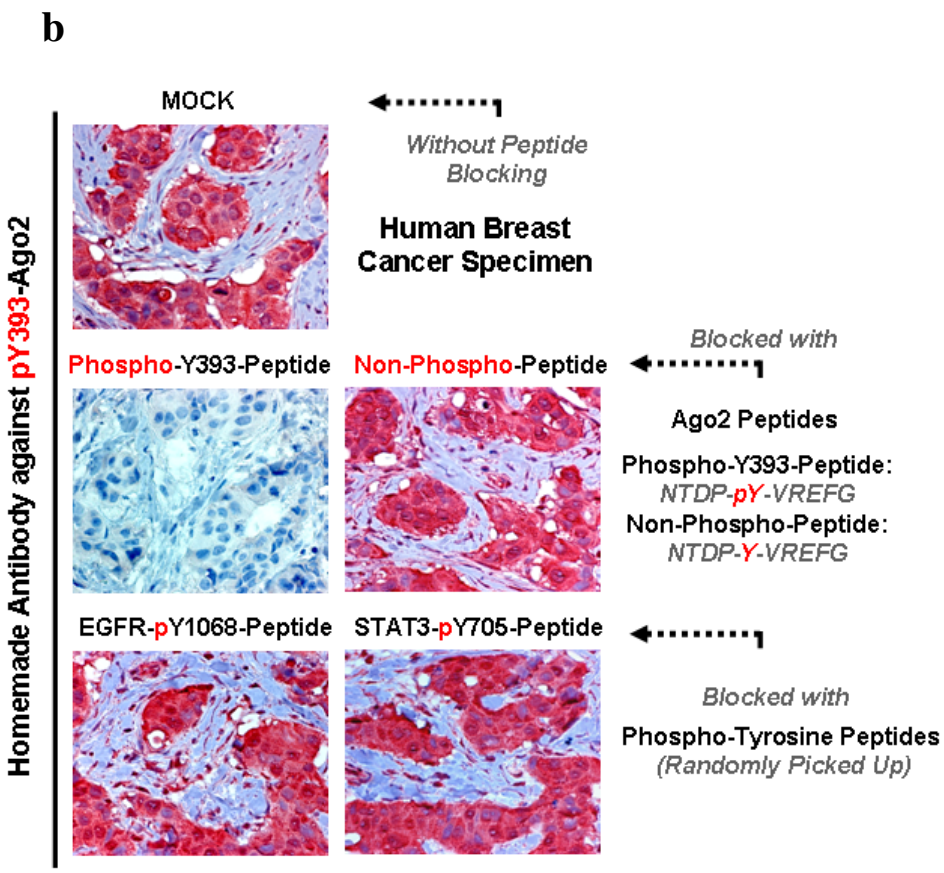

Figure 3-29 Characterization of mouse polyclonal antibody against phospho-Y393-Ago2 (homemade).

b, Peptide competition assay for p-Y393-Ago2 antibody by immunohistochemical staining. Human breast tumor sample showing high expression of EGFR (data not shown) also showed positively staining of p-Y393-Ago2 using the homemade antibody. Importantly, the recognition capacity of this antibody can be completely blocked with phospho-Y393-Ago2-peptide but not the control non-phospho-Ago2-peptide or the other randomly chosen phospho-tyrosine peptides, demonstrating its fidelity in IHC staining for detecting Ago2-Y393 phosphorylation *in vivo*.

3.3.2 Structural analysis of human Ago2

To gain more insight into phospho-Y393-Ago2, we analyzed the crystal structure of human Ago2 (Schirle and MacRae, 2012) (hAgo2) and found that the side chain of Y393 protrudes from an exterior orientation towards a cavity between the N domain, an interaction surface for EGFR, and the linker L2 (Fig. 3-25c). Y393 is exposed to solvent and some distance from both the guide RNA-binding channel and the PIWI box, a Dicer-binding region of hAgo2 (Tahbaz et al., 2004). Given that Dicer is a large protein, it is conceivable that Dicer could still interact with both the Dicer-specific PIWI box and Y393 due to their location on the same surface of hAgo2 (Fig. 3-25c). If so, phosphorylation of Y393 could inhibit this interaction as previously observed (Figs. 3-25b, 3-26, and 3-27).

3.3.3 EGFR-mediated phosphorylation of Ago2 at Y393 suppresses miRNA maturation in response to hypoxia

The recruitment of Ago2 to Dicer is critical for loading miRNA precursors onto RISC loading complex (Maniataki and Mourelatos, 2005) and facilitating miRNA maturation (Chendrimada et al., 2005; Maniataki and Mourelatos, 2005) from pre- to mature miRNAs. We therefore investigated whether Ago2-Y393 phosphorylation plays a role in EGFR-suppressed miRNA maturation in response to hypoxia. Compared with Ago2-Y393F mutant, induction of Ago2-WT significantly reduced the expression of most mHESM but not those that do not belong to the mHESM cluster (defined as non-mHESM) in response to hypoxia (Fig. 3-28b). Structural analysis of miRNA precursors determined that a majority of mHESM regulated by p-Y393-Ago2 contained a long-loop structure, which is not present in non-mHESM (Fig. 3-28b). Interestingly, mHESM that were not significantly affected by Ago2-Y393 phosphorylation also had short-loop structures in their precursors similar to

what we found in non-mHESM (Fig. 3-28b), suggesting the importance of long-loop structure in regulation specificity. Similar expression patterns of mature miRNAs were also observed in other paired stable clones (Figs. 3-30, 3-31). Silencing endogenous EGFR significantly diminished the expression difference of long-loop mHESM present in miR-31, miR-192, and miR-193a-5p between Ago2-WT and Ago2-Y393F mutant cells (Fig. 3-32). The levels of their primary transcripts were reduced by EGFR knockdown under hypoxia but similar between WT and Y393F Ago2 cells (Fig. 3-32b). This evidence supports phospho-Y393-Ago2-suppressed miRNA maturation as a downstream event of EGFR under hypoxia. Moreover, decreased expression of long-loop mHESM as shown in miR-31, miR-192 and miR-193a-5p under hypoxia resulted in the de-repression of miRNA targets (Fig. 3-25d) as measured by miR-Reporter luciferase activity. In contrast, the expression of miR-21 (non-mHESM) and repression of its target were not significantly affected by Ago2-Y393 phosphorylation (Fig. 3-25d). These results underline the functional importance of p-Y393-Ago2-mediated suppression of long-loop mHESM under hypoxia.

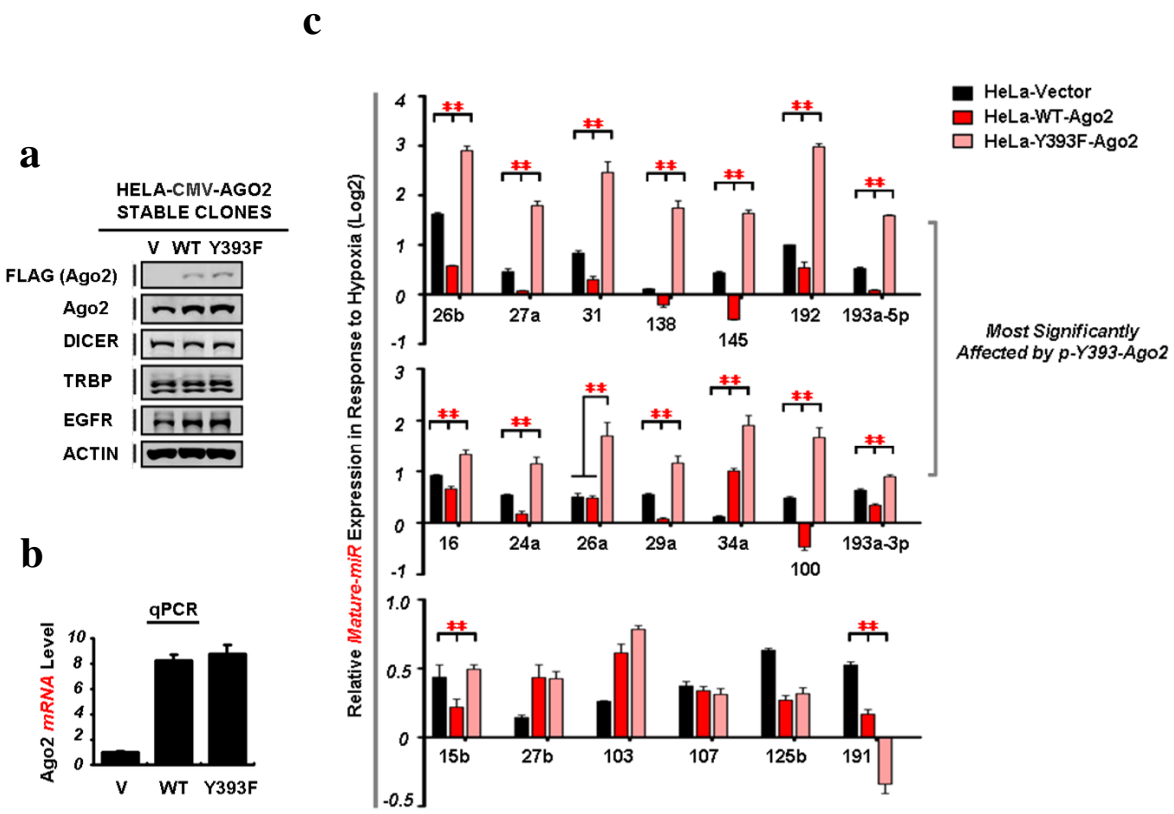

Figure 3-30 Ago2-Y393 phosphorylation reduces the production of most mHESM in HeLa non-inducible stable transfectants in response to hypoxia.

a, Western blot verification for non-inducible Ago2 stable clones generated in HeLa cell line, as indicated. **b,** qPCR verification for the mRNA expression of WT and Y393F Ago2 in HeLa non-inducible stable transfectants. β-actin mRNA was used as internal control. **c,** Normalized relative expression (Log2) of mature mHESM in HeLa non-inducible Ago2 stable clones, as verified in panels **a** and **b**, in response to hypoxia. Statistical analysis was carried out using student's *t* test (comparing WT- and Mut-Ago2). Data are shown as mean ± s.d., *n*=4, **indicates P<0.01.

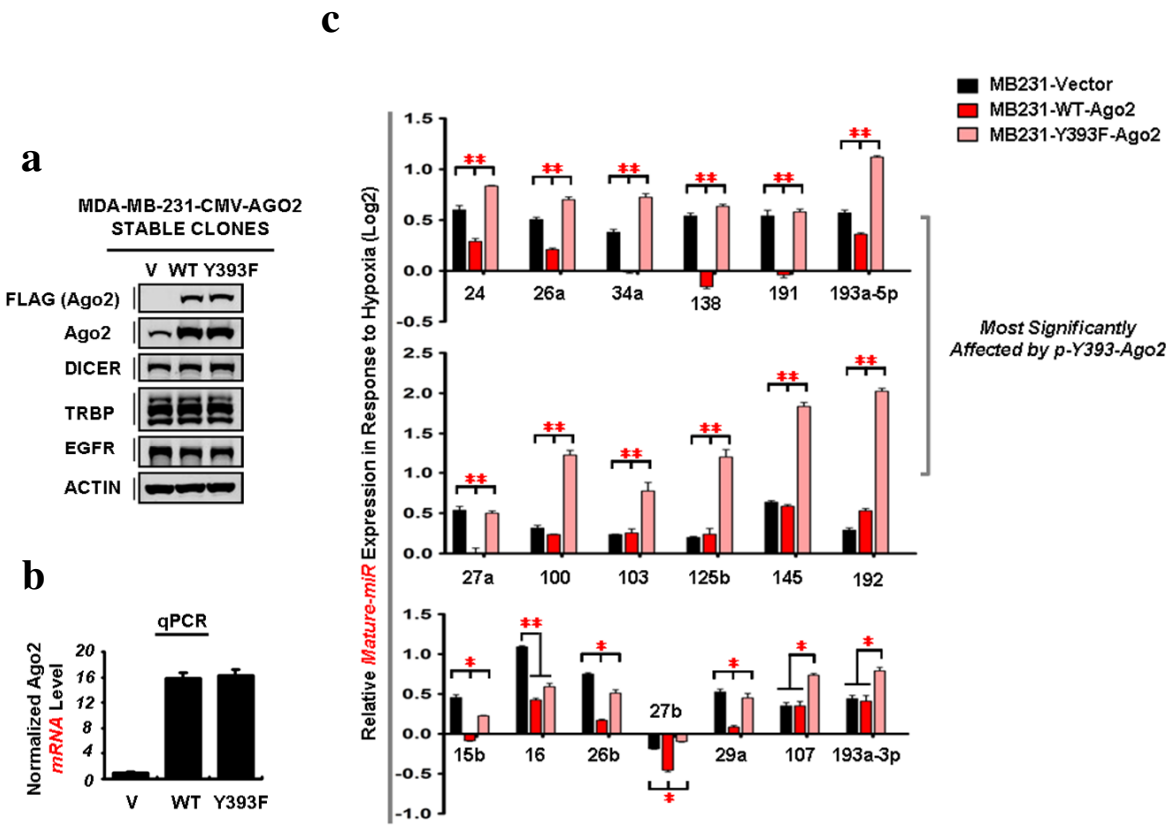

Figure 3-31 Ago2-Y393 phosphorylation suppresses the production of most mHESM in MDA-MB-231 stable transfectants in response to hypoxia.

a, Western blot verification for Ago2 stable clones generated in MDA-MB-231 cell line, as indicated. **b,** qPCR verification for the mRNA expression of WT and Y393F Ago2 in MDA-MB-231 stable transfectants. β-actin mRNA was used as internal control. **c,** Normalized relative expression (Log2) of mature mHESM in MDA-MB-231 Ago2 stable clones, as verified in panels **a** and **b**, in response to hypoxia. Note: miR-31 was not expressed in MDA-MB-231 cell line. Statistical analysis was carried out using student's *t* test (comparing WT and Y393F Ago2). Data are shown as mean ± s.d., *n*=4, *indicates P<0.05, **indicates P<0.01.

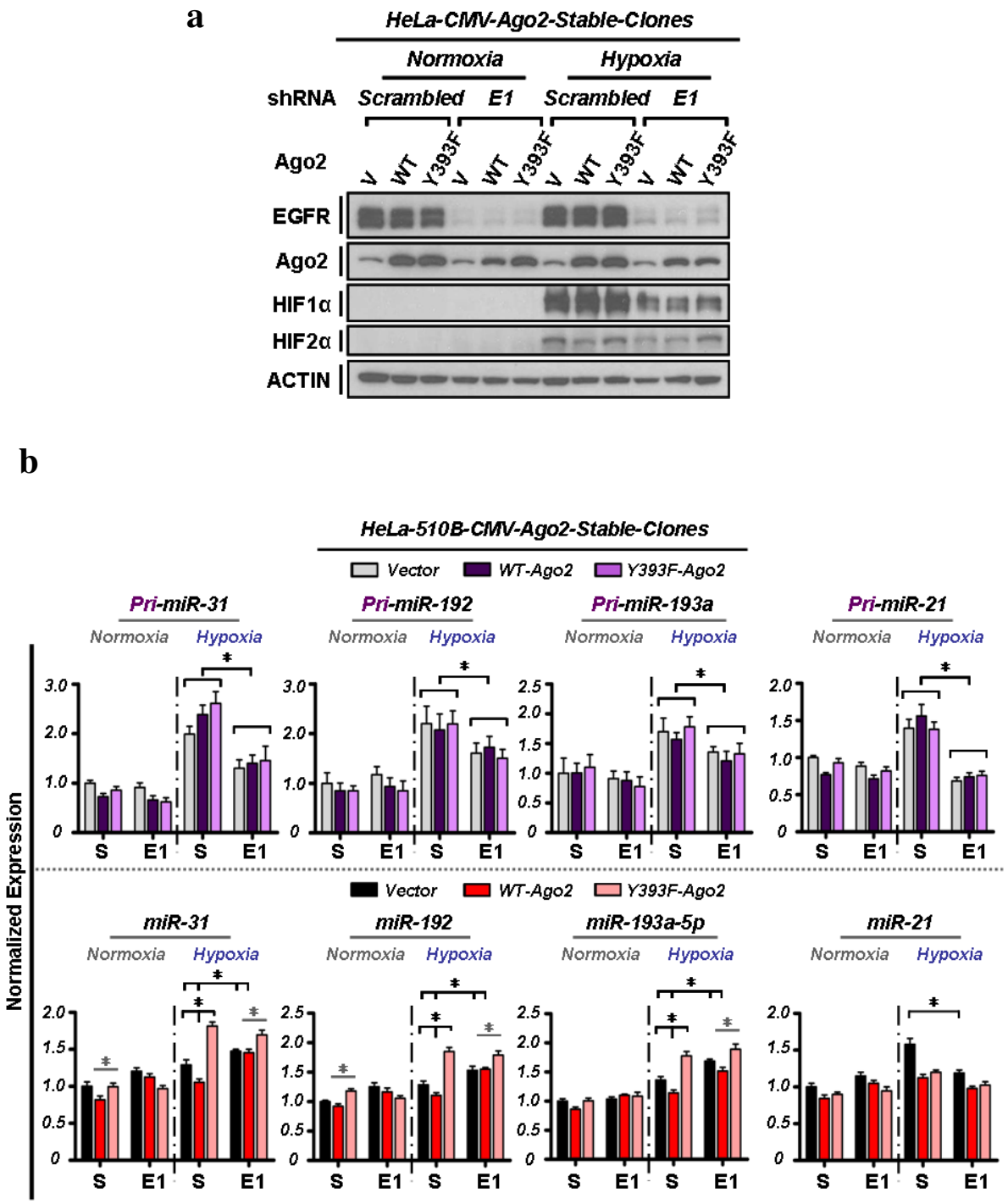

Figure 3-32 EGFR is the tyrosine kinase that suppresses the processing of long-loop mHESM through phosphorylation of Ago2 at Y393 in response to hypoxia.

Figure 3-32. EGFR is the tyrosine kinase that suppresses the processing of long-loop mHESM through phosphorylation of Ago2 at Y393 in response to hypoxia.

a, Western blot analysis of HeLa CMV Ago2 stable clones expressing scrambled control or EGFR shRNA-E1 that cultured under normoxia or hypoxia for 24 hr. HIF1α and HIF2α were used as positive control for cell hypoxic response. β-actin was used as protein loading control. **b,** Top, normalized expression of pri-miRNAs in HeLa CMV Ago2 stable clones expressing scrambled control or EGFR shRNA-E1, as verified in panel **a**, in response to hypoxia. Bottom, corresponding normalized expression of mature miR-31, miR-192, miR-193a-5p (long-loop mHESM) and miR-21 (non-mHESM). Silencing EGFR suppressed the expression of pri-miR-31, pri-miR-192 and pri-miR-193a (long-loop mHESM representatives) to a similar level among those stable transfectants under hypoxia; however, it enhanced the level of corresponding mature miRNAs in vector control and WT but not Y393F Ago2 cells. The expression of pri- and mature miR-21 (non-mHESM) was decreased by EGFR knockdown, but was similar between WT and Y393F Ago2 stable clones. These results indicate that increased expression of mature long-loop mHESM in vector control and WT Ago2 cells after EGFR knockdown was not caused by transcriptional upregulation but instead de-repression of miRNA maturation. S, scrambled control; E1, EGFR shRNA-E1. Statistical analysis was carried out using Student's *t* test and the significance shown in the diagram was based on the difference between vector control or WT and Y393F Ago2, or between scrambled control and EGFR knockdown groups, as indicated. Data are shown as mean ± s.d., n=4, * indicates $P<0.05$.

3.3.4 Y393-phosphorylation of Ago2 attenuates its interaction with Dicer resulting in suppressed miRNA maturation and reduced RISC activity

The long-loop structure in miRNA precursors is a known characteristic of Dicer's preference (Tsutsumi et al., 2011). Reduction in Dicer-Ago2 interaction resulted in less loading of the precursors of miR-31, miR-192 and miR-193a-5p (long-loop mHESM), but not miR-21 (short-loop non-mHESM), onto p-Y393-Ago2 under hypoxia (Fig. 3-33). To examine the functional relevance of decreased Dicer-pAgo2 association, we knocked down Dicer in HeLa TetOff-inducible Ago2 stable clones (Figs. 3-25e, 3-34a,b) and found the differences between WT and Y393F Ago2 in miRNA precursor loading (Fig. 3-25e) and mature miRNA expression (Fig. 3-34c) were significantly diminished. These results suggest that the maturation of long-loop mHESM is suppressed by Ago2-Y393 phosphorylation through Dicer. Moreover, Y393F Ago2 was capable of loading more mature mHESM (Fig. 3-25e), which is consistent with its enhanced RISC activity as indicated by luciferase reporter assay (Fig. 3-25d). However, the mature miRNA loading difference between WT and Y393F Ago2 was Dicer-dependent (Fig. 3-25e), and similar to what we observed in mature miRNA expression (Fig. 3-34c). These data suggest that Ago2-Y393 phosphorylation decreases Dicer-Ago2 interaction along with reduced miRNA precursor loading, which consequently suppresses the maturation of long-loop mHESM and decreases the loading of corresponding mature miRNAs onto RISC under hypoxia.

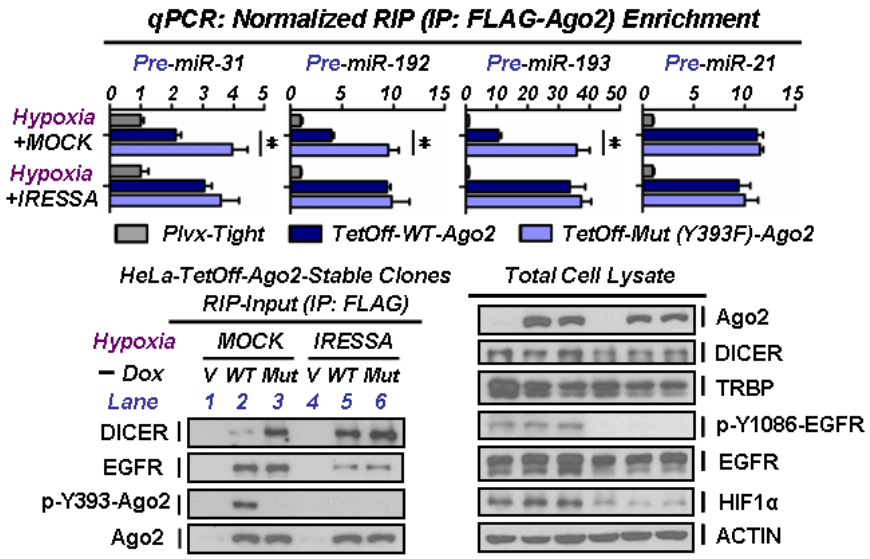

Figure 3-33 The precursors of long-loop mHESM as shown in pre-miR-31, pre-miR-192 and pre-miR-193 but not pre-miR-21 (non-mHESM) were less loaded onto p-Y393-Ago2 under hypoxia.

Top, qRT-PCR showing the loading difference between WT and Y393F mutant Ago2 in long-loop mHESM precursors was significantly diminished by TKi (Iressa) treatment under hypoxia. RNA was extracted from anti-FLAG immunoprecipitates in HeLa TetOff-inducible Ago2 stable clones that cultured under hypoxia treated with Mock (DMSO) or Iressa (1 μM) for 24 hr as indicated. Data were normalized to each corresponding negative control (anti-FLAG immunoprecipitate from HeLa TetOff Plvx-Tight (vector control) stable transfectant cultured under hypoxia). Statistical analysis was carried out using Student's *t* test and data are shown as mean ± s.d., *n*=3, * indicates $P<0.05$. Bottom, IP-western control for RIP (RNA-binding protein immunoprecipitation) assay. p-Y1086-EGFR was used as an indicator for the inhibitory efficacy of Iressa treatment. HIF1α was used as a positive control for cell hypoxic response. β-actin was used as protein loading control.

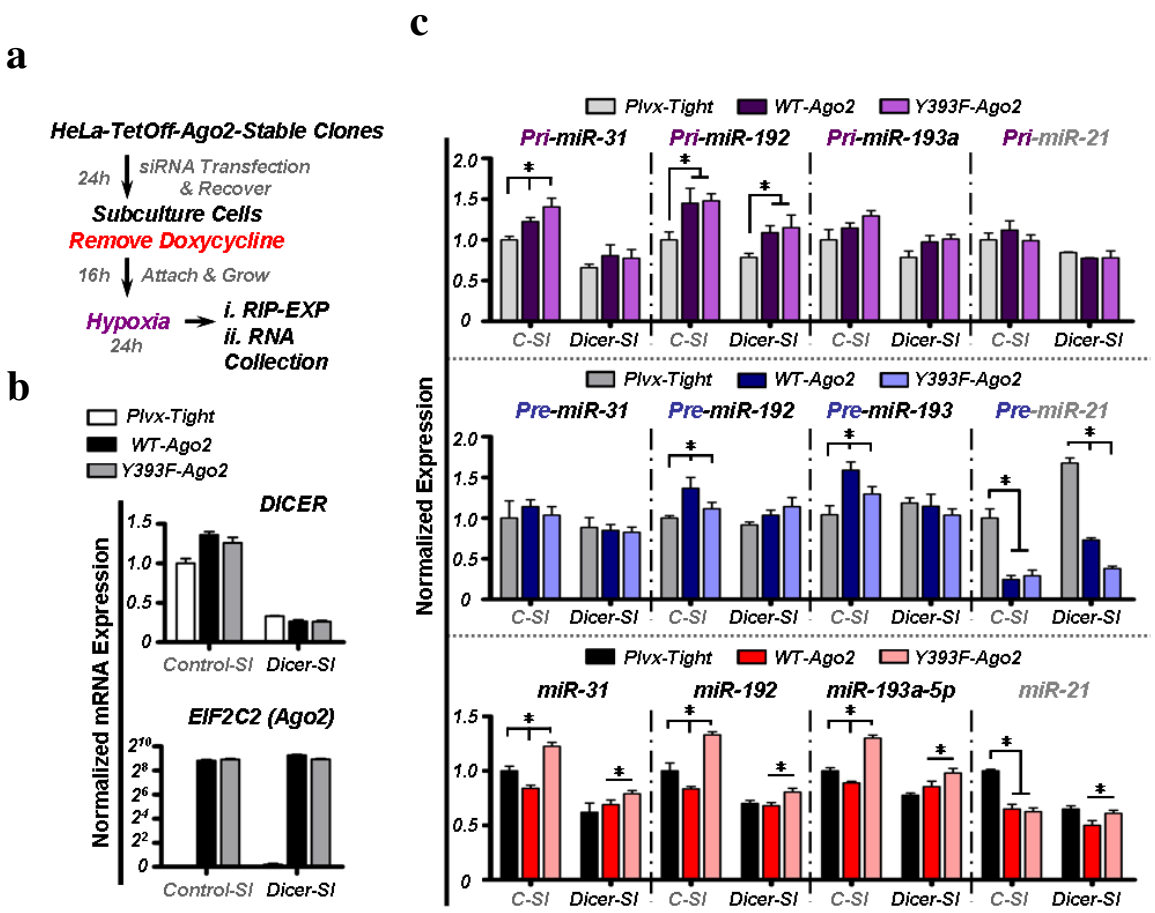

Figure 3-34 The maturation of long-loop mHESM was suppressed by Ago2-Y393 phosphorylation through Dicer.

a, Experimental flow chat. **b,** qPCR verification for the mRNA expression of Dicer and Ago2 in HeLa TetOff-inducible Ago2 stable clones expressing control siRNA pool or Dicer siRNA pool (Dharmacon, On-Target Plus siRNA) that were cultured under hypoxia for 24h, as indicated in flow chat **a**. β-actin mRNA was used as internal control. **c,** Normalized expression of mature miR-31, miR-192, miR-193a-5p (long-loop mHESM) and miR-21 (non-mHESM) as well as their precursors and primary transcripts in HeLa TetOff-inducible Ago2 stable clones expressing control siRNA pool or Dicer siRNA pool that were cultured under hypoxia for 24h, as indicated in flow chat **a**. Statistical analysis was carried out using student's *t* test (comparing vector control or WT to Y393F Ago2). Data are shown as mean ± s.d., *n*=3, *indicates P<0.05.

3.3.5 A long-loop structure in pre-miRNA confers regulation specificity

To demonstrate that the long-loop structure of pre-miRNAs indeed serves as one of the determinants that distinguish mHESM regulated by p-Y393-Ago2 from the others, we mutated pre-miR-192-WT (long-loop) into pre-miR-192-3M (short-loop) and stably expressed them in HeLa TetOff-inducible Ago2 stable clones (top, Fig. 3-25f). Compared with Ago2-Y393F mutant, induction of Ago2-WT attenuated the maturation of pre-miR-192-WT but not pre-miR-192-3M, which virtually lost its processing efficacy without the long-loop structure (Figs. 3-25f, 3-35). Conversely, Ago2-WT was able to suppress pre-miR-21-3M with a regenerated long-loop structure (Figs. 3-25g, 3-36) that is not present in miR-21-WT (Fig. 3-25g, 3-37). These results support a long-loop-dependent mechanism by which p-Y393-Ago2 confers regulation specificity on miRNA maturation.

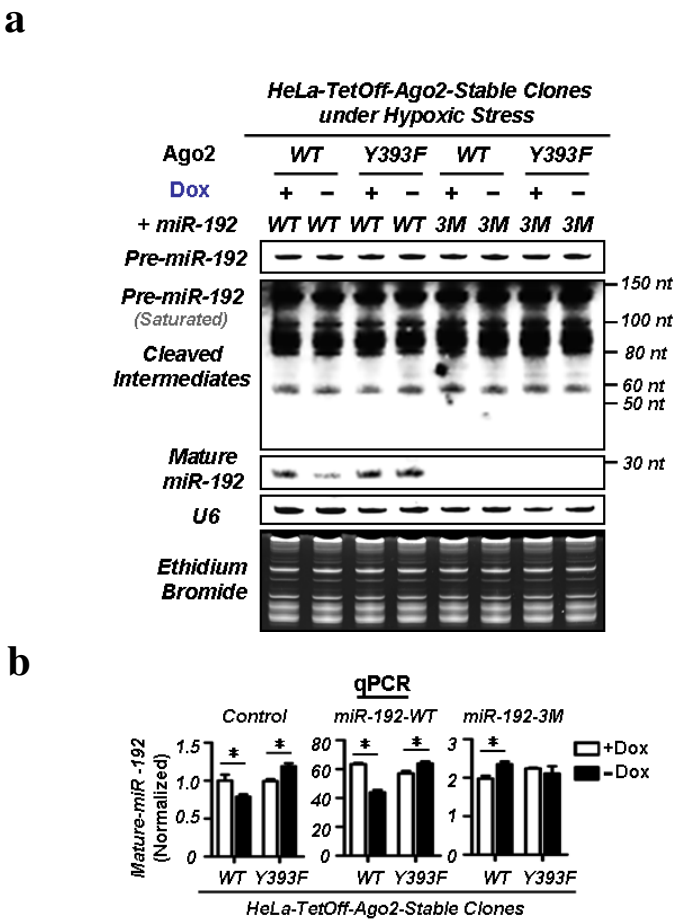

Figure 3-35 The long-loop structure in pre-miR-192 (long-loop mHESM) is required for p-Y393-Ago2-suppressed maturation under hypoxia.

a, Pre-miR-192-WT (long-loop) and pre-miR-192-3M (3 nucleotides were mutated, short-loop) were stably expressed in HeLa TetOff-inducible Ago2 stable clones. Total RNA was extracted from the stable transfectants as indicated and subjected to Northern Blot analysis. The detected mature miR-192 signal was too weak compared with the precursors; therefore, data was shown in different exposure time. **b,** Corresponding qPCR analysis. Control, stable expression of vector control; miR-192-WT, stable expression of pre-miR-192-WT; miR-192-3M, stable expression of pre-miR-192-3M in HeLa TetOff-inducible Ago2 stable clones. All the data were first normalized based on U6 internal control and then to the control group (HeLa TetOff WT Ago2, expressing vector control with doxycycline treatment). Statistical analysis was carried out using Student's t test and data are shown as mean ± s.d., *n*=3, * indicates P<0.05.

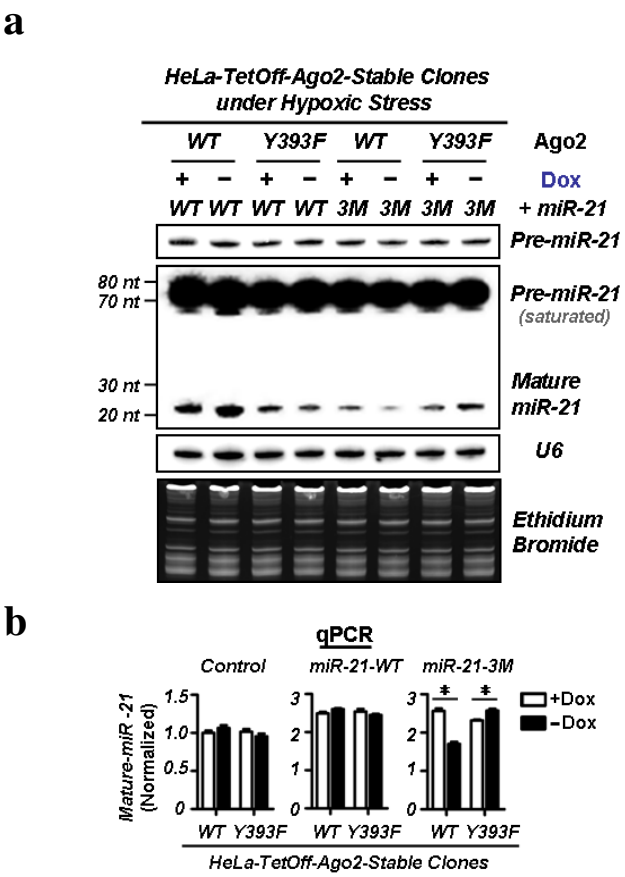

Figure 3-36 Regeneration of a long-loop structure in pre-miR-21-3M renders it to be suppressed by Ago2-Y393 phosphorylation under hypoxia.

a, Pre-miR-21-WT (short-loop) and pre-miR-21-3M (3 nucleotides were mutated, long-loop) were stably expressed in HeLa TeOff-inducible Ago2 stable clones. Total RNA was extracted from the stable transfectants as indicated and subjected to Northern Blot analysis. EB staining shows the integrity of RNA samples and U6 was used as RNA loading control. **b,** Corresponding qPCR analysis. Control, stable expression of vector control; miR-21-WT, stable expression of pre-miR-21-WT; miR-21-3M, stable expression of pre-miR-21-3M in HeLa TetOff-inducible Ago2 stable clones. All the data were first normalized based on U6 internal control and then to the control group (HeLa TetOff WT Ago2, expressing vector control with doxycycline treatment). Statistical analysis was carried out using Student's t test and data are shown as mean ± s.d., *n*=3, * indicates P<0.05.

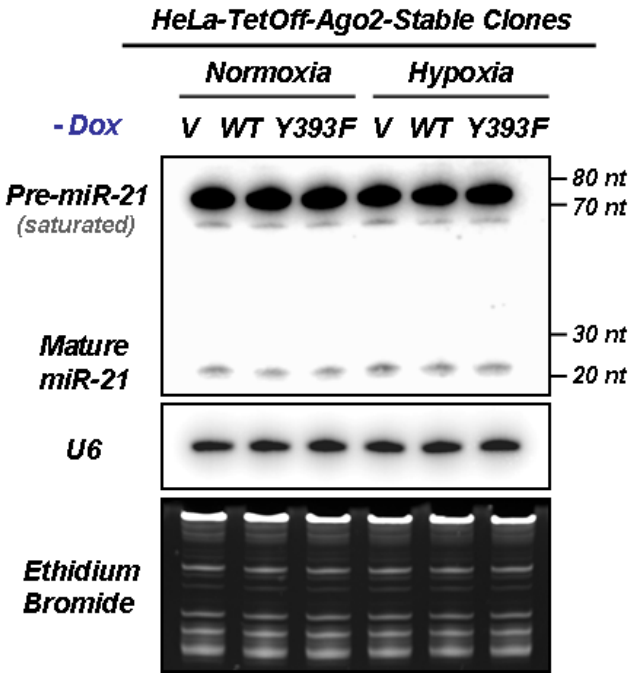

Figure 3-37 The maturation of endogenous miR-21 was not significantly affected by Ago2-Y393 phosphorylation.

Total RNA was extracted from HeLa TetOff-inducible Ago2 stable clones cultured under normoxia or hypoxia for 24 hr and subjected to Northern Blot analysis. V, vector control (Plvx-Tight); WT, WT Ago2; Y393F, Y393F Ago2. EB staining shows the integrity of RNA samples and U6 was used as RNA loading control.

3.4 Functional assessments of Ago2-Y393-phosphorylation under hypoxia

3.4.1 Ago2-Y393-phosphorylation promotes cell survival and enhances cell invasiveness in response to hypoxia

Hypoxic tumor microenvironment promotes metastatic phenotype by facilitating tumor cell survival through evasion of apoptosis (Bertout et al., 2008). Given that most mHESM suppressed by p-Y393-Ago2 are tumor-suppressor-like (Figs. 3-20, 3-28b), we further investigated the pathophysiological role of Ago2 phosphorylation in response to hypoxia. Compared with vector control and Ago2-WT, a higher proportion of cells expressing Ago2-Y393F mutant underwent apoptosis following hypoxia exposure for 3 days (Fig. 3-38), indicating that they were more susceptible to hypoxic stress. Knockdown of endogenous EGFR reduced cell survival and diminished the differences in apoptosis between Ago2-WT and Ago2-Y393F stable transfectants (Fig. 3-39a), suggesting that the phosphorylation of Ago2, rather than the mutation itself, is critical for cell survival under hypoxia. We did not observe any significant changes between Ago2-WT and Ago2-Y393F mutant in cell proliferation rate (Fig. 3-40a,b) or anchorage-independent growth (Fig. 3-40c,d). Interestingly, Ago2-WT but not Ago2-Y393F mutant significantly increased cell migration in response to hypoxia (Figs. 3-39b, 3-41, 3-42). TKI treatment abrogated Ago2-WT-enhanced migration but failed to inhibit Ago2-Y393F mutant cells, indicating that Ago2-Y393 phosphorylation is important for EGFR-enhanced cell migration under hypoxia. Similar results were also obtained from three-dimensional invasion assay with or without TKI treatment (Figs. 3-39c, 3-43). These results demonstrate the functional importance of Ago2-Y393 phosphorylation in blocking cell apoptosis and enhancing cell invasiveness under hypoxia.

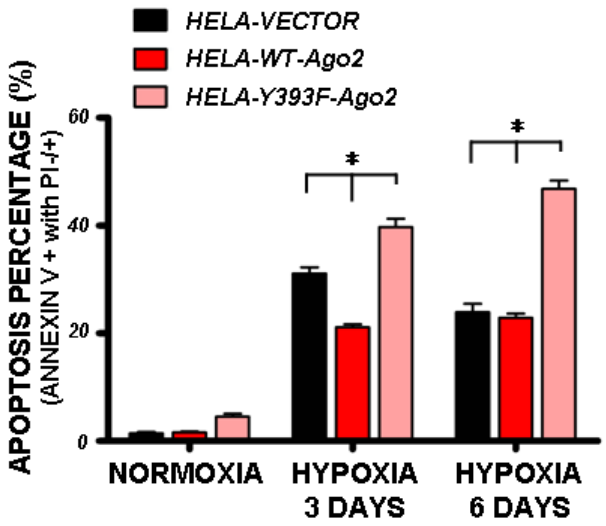

Figure 3-38 Y393F mutant Ago2 cells are more susceptible to apoptosis in response to hypoxia.

Apoptosis analysis of HeLa CMV Ago2 stable clones by FACS analysis. Data are shown as mean ± s.d., *n*=3. * indicates P<0.05.

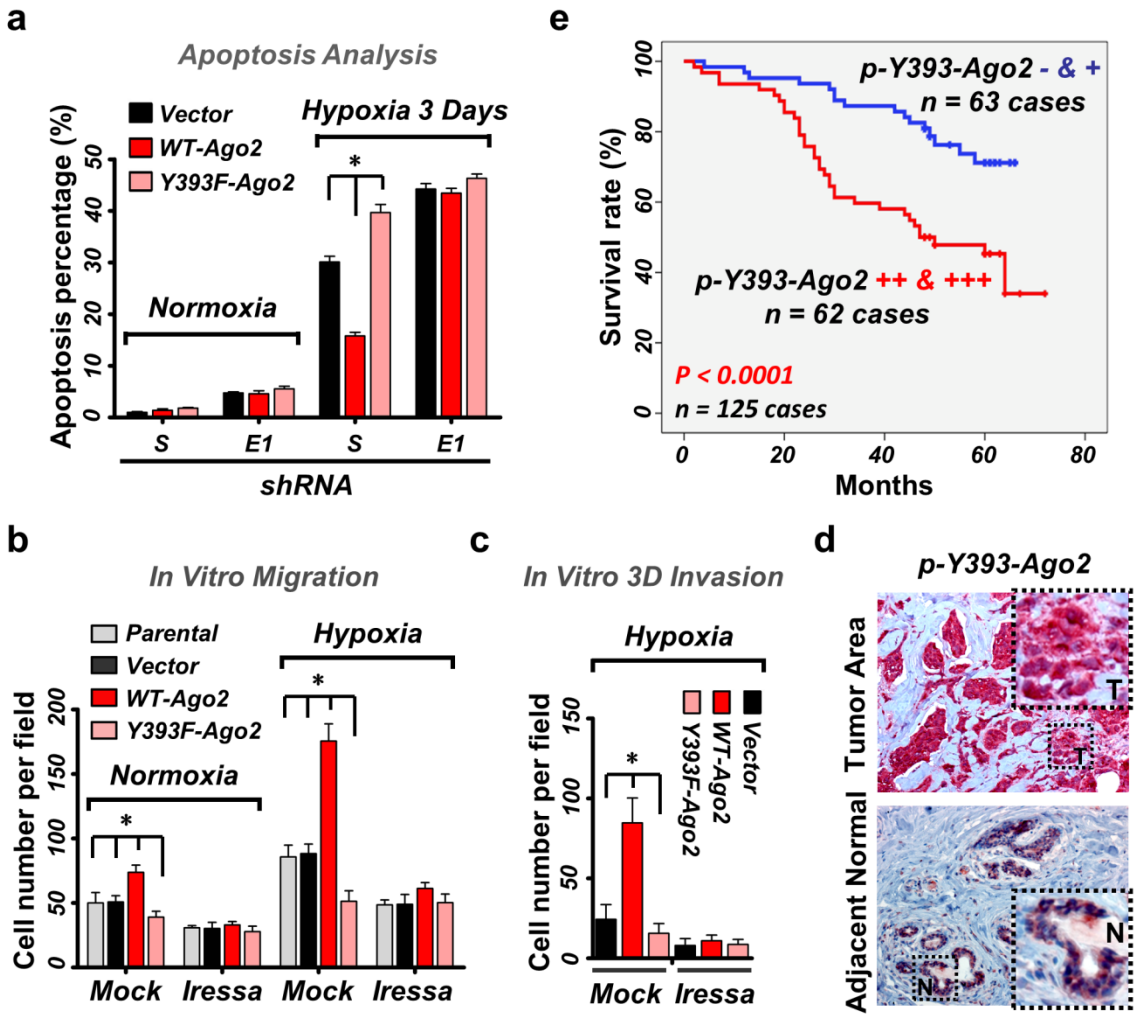

Figure 3-39 Ago2-Y393 phosphorylation mediates EGFR-enhanced cell survival and invasiveness under hypoxia, and significantly correlates with poorer overall survival in breast cancer patients.

a, Cell apoptosis analyzed by FACS, *n*=3. **b,** *In vitro* migration assay. Result was calculated based on five randomly selected fields per membrane in triplicate, *n*=3. **c,** *In vitro* 3-D invasion assay, *n*=5. **d,** Representative IHC images of p-Y393-Ago2 in human breast tumor and its adjacent normal tissue. **e,** Correlation between p-Y393-Ago2 and overall survival in breast cancer patients (*n*=125). P<0.0001, Kaplan-Meier survival analysis. All data represent mean ± s.d.; * indicates P<0.05, *t* test.

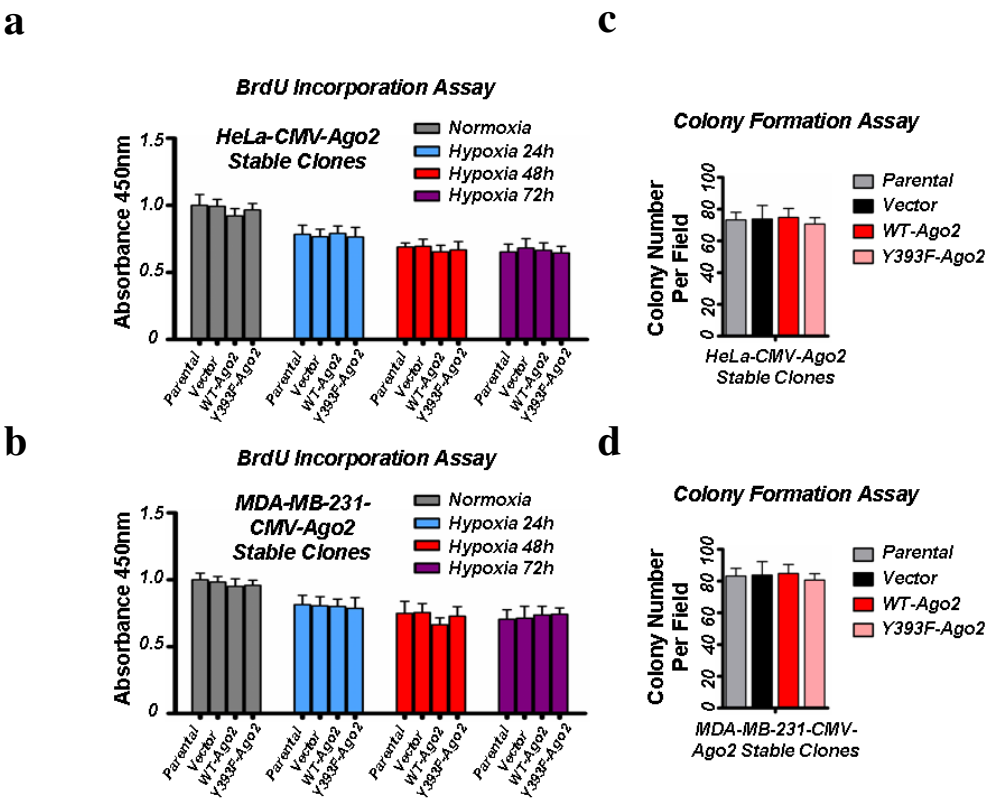

Figure 3-40 Cell proliferation and anchorage-independent cell growth are not significantly affected by WT or Y393F mutant Ago2.

Cell proliferation was detected by BrdU Cell Proliferation Assay Kit (Cell Signaling). **a,** 5×10^3 HeLa CMV Ago2 stable transfectant cells, **b,** 2×10^3 MDA-MB-231 CMV Ago2 stable transfectant cells, were seeded at 96 well-plates and cultured under normoxia for 24 hr or hypoxia for 24, 48 and 72 hr. 10 μM BrdU was added to the plate and cells were incubated for 4 hr. Data are shown as mean ± s.d., *n*=5. Soft agar colony formation 15 days after culture. **c,** 1×10^4 HeLa CMV Ago2 stable transfectant cells or **d,** 5×10^3 MDA-MB-231 CMV Ago2 stable transfectant cells on agarose gel. Colonies that grew beyond 50 μm in diameter were scored as positive. Colony number was counted based on three random chosen areas per dish in triplicate. Data are shown as mean ± s.d., *n*=3.

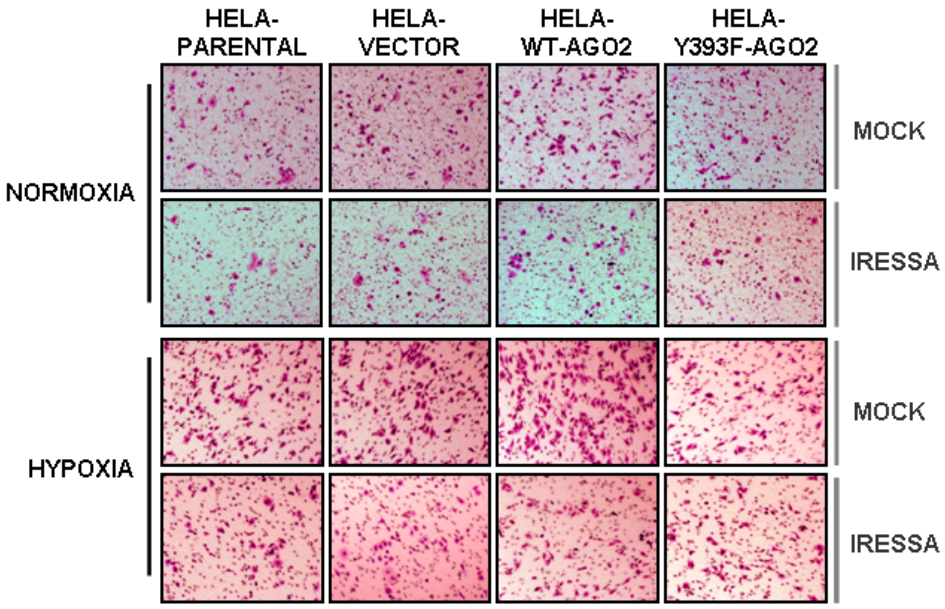

Figure 3-41 Ago2-Y393 phosphorylation enhances cell migration under hypoxia, which can be blocked by Iressa treatment.

Representative photographs of *in vitro* cell migration assay shown in Figure 3-39b. The average number of migrated cells per field (counted visually under a light microscope at original magnification ×200) shown in Figure 3-39b was calculated based on five randomly selected fields per membrane in triplicate.

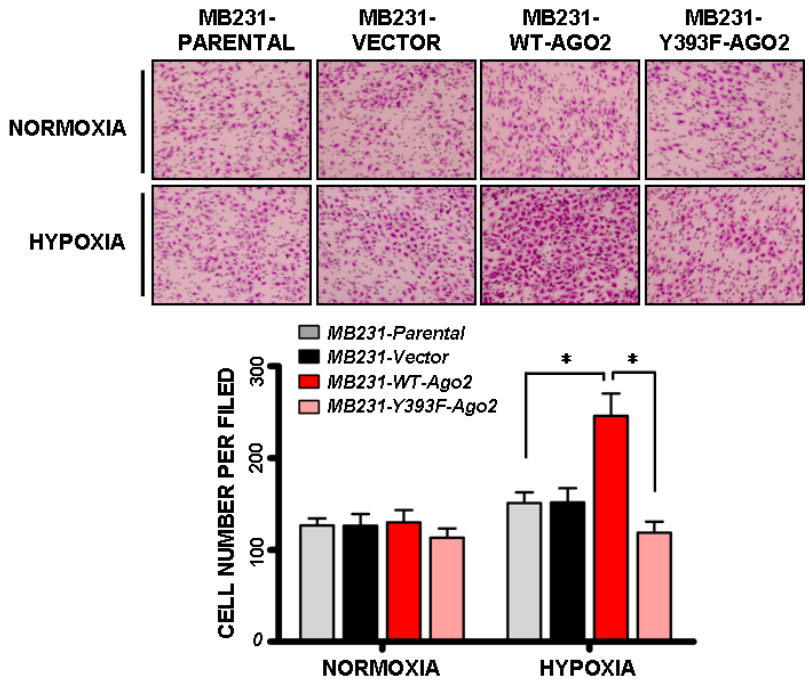

Figure 3-42 Ago2-Y393 phosphorylation enhances cell migration in response to hypoxia.

Top, Representative photographs of *in vitro* cell migration assay using MDA-MB-231 CMV Ago2 stable clones cultured under normoxia or hypoxia, as indicated. Bottom, corresponding quantitation data are shown as mean ± s.d., *n*=3. *indicates P<0.05. The average number of migrated cells per field (counted visually under a light microscope at original magnification ×200) was calculated based on five randomly selected fields per membrane in triplicate.

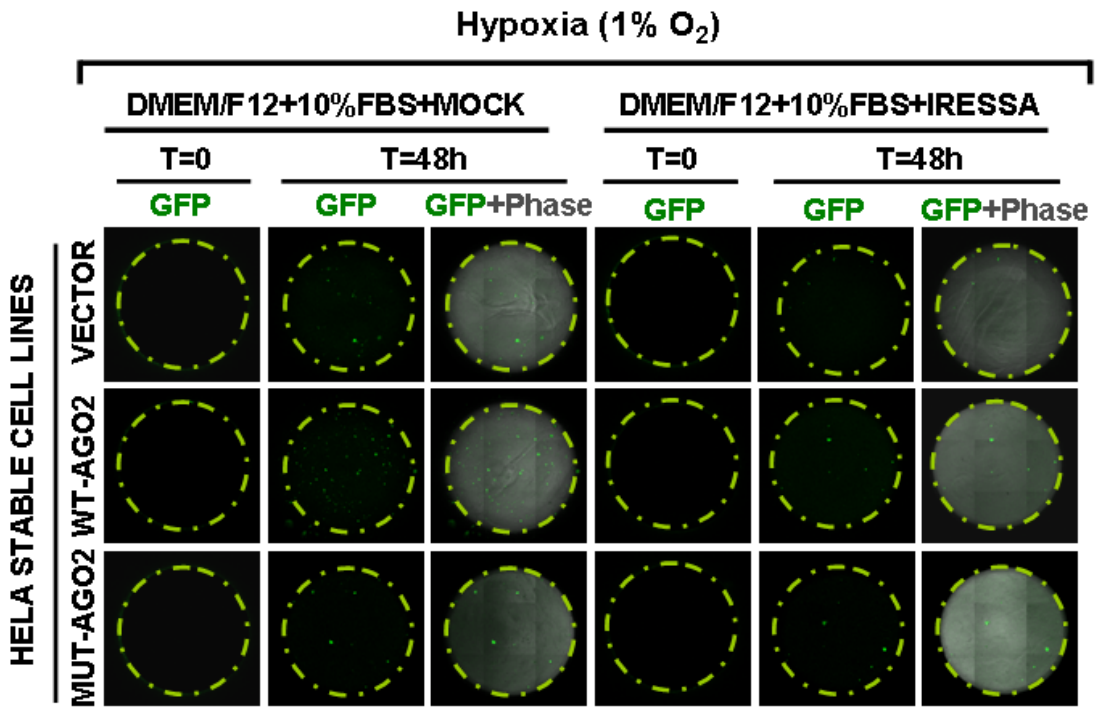

Figure 3-43 Ago2-Y393 phosphorylation mediates EGFR-enhanced cell invasiveness under hypoxia.

Representative images of *in vitro* 3-D invasion assay shown in Figure 3-39c. 9 images were taken by microscope and merged together to show the whole area (marked by yellow circle) for cell invasion in each well (each experimental group contained 5 wells as repeats). HeLa-CMV-Ago2-EF1-CopGFP stable cells are highlighted by their own GFP fluorescence. The number of invaded cells was calculated based on the total cell number in each invasion area as marked by yellow circle after 48 hr as indicated.

3.4.2 Phospho-Y393-Ago2 is specifically enriched in hypoxic primary tumors and significantly correlates with poorer overall survival in breast cancer patients

Finally, we utilized orthotopic xenograft breast cancer model to establish the relationship between hypoxia, EGFR, and p-Y393-Ago2, and showed that p-Y393-Ago2 along with EGFR is upregulated during tumor progression and specifically enriched in hypoxic tumor areas (Fig. 3-44). To further examine the clinical relevance of Ago2-Y393 phosphorylation, we analyzed the expression patterns of p-Y393-Ago2, EGFR, and the degree of hypoxia (indicated by HIF1α and HIF2α (Bertout et al., 2008)) in primary breast tumors in consecutive sections collected from 128 human breast cancer patients. In adjacent normal breast tissues, the expression of p-Y393-Ago2 was low but highly elevated in hypoxic breast tumors (Fig. 3-39d). We observed significant positive correlations between p-Y393-Ago2, EGFR, HIF1α and HIF2α (Fig. 3-45a, Table. 3-1) and further validated that Ago2-Y393 phosphorylation was enriched in hypoxic subareas of breast tumors with positive expression of EGFR (Fig. 3-45b). Moreover, higher expression of p-Y393-Ago2 correlated significantly with poorer overall survival in breast cancer patients (Fig. 3-39e), supporting its clinical importance as a potential prognostic marker for breast cancer patient survival.

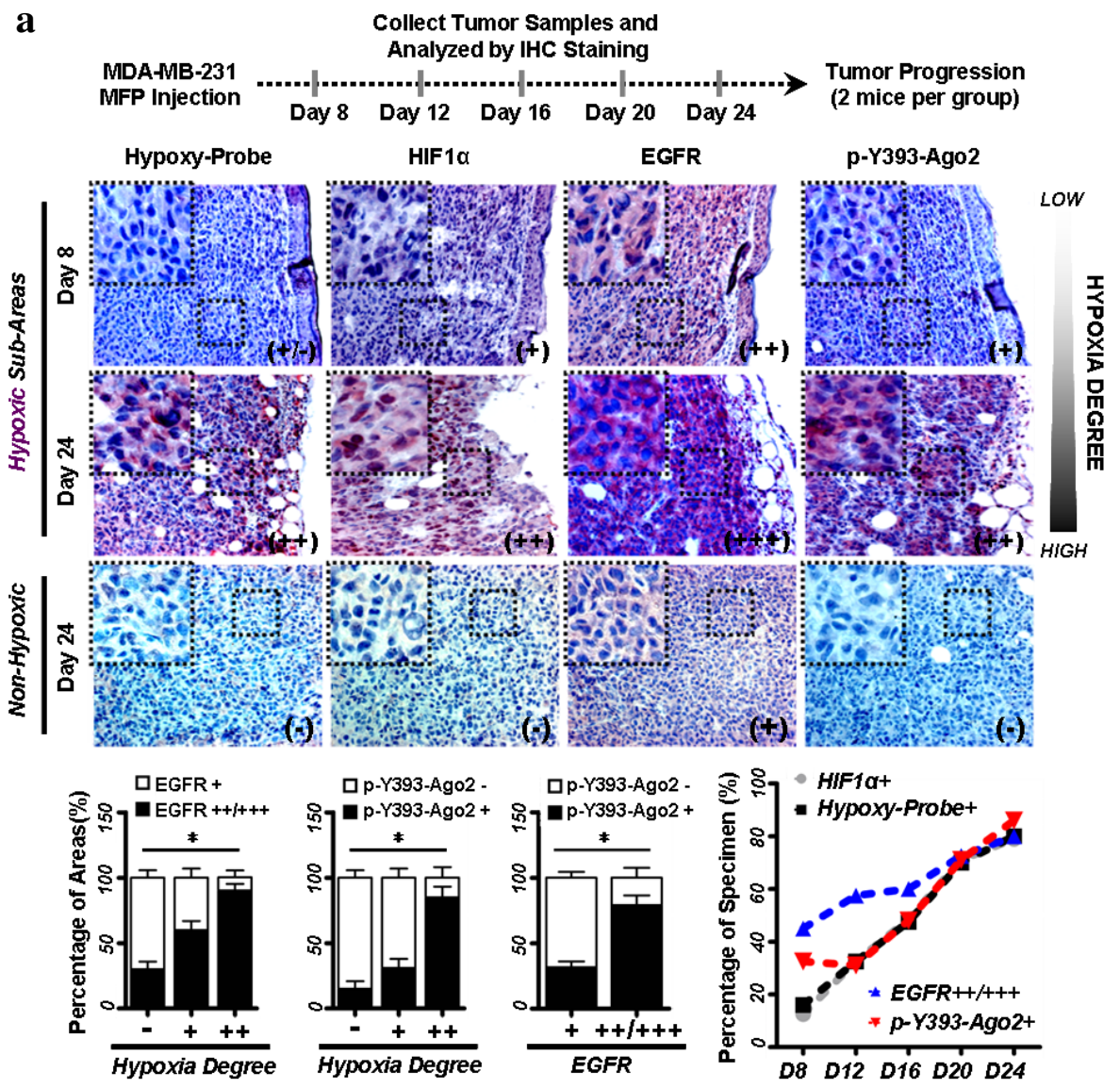

Figure 3-44 The expression of phospho-Y393-Ago2 is upregulated during tumor progression and specifically enriched in the hypoxic tumor subareas.

a, Top, experimental design for orthotopic breast cancer mouse model using MDA-MB-231 cells (1×10^6 cells per mouse). Middle, representative IHC images of consecutive sections from collected primary tumors (day 8 and day 24). Bottom, quantitative diagrams showing the expression patterns of EGFR, p-Y393-Ago2 and the degree of hypoxia (based on the average score for hypoxy-probe(Hutchison et al., 2004) and HIF1α) in primary tumors. Data at bottom right are shown as mean, *n*=2. Data at bottom left are shown as mean ± s.d. Statistical analyses were performed by ANOVA or by Student's *t* test, *n*=10 (score was based on tumor sub-areas).

b

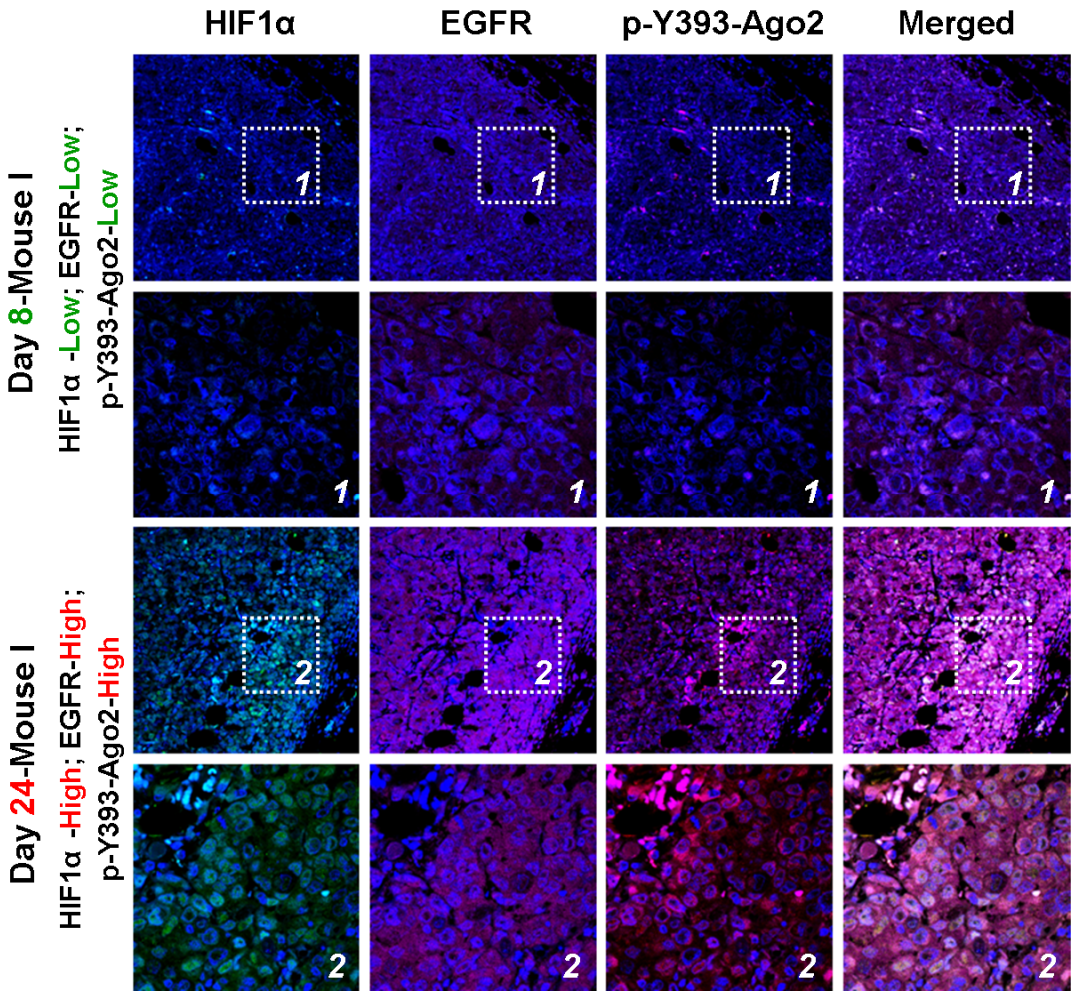

Figure 3-44. The expression of phospho-Y393-Ago2 is upregulated during tumor progression and specifically enriched in the hypoxic tumor subareas.

b, Primary tumors (mouse xenograft model) collected on Day 8 and Day 24 were fixed and stained with antibodies against endogenous HIF1α (green), EGFR (magenta), p-Y393-Ago2 (red), and DAPI (blue).

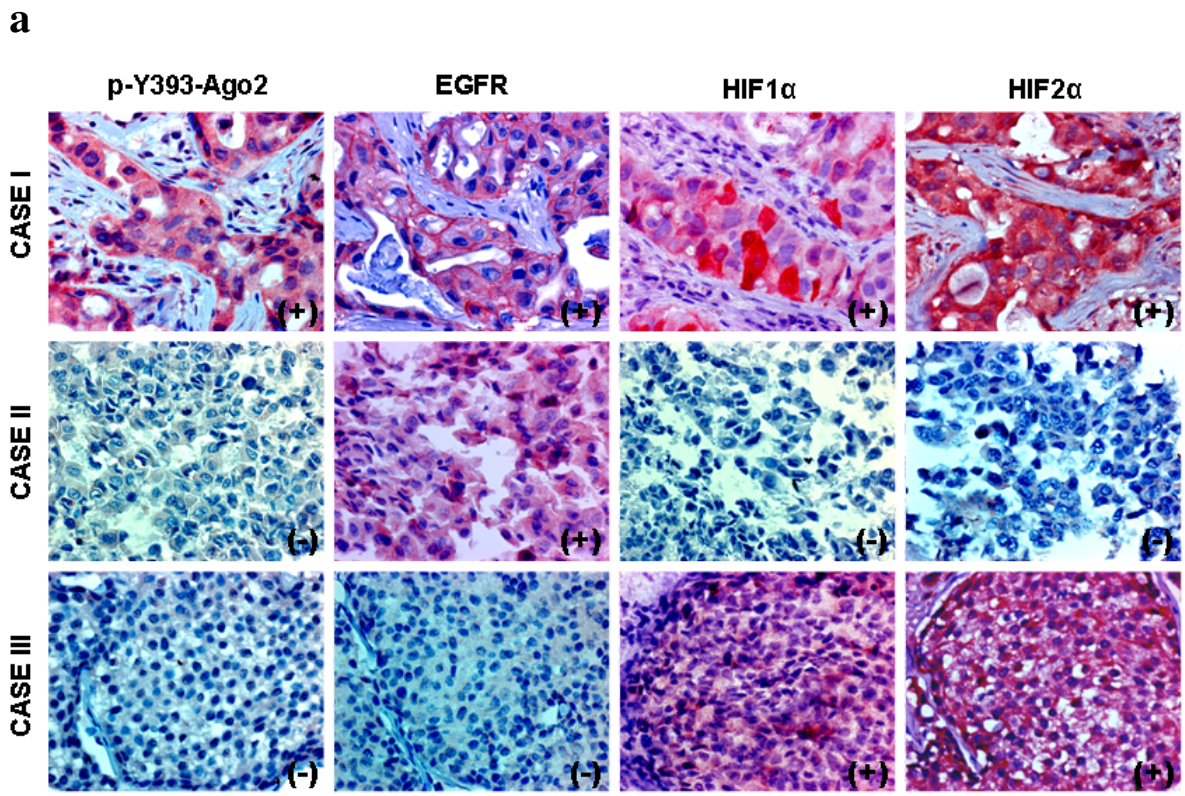

Figure 3-45 Phospho-Y393-Ago2 is specifically enriched in human primary breast tumor hypoxic subareas with positive expression of EGFR.

a, Human primary breast tumors (128 cases) were examined by IHC staining and the positive correlations between phospho-Y393-Ago2, EGFR and HIF1/2α are shown in Supplementary Table 1. Representative IHC staining images show that the expression of p-Y393-Ago2 was elevated in hypoxic breast tumor (HIF1/2α positive) with positive expression of EGFR. p-Y393-Ago2 was hardly detected when HIF1/2α or EGFR was not expressed.

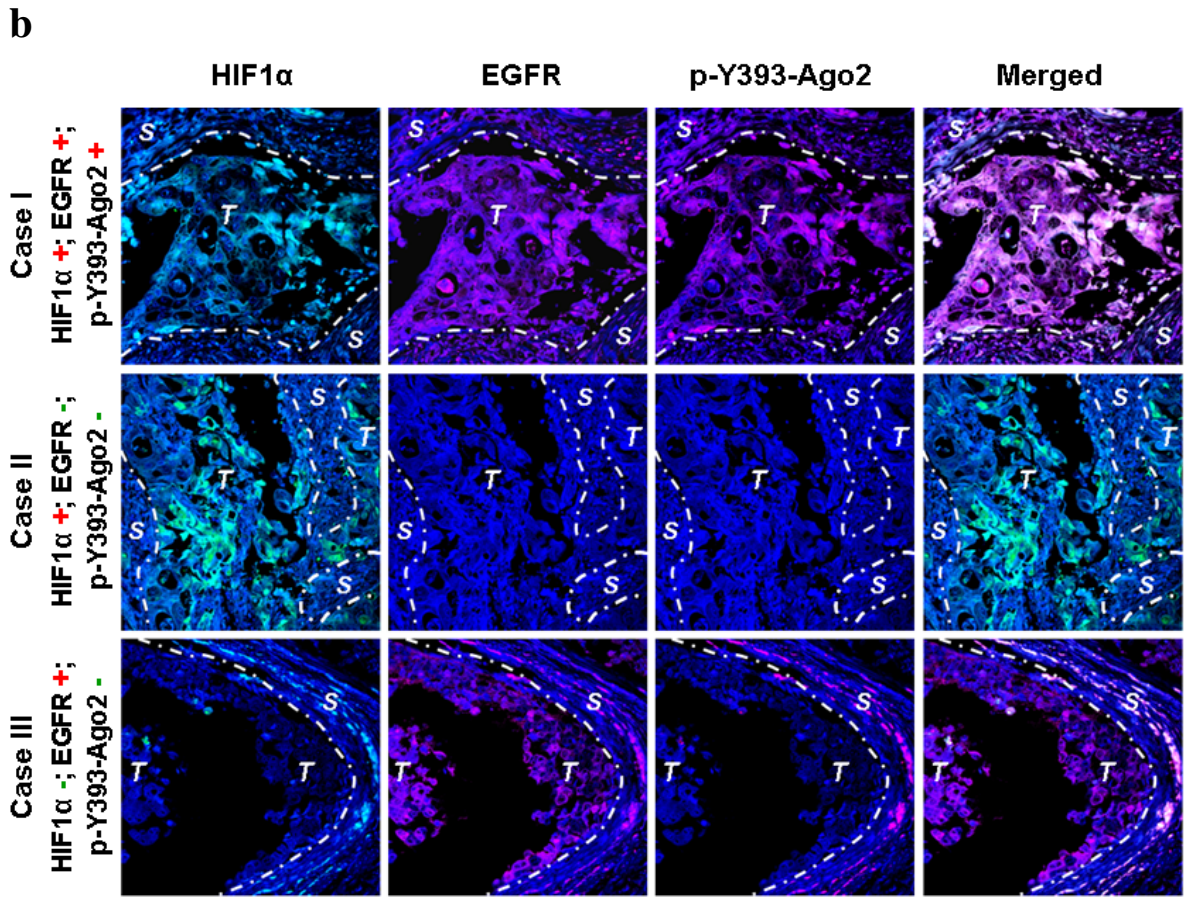

Figure 3-45 Phospho-Y393-Ago2 is specifically enriched in human primary breast tumor hypoxic subareas with positive expression of EGFR.

b, Three cases as indicated were chosen to show the colocalization between p-Y393-Ago2, EGFR and the hypoxic microenvironment (indicated by HIF1α) by immunofluorescence analysis. Breast tumor samples were fixed and stained with antibodies against endogenous HIF1α (green), EGFR (magenta), p-Y393-Ago2 (red), and DAPI (blue). S: surrounding tissue; T: human breast tumor area.

Table 3-1 p-Y393-Ago2 positively correlates with EGFR, HIF1α, HIF2α in human breast carcinoma

	EGFR			HIF1α			HIF2α		
p-Y393-Ago2	-/+	++	+++	-/+	++	+++	-/+	++	+++
-/+	18(14.1%)	4(3.1%)	3(2.3%)	14(10.9%)	3(2.3%)	9(7.0%)	15(11.7%)	6(4.7%)	5(3.9%)
++	27(21.1%)	7(5.5%)	8(6.3%)	9(7.0%)	8(6.3%)	19(14.8%)	11(8.6%)	12(9.4%)	14(10.9%)
+++	29(22.7%)	9(7.0%)	23(18%)	13(10.2%)	9(7.0%)	44(34.4%)	11(8.6%)	17(13.3%)	37(28.9%)
Total	74(57.8%)	20(15.6%)	34(26.6%)	36(28.1%)	20(15.6%)	72(56.3%)	37(28.9%)	35(27.3%)	56(43.8%)
p-Value	P<0.04			P<0.01			P<0.001		

Expression patterns of p-Y393-Ago2, EGFR, HIF1α and HIF2α in the consecutive sections from human breast tumors were determined and summarized. (-/+): negative-low; (++): positive-medium; (+++): positive-high. The correlation between p-Y393-Ago2, EGFR, HIF1α and HIF2α was analyzed using SPSS 16.0 Pearson Chi-Square Test. P-value that less than 0.05 was set as the criterion for statistical significance.

3.5 Discussion and future directions

In this study, we identified a novel role of EGFR in miRNA maturation via Ago2-Y393 phosphorylation. While these results support EGFR as the tyrosine kinase that suppresses miRNA maturation through Ago2-Y393 phosphorylation under hypoxia, there may be other tyrosine kinases that can also contribute to phospho-Ago2-mediated miRNA processing as indicated by Figure 3-32. Additionally, several interesting questions are raised from our data and need to be further studied in future.

Q1. What is the complete molecular mechanism by which phosphorylated Ago2 affects processing of miRNAs to their mature form? Is it entirely due to a reduction in phosphorylated Ago2/Dicer interaction?

The steady level of a mature miRNA is control by both biogenesis and turnover. Ago2 regulates miRNA maturation and also stabilizes the mature miRNA after loading into RISC, enhancing the expression of mature miRNA as a net result. To demonstrate the functional importance of reduced pAgo2-Dicer interaction, we knocked down endogenous Dicer in HeLa TetOff inducible Ago2 stable clones to decelerate miRNA maturation under hypoxia. If reduced mature miRNA expression in WT Ago2 cells is solely caused by suppressed miRNA maturation through decreased p-Y393-Ago2-Dicer interaction, restriction of their maturation process by silencing core enzyme Dicer would significantly diminish the difference of miRNA expression in WT and Y393F Ago2 stable clones. On the other hand, if it is a consequence of decreased mature miRNA stability (likely due to reduced binding affinity with p-Y393-Ago2), expression difference of mature miRNAs should not be affected even after knocking down Dicer. Indeed, after silencing Dicer the expression

difference in mature miRNAs between WT and Y393F Ago2 was significantly diminished, suggesting that the maturation of those long-loop mHESM is suppressed by Ago2-Y393 phosphorylation through Dicer, which in turn contributes to the decreased level of mature long-loop mHESM in WT Ago2 cells. Moreover, silencing Dicer diminished the loading difference between WT and Y393F Ago2 under hypoxia. This result suggests that enhanced precursor loading of Y393F Ago2 was largely due to its increased association with Dicer. Correspondingly, more mature long-loop mHESM were loaded onto Y393F-Ago2, consistent with its enhanced RISC activity as indicated by luciferase reporter assay. However, the mature miRNA loading difference between WT and Y393F Ago2 was Dicer-dependent and similar to the one we observed in mature miRNA expression. Therefore, reduced mature miRNA loading of WT Ago2 could be a consequence of suppressed mature miRNA expression. Nonetheless, the potential contribution from pAgo2-mediated miRNA stability control cannot be completely excluded. To fully address this issue, we need to perform in vitro small RNA loading assay to see whether Ago2's binding affinity towards long-loop mHESM or other short-loop miRNAs is altered by phosphorylation at Y393.

Q2. How does the long-loop structure of miRNAs contribute to the selective targeting by EGFR? Is Ago2 the only downstream target of EGFR involving in miRNA regulation in response to hypoxia?

The structure of miRNA precursors that selectively targeted by EGFR in response to hypoxia was shown in Figure 3-28. The majority of mHESM that are also regulated by Ago2-Y393 phosphorylation do have a long-loop structure in their precursors and we already showed that the long-loop structure is required and sufficient for phospho-Y393-Ago2-mediated suppression on miRNA maturation under hypoxia. However, other mHESM

(not affected by Ago2-Y393 phosphorylation), lacking the long-loop structure in their precursors were regulated by EGFR in response to hypoxia, suggesting that Ago2-Y393 phosphorylation is only one of the major downstream events that responsible for EGFR-suppressed miRNA maturation in response to hypoxia. Also, the long-loop structure in miRNA precursors is important for p-Y393-Ago2-mediated miRNA regulation but is not required for the selective targeting by EGFR. Recently, several EGFR-downstream kinases have been proposed to play a role in miRNA biogenesis pathway, including Erk, which phosphorylates TRBP to enhance the general miRNA processing but specifically reduce the expression of let-7 family (Paroo et al., 2009), and AKT3 (Horman et al., 2013), which phosphorylates Ago2 at Ser387, resulting in enhanced translational repression but reduced cleavage activity. Nonetheless, whether EGFR has additional direct binding partners involved in miRNA processing remain unknown and worth to be investigated in future.

Q3. What is the effect of phosphorylated Ago2 on RISC complex formation?

Different from RISC loading complex (which consists of Dicer, TRBP and Ago2 (Chendrimada et al., 2005; Diederichs and Haber, 2007)) involved in miRNA maturation, RISC complex is responsible for the executing step of miRNA-mediated gene silencing (Eulalio et al., 2008) and is constituted by many proteins, including Ago2, GW182, TNRC6A/B/C and etc. RISC complex also associates with 5' decapping complex, including Dcp1A, Dcp2 and XRN-1, for miRNA-mediated mRNA destabilization (Parker and Sheth, 2007). In 293T overexpression system, Ago2-GW182 and Ago2-Dcp1A interactions were slightly affected by Ago2-Y393 phosphorylation (Fig. 3-46). The data itself cannot support nor exclude the possibility that Ago2-Y393 phosphorylation may affect RISC formation as multiple proteins were involved in this complex. I believe that this could be an interesting

direction that worth to be pursued further, since Ago2 is known to be the catalytic core of RISC and plays essential roles in miRNA-mediated gene silencing.

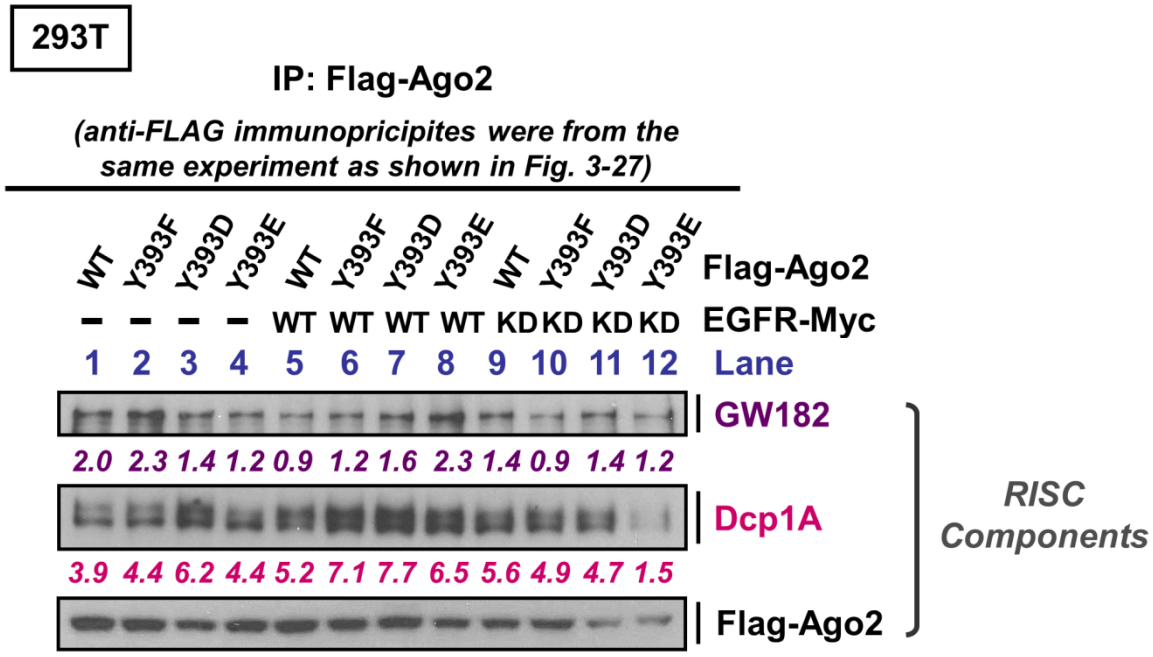

Figure 3-46 The association between Ago2 and other RISC components is also affected by Ago2-Y393-phosphorylation.

Protein samples of immunoprecipition are from the same experiment as shown in Figure 3-27. Anti-FLAG immunoprecipitates were blotted with GW182 or Dcp1A antibody to show the interactions between Ago2 and other RISC components.

Q4. What are the targeted proteins that upregulated by p-Y393-Ago2 due to suppressed miRNA maturation in response to hypoxia stress?

To address this question, we first screened mRNAs that were affected by EGFR under hypoxia and were predicted to be targeted by multiple long-loop mHESM. We chose LOX as an example (Fig. 3-47). First of all, Y393F Ago2, compared with WT, was loaded with more LOX mRNAs under hypoxia (pink *vs.* red, Fig. 3-48; RIP input is shown in Fig. 3-25e), suggesting LOX as a potential target regulated by Ago2-Y393 phosphorylation. Moreover, the difference between WT and Y393F Ago2 in LOX mRNA loading was significantly diminished after silencing Dicer (Fig. 3-48), implying that reduced LOX mRNA loading in WT Ago2 was largely due to suppressed expression of long-loop mHESM. To examine the readout of targeting repression, we analyzed LOX expression in HeLa CMV Ago2 stable clones and found that Y393F Ago2 cells expressed lower level of LOX in response to hypoxia (Fig. 3-49), consistent with its enhanced LOX mRNA loading as shown in figure 3-48. A similar result was observed in MDA-MB-231 CMV Ago2 stable clones (Fig. 3-50). Importantly, TKi treatments (1 μM Iressa and 50 nM AG1478 for 24 hr) diminished the expression difference of LOX between WT and Y393F Ago2 stable clones, indicating that LOX is regulated by Ago2-Y393 phosphorylation downstream of EGFR activation under hypoxia. However, LOX is only one of the examples that regulated by phosphorylated Ago2 in response to hypoxia. We believe more endogenous proteins are regulated by Ago2-Y393 phosphorylation, which collectively play important roles in cellular response against hypoxic stress. To this end, we plan to use non-biased antibody array to explore the profile of target proteins that are regulated by phospho-Y393-Ago2 under hypoxia. This result will

help us further understand the functional role of Ago2 phosphorylation in miRNA-mediated gene slicing, specifically in response to hypoxic stress.

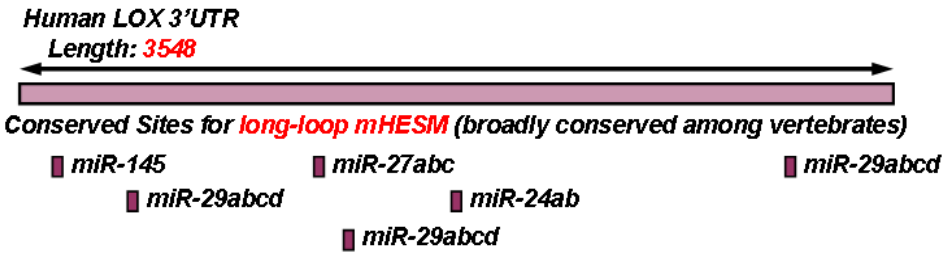

Figure 3-47 The 3'UTR of LOX mRNA are predicted to be targeted by multiple long-loop mHESM.

Conserved miRNA targeting sites (predicted by TargetScan) are shown as indicated.

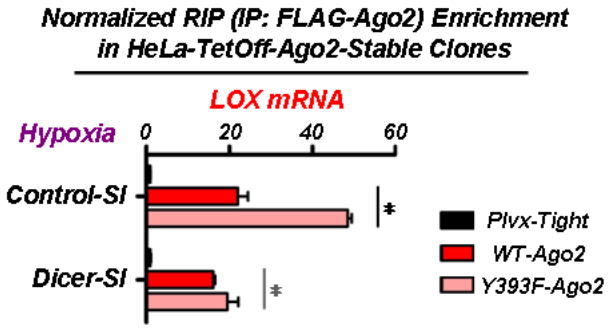

Figure 3-48 Ago2-Y393 phosphorylation reduces the loading of LOX mRNA, a process that is dependent on Dicer.

RIP enrichment of LOX mRNA as indicated. RIP input controls are shown in Figure 3-25e.

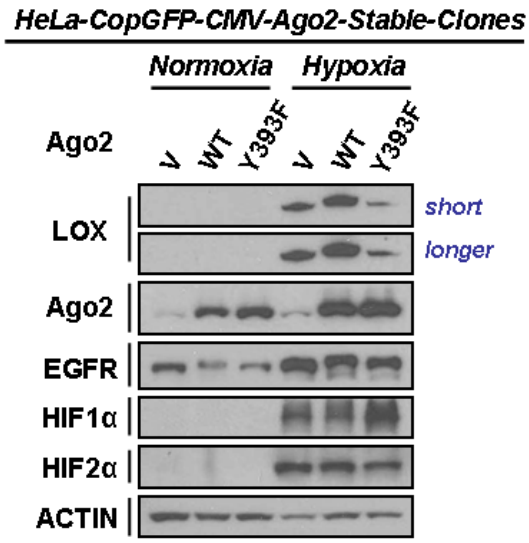

Figure 3-49 LOX is regulated by Ago2-Y393 phosphorylation in response to hypoxia.

Western blot analysis of HeLa Ago2 stable transfectants as indicated. HIF1α and HIF2α are used as positive controls for cellular hypoxic response. β-actin is used as loading control.

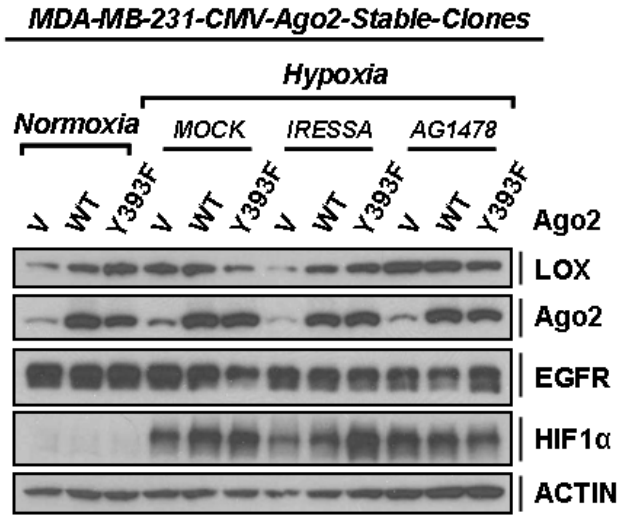

Figure 3-50 EGFR kinase inhibitors diminish the expression difference of LOX in WT and Y393F Ago2 stable clones under hypoxia.

Western blot analysis of MDA-MB-231 Ago2 stable transfectants as indicated. HIF1α is used as positive control for cellular hypoxic response. β-actin is used as loading control.

Q5. What's the biological function of Ago2-Y393 phosphorylation in primary tumor growth and metastasis?

To assess the *in vivo* biological function of Ago2-Y393 phosphorylation, we injected MDA-MB-231 parental and Ago2 stable tranfectants, including vector control, WT and Y393F Ago2, into mouse mammary fat pads, an orthotopic tumor model for breast cancer. Consistent with *in vitro* proliferation assays (Fig. 3-40), we didn't observe significant difference in primary tumor growth among those experimental groups (Fig. 3-51). Interestingly, higher frequency of primary tumor relapse as well as distal metastasis (lymph node metastasis and lung micro-metastasis) was found in WT Ago2 cells after primary tumor removal for 4 weeks (Figs. 3-51, 3-52), suggesting that Ago2-Y393 phosphorylation plays a pivotal role in cancer progression. We reasoned that high frequency of primary tumor relapse could due to enhanced local invasion. Indeed, more WT-Ago2 cells invaded into the surrounding blood vessels when the primary tumors were removed (Fig. 3-53). However, the key events downstream of Ago2-Y393 phosphorylation that specifically contribute to the development of malignancy remain unclear and need to be systemically investigated in future.

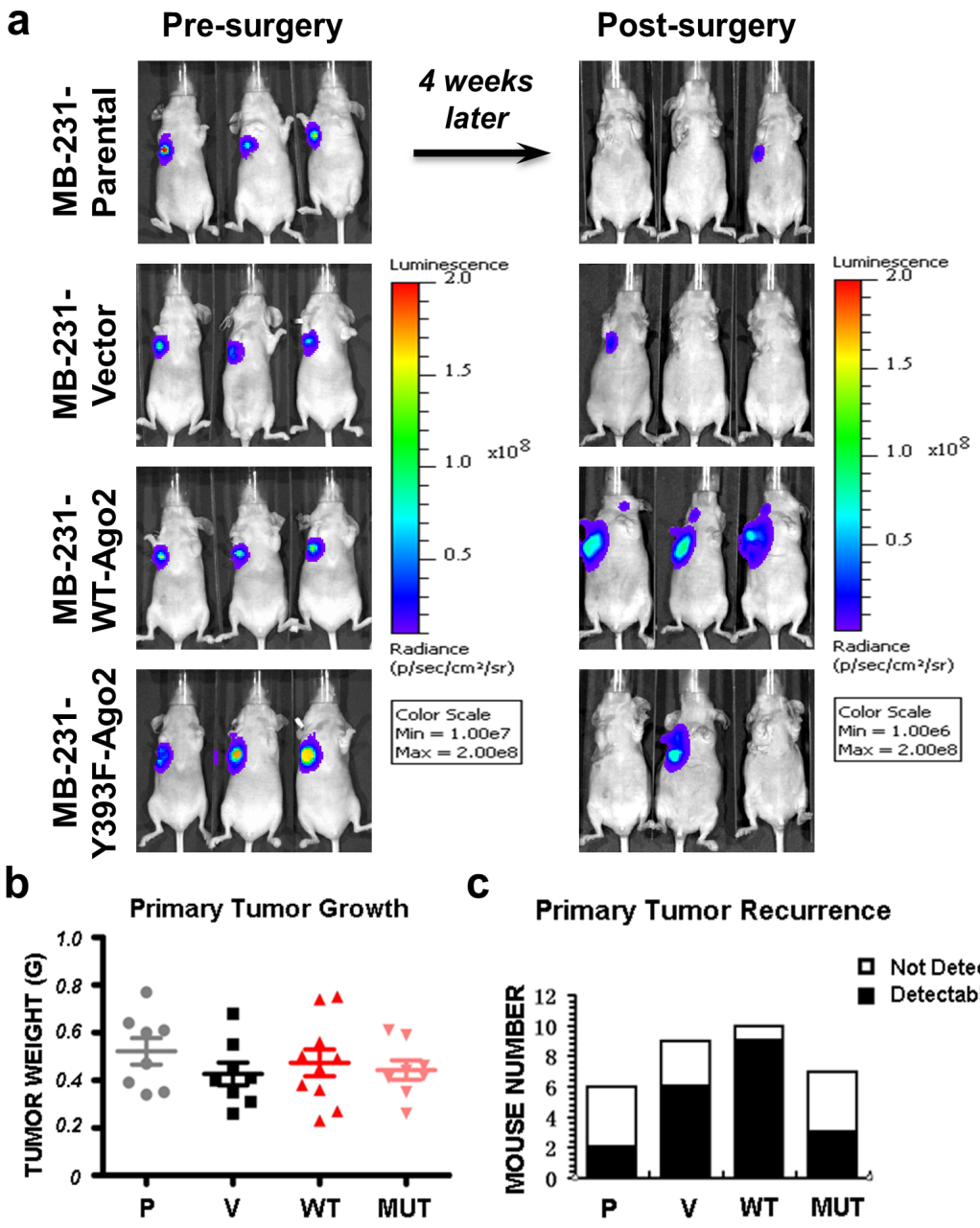

Figure 3-51 Ago2-Y393 phosphorylation enhances primary tumor relapse while has no significant effects on primary tumor growth.

a, Representative luminescence images for primary tumors before surgery and tumor relapses after surgery. **b,** Primary tumor weight as indicated. **c,** Percentage of primary tumor relapse in different groups as indicated. P, parental; V, vector; WT, WT Ago2; MUT, Y393F Ago2.

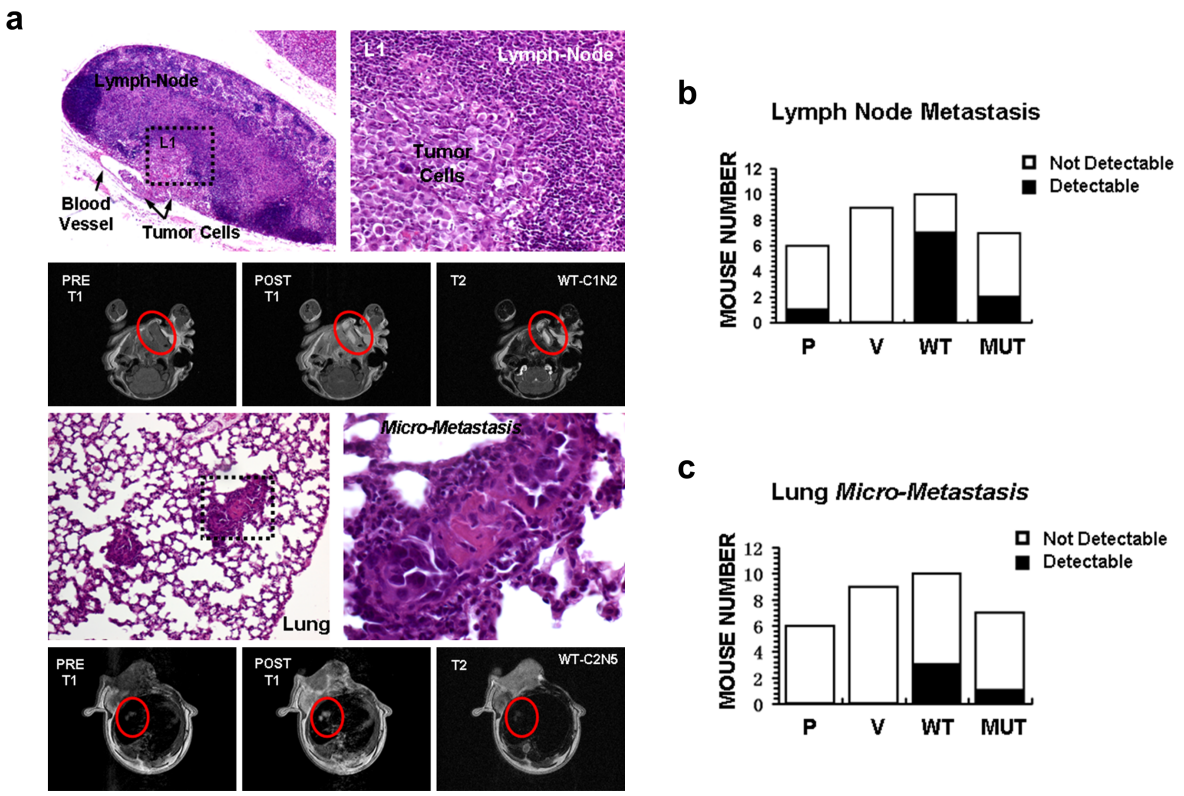

Figure 3-52 Ago2-Y393 phosphorylation promotes distal metastasis.

a, Representative HE-staining and MRI images for lymph node metastasis and lung micro-metastasis. **b,** quantification of lymph node metastasis as indicated. **c,** quantification of lung micro-metastasis as indicated. P, parental; V, vector; WT, WT Ago2; MUT, Y393F Ago2.

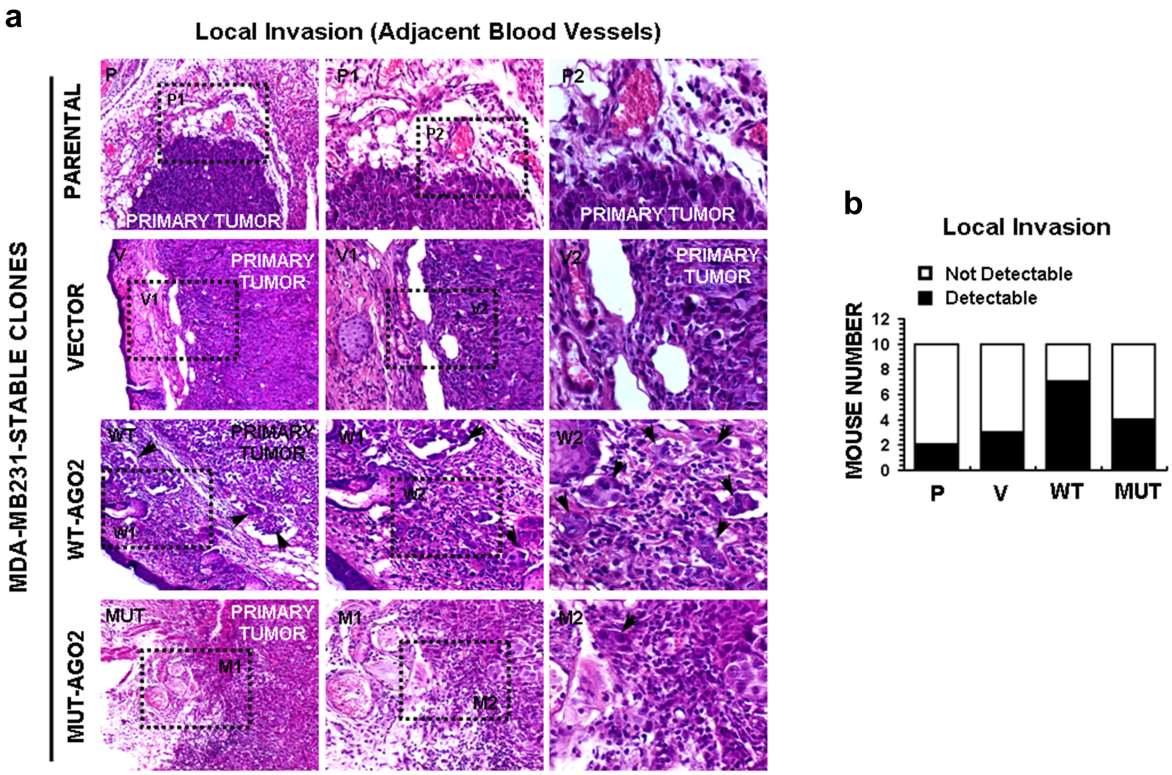

Figure 3-53 Ago2-Y393 phosphorylation facilitates tumor cells invading into adjacent blood vessels.

a, Representative HE-staining images for tumor invasion into adjacent blood vessels. **b,** quantification of primary tumor local invasion as indicated. P, parental; V, vector; WT, WT Ago2; MUT, Y393F Ago2.

Our Proposed Model

Our research work demonstrates EGFR as a novel direct mediator that modulates miRNA maturation in response to hypoxia through phosphorylation of Ago2 at Tyr393 (Fig. 3-54). This work opens a new direction to further understand the regulation of miRNA machinery in response to stress signaling, which is likely to have important clinical implications.

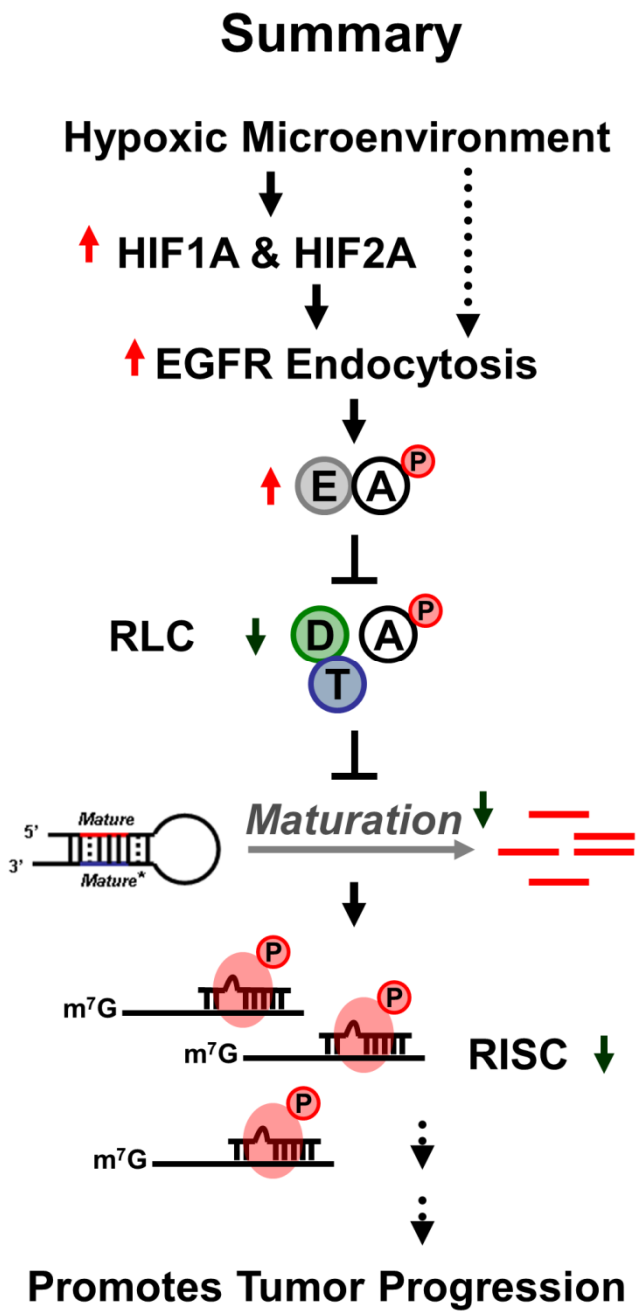

Figure 3-54 Proposed model for EGFR-regulated miRNA maturation in response to hypoxia through phosphorylation of Ago2.

E, EGFR; A, Ago2; D, Dicer; T, TRBP; RISC, RNA-Induced Silencing Complex.

Bibliography

Abd El-Rehim, D.M., Pinder, S.E., Paish, C.E., Bell, J.A., Rampaul, R.S., Blamey, R.W., Robertson, J.F., Nicholson, R.I., and Ellis, I.O. (2004). Expression and co-expression of the members of the epidermal growth factor receptor (EGFR) family in invasive breast carcinoma. Br J Cancer *91*, 1532-1542.

Anthis, N.J., Haling, J.R., Oxley, C.L., Memo, M., Wegener, K.L., Lim, C.J., Ginsberg, M.H., and Campbell, I.D. (2009). Beta integrin tyrosine phosphorylation is a conserved mechanism for regulating talin-induced integrin activation. J Biol Chem *284*, 36700-36710.

Basu, R.K., Hubchak, S., Hayashida, T., Runyan, C.E., Schumacker, P.T., and Schnaper, H.W. (2011). Interdependence of HIF-1alpha and TGF-beta/Smad3 signaling in normoxic and hypoxic renal epithelial cell collagen expression. Am J Physiol Renal Physiol *300*, F898-905.

Bates, G.J., Nicol, S.M., Wilson, B.J., Jacobs, A.M., Bourdon, J.C., Wardrop, J., Gregory, D.J., Lane, D.P., Perkins, N.D., and Fuller-Pace, F.V. (2005). The DEAD box protein p68: a novel transcriptional coactivator of the p53 tumour suppressor. The EMBO journal *24*, 543-553.

Bertout, J.A., Patel, S.A., and Simon, M.C. (2008). The impact of O2 availability on human cancer. Nature reviews Cancer *8*, 967-975.

Blenkiron, C., Goldstein, L.D., Thorne, N.P., Spiteri, I., Chin, S.F., Dunning, M.J., Barbosa-Morais, N.L., Teschendorff, A.E., Green, A.R., Ellis, I.O., Tavare, S., Caldas, C., and Miska,

E.A. (2007). MicroRNA expression profiling of human breast cancer identifies new markers of tumor subtype. Genome biology *8*, R214.

Briata, P., Forcales, S.V., Ponassi, M., Corte, G., Chen, C.Y., Karin, M., Puri, P.L., and Gherzi, R. (2005). p38-dependent phosphorylation of the mRNA decay-promoting factor KSRP controls the stability of select myogenic transcripts. Molecular cell *20*, 891-903.

Cao, C., Lu, S., Jiang, Q., Wang, W.J., Song, X., Kivlin, R., Wallin, B., Bagdasarian, A., Tamakloe, T., Chu, W.M., Marshall, J., Kouttab, N., Xu, A., and Wan, Y. (2008). EGFR activation confers protections against UV-induced apoptosis in cultured mouse skin dendritic cells. Cell Signal *20*, 1830-1838.

Caretti, G., Schiltz, R.L., Dilworth, F.J., Di Padova, M., Zhao, P., Ogryzko, V., Fuller-Pace, F.V., Hoffman, E.P., Tapscott, S.J., and Sartorelli, V. (2006). The RNA helicases p68/p72 and the noncoding RNA SRA are coregulators of MyoD and skeletal muscle differentiation. Developmental cell *11*, 547-560.

Causevic, M., Hislop, R.G., Kernohan, N.M., Carey, F.A., Kay, R.A., Steele, R.J., and Fuller-Pace, F.V. (2001). Overexpression and poly-ubiquitylation of the DEAD-box RNA helicase p68 in colorectal tumours. Oncogene *20*, 7734-7743.

Cheloufi, S., Dos Santos, C.O., Chong, M.M., and Hannon, G.J. (2010). A dicer-independent miRNA biogenesis pathway that requires Ago catalysis. Nature *465*, 584-589.

Chendrimada, T.P., Gregory, R.I., Kumaraswamy, E., Norman, J., Cooch, N., Nishikura, K., and Shiekhattar, R. (2005). TRBP recruits the Dicer complex to Ago2 for microRNA processing and gene silencing. Nature *436*, 740-744.

Cheng, T.L., Wang, Z., Liao, Q., Zhu, Y., Zhou, W.H., Xu, W., and Qiu, Z. (2014). MeCP2 Suppresses Nuclear MicroRNA Processing and Dendritic Growth by Regulating the DGCR8/Drosha Complex. Developmental cell *28*, 547-560.

Choudhry, H., and Catto, J.W. (2011). Epigenetic regulation of microRNA expression in cancer. Methods Mol Biol *676*, 165-184.

Cifuentes, D., Xue, H., Taylor, D.W., Patnode, H., Mishima, Y., Cheloufi, S., Ma, E., Mane, S., Hannon, G.J., Lawson, N.D., Wolfe, S.A., and Giraldez, A.J. (2010). A novel miRNA processing pathway independent of Dicer requires Argonaute2 catalytic activity. Science *328*, 1694-1698.

Cikaluk, D.E., Tahbaz, N., Hendricks, L.C., DiMattia, G.E., Hansen, D., Pilgrim, D., and Hobman, T.C. (1999). GERp95, a membrane-associated protein that belongs to a family of proteins involved in stem cell differentiation. Mol Biol Cell *10*, 3357-3372.

Clark, E.L., Coulson, A., Dalgliesh, C., Rajan, P., Nicol, S.M., Fleming, S., Heer, R., Gaughan, L., Leung, H.Y., Elliott, D.J., Fuller-Pace, F.V., and Robson, C.N. (2008). The RNA helicase p68 is a novel androgen receptor coactivator involved in splicing and is overexpressed in prostate cancer. Cancer Res *68*, 7938-7946.

Daniels, S.M., Melendez-Pena, C.E., Scarborough, R.J., Daher, A., Christensen, H.S., El Far, M., Purcell, D.F., Laine, S., and Gatignol, A. (2009). Characterization of the TRBP domain required for dicer interaction and function in RNA interference. BMC molecular biology *10*, 38.

Davis, B.N., Hilyard, A.C., Lagna, G., and Hata, A. (2008). SMAD proteins control DROSHA-mediated microRNA maturation. Nature *454*, 56-61.

Debnath, J., Muthuswamy, S.K., and Brugge, J.S. (2003). Morphogenesis and oncogenesis of MCF-10A mammary epithelial acini grown in three-dimensional basement membrane cultures. Methods *30*, 256-268.

Diederichs, S., and Haber, D.A. (2007). Dual role for argonautes in microRNA processing and posttranscriptional regulation of microRNA expression. Cell *131*, 1097-1108.

Endoh, H., Maruyama, K., Masuhiro, Y., Kobayashi, Y., Goto, M., Tai, H., Yanagisawa, J., Metzger, D., Hashimoto, S., and Kato, S. (1999). Purification and identification of p68 RNA helicase acting as a transcriptional coactivator specific for the activation function 1 of human estrogen receptor alpha. Mol Cell Biol *19*, 5363-5372.

Erler, J.T., Bennewith, K.L., Nicolau, M., Dornhofer, N., Kong, C., Le, Q.T., Chi, J.T., Jeffrey, S.S., and Giaccia, A.J. (2006). Lysyl oxidase is essential for hypoxia-induced metastasis. Nature *440*, 1222-1226.

Eulalio, A., Huntzinger, E., and Izaurralde, E. (2008). Getting to the root of miRNA-mediated gene silencing. Cell *132*, 9-14.

Faller, M., Matsunaga, M., Yin, S., Loo, J.A., and Guo, F. (2007). Heme is involved in microRNA processing. Nature structural & molecular biology *14*, 23-29.

Franovic, A., Gunaratnam, L., Smith, K., Robert, I., Patten, D., and Lee, S. (2007). Translational up-regulation of the EGFR by tumor hypoxia provides a nonmutational

explanation for its overexpression in human cancer. Proc Natl Acad Sci U S A *104*, 13092-13097.

Fukuda, T., Yamagata, K., Fujiyama, S., Matsumoto, T., Koshida, I., Yoshimura, K., Mihara, M., Naitou, M., Endoh, H., Nakamura, T., Akimoto, C., Yamamoto, Y., Katagiri, T., Foulds, C., Takezawa, S., Kitagawa, H., Takeyama, K., O'Malley, B.W., and Kato, S. (2007). DEAD-box RNA helicase subunits of the Drosha complex are required for processing of rRNA and a subset of microRNAs. Nat Cell Biol *9*, 604-611.

Fuller-Pace, F.V., and Moore, H.C. (2011). RNA helicases p68 and p72: multifunctional proteins with important implications for cancer development. Future Oncol *7*, 239-251.

Garre, P., Perez-Segura, P., Diaz-Rubio, E., Caldes, T., and de la Hoya, M. (2010). Reassessing the TARBP2 mutation rate in hereditary nonpolyposis colorectal cancer. Nature genetics *42*, 817-818; author reply 818.

Gherzi, R., Trabucchi, M., Ponassi, M., Ruggiero, T., Corte, G., Moroni, C., Chen, C.Y., Khabar, K.S., Andersen, J.S., and Briata, P. (2006). The RNA-binding protein KSRP promotes decay of beta-catenin mRNA and is inactivated by PI3K-AKT signaling. PLoS biology *5*, e5.

Gibbings, D., Mostowy, S., Jay, F., Schwab, Y., Cossart, P., and Voinnet, O. (2012). Selective autophagy degrades DICER and AGO2 and regulates miRNA activity. Nat Cell Biol *14*, 1314-1321.

Gibbings, D.J., Ciaudo, C., Erhardt, M., and Voinnet, O. (2009). Multivesicular bodies associate with components of miRNA effector complexes and modulate miRNA activity. Nat Cell Biol *11*, 1143-1149.

Gould, G.W., and Lippincott-Schwartz, J. (2009). New roles for endosomes: from vesicular carriers to multi-purpose platforms. Nature reviews Molecular cell biology *10*, 287-292.

Grant, B.D., and Donaldson, J.G. (2009). Pathways and mechanisms of endocytic recycling. Nature reviews Molecular cell biology *10*, 597-608.

Gross, T.J., Powers, L.S., Boudreau, R.L., Brink, B., Reisetter, A., Goel, K., Gerke, A.K., Hassan, I.H., and Monick, M.M. (2014). A microRNA processing defect in smokers' macrophages is linked to SUMOylation of the endonuclease DICER. J Biol Chem.

Guil, S., and Caceres, J.F. (2007). The multifunctional RNA-binding protein hnRNP A1 is required for processing of miR-18a. Nature structural & molecular biology *14*, 591-596.

Haines, G.K., Ghadge, G.D., Becker, S., Kies, M., Pelzer, H., Thimmappaya, B., and Radosevich, J.A. (1993). Correlation of the expression of double-stranded RNA-dependent protein kinase (p68) with differentiation in head and neck squamous cell carcinoma. Virchows Archiv B, Cell pathology including molecular pathology *63*, 289-295.

Halatsch, M.E., Schmidt, U., Behnke-Mursch, J., Unterberg, A., and Wirtz, C.R. (2006). Epidermal growth factor receptor inhibition for the treatment of glioblastoma multiforme and other malignant brain tumours. Cancer Treat Rev *32*, 74-89.

Heo, I., Joo, C., Kim, Y.K., Ha, M., Yoon, M.J., Cho, J., Yeom, K.H., Han, J., and Kim, V.N. (2009). TUT4 in concert with Lin28 suppresses microRNA biogenesis through pre-microRNA uridylation. Cell *138*, 696-708.

Hill, D.A., Ivanovich, J., Priest, J.R., Gurnett, C.A., Dehner, L.P., Desruisseau, D., Jarzembowski, J.A., Wikenheiser-Brokamp, K.A., Suarez, B.K., Whelan, A.J., Williams, G., Bracamontes, D., Messinger, Y., and Goodfellow, P.J. (2009). DICER1 mutations in familial pleuropulmonary blastoma. Science *325*, 965.

Horman, S.R., Janas, M.M., Litterst, C., Wang, B., MacRae, I.J., Sever, M.J., Morrissey, D.V., Graves, P., Luo, B., Umesalma, S., Qi, H.H., Miraglia, L.J., Novina, C.D., and Orth, A.P. (2013). Akt-mediated phosphorylation of argonaute 2 downregulates cleavage and upregulates translational repression of MicroRNA targets. Molecular cell *50*, 356-367.

Hsu, J.M., Chen, C.T., Chou, C.K., Kuo, H.P., Li, L.Y., Lin, C.Y., Lee, H.J., Wang, Y.N., Liu, M., Liao, H.W., Shi, B., Lai, C.C., Bedford, M.T., Tsai, C.H., and Hung, M.C. (2011). Crosstalk between Arg 1175 methylation and Tyr 1173 phosphorylation negatively modulates EGFR-mediated ERK activation. Nat Cell Biol *13*, 174-181.

Hsu, S.C., Miller, S.A., Wang, Y., and Hung, M.C. (2009). Nuclear EGFR is required for cisplatin resistance and DNA repair. Am J Transl Res *1*, 249-258.

Huo, L., Wang, Y.N., Xia, W., Hsu, S.C., Lai, C.C., Li, L.Y., Chang, W.C., Wang, Y., Hsu, M.C., Yu, Y.L., Huang, T.H., Ding, Q., Chen, C.H., Tsai, C.H., and Hung, M.C. (2011). RNA helicase A is a DNA-binding partner for EGFR-mediated transcriptional activation in the nucleus. Proc Natl Acad Sci U S A *107*, 16125-16130.

Hutchison, G.J., Valentine, H.R., Loncaster, J.A., Davidson, S.E., Hunter, R.D., Roberts, S.A., Harris, A.L., Stratford, I.J., Price, P.M., and West, C.M. (2004). Hypoxia-inducible factor 1alpha expression as an intrinsic marker of hypoxia: correlation with tumor oxygen, pimonidazole measurements, and outcome in locally advanced carcinoma of the cervix. Clin Cancer Res *10*, 8405-8412.

Hutvagner, G., and Simard, M.J. (2008). Argonaute proteins: key players in RNA silencing. Nature reviews Molecular cell biology *9*, 22-32.

Iki, T., Yoshikawa, M., Nishikiori, M., Jaudal, M.C., Matsumoto-Yokoyama, E., Mitsuhara, I., Meshi, T., and Ishikawa, M. (2010). In vitro assembly of plant RNA-induced silencing complexes facilitated by molecular chaperone HSP90. Molecular cell *39*, 282-291.

Iliopoulos, D., Jaeger, S.A., Hirsch, H.A., Bulyk, M.L., and Struhl, K. (2010). STAT3 activation of miR-21 and miR-181b-1 via PTEN and CYLD are part of the epigenetic switch linking inflammation to cancer. Molecular cell *39*, 493-506.

Ivan, M., Kondo, K., Yang, H., Kim, W., Valiando, J., Ohh, M., Salic, A., Asara, J.M., Lane, W.S., and Kaelin, W.G., Jr. (2001). HIFalpha targeted for VHL-mediated destruction by proline hydroxylation: implications for O2 sensing. Science *292*, 464-468.

Iwasaki, S., Kobayashi, M., Yoda, M., Sakaguchi, Y., Katsuma, S., Suzuki, T., and Tomari, Y. (2010). Hsc70/Hsp90 chaperone machinery mediates ATP-dependent RISC loading of small RNA duplexes. Molecular cell *39*, 292-299.

Jalal, C., Uhlmann-Schiffler, H., and Stahl, H. (2007). Redundant role of DEAD box proteins p68 (Ddx5) and p72/p82 (Ddx17) in ribosome biogenesis and cell proliferation. Nucleic Acids Res *35*, 3590-3601.

Jensen, E.D., Niu, L., Caretti, G., Nicol, S.M., Teplyuk, N., Stein, G.S., Sartorelli, V., van Wijnen, A.J., Fuller-Pace, F.V., and Westendorf, J.J. (2008). p68 (Ddx5) interacts with Runx2 and regulates osteoblast differentiation. Journal of cellular biochemistry *103*, 1438-1451.

Jiang, J., Lee, E.J., Gusev, Y., and Schmittgen, T.D. (2005). Real-time expression profiling of microRNA precursors in human cancer cell lines. Nucleic Acids Res *33*, 5394-5403.

Jiang, X., Huang, F., Marusyk, A., and Sorkin, A. (2003). Grb2 regulates internalization of EGF receptors through clathrin-coated pits. Mol Biol Cell *14*, 858-870.

Johnston, M., Geoffroy, M.C., Sobala, A., Hay, R., and Hutvagner, G. (2010). HSP90 protein stabilizes unloaded argonaute complexes and microscopic P-bodies in human cells. Mol Biol Cell *21*, 1462-1469.

Kawai, S., and Amano, A. (2012). BRCA1 regulates microRNA biogenesis via the DROSHA microprocessor complex. The Journal of cell biology *197*, 201-208.

Kim, V.N. (2005). MicroRNA biogenesis: coordinated cropping and dicing. Nature reviews Molecular cell biology *6*, 376-385.

Kim, V.N., Han, J., and Siomi, M.C. (2009). Biogenesis of small RNAs in animals. Nature reviews Molecular cell biology *10*, 126-139.

Knodler, L.A., and Steele-Mortimer, O. (2005). The Salmonella effector PipB2 affects late endosome/lysosome distribution to mediate Sif extension. Mol Biol Cell *16*, 4108-4123.

Koch, C.A., Anderson, D., Moran, M.F., Ellis, C., and Pawson, T. (1991). SH2 and SH3 domains: elements that control interactions of cytoplasmic signaling proteins. Science *252*, 668-674.

Kumar, M.S., Pester, R.E., Chen, C.Y., Lane, K., Chin, C., Lu, J., Kirsch, D.G., Golub, T.R., and Jacks, T. (2009). Dicer1 functions as a haploinsufficient tumor suppressor. Genes & development *23*, 2700-2704.

Kwak, P.B., and Tomari, Y. (2012). The N domain of Argonaute drives duplex unwinding during RISC assembly. Nature structural & molecular biology *19*, 145-151.

Lambertz, I., Nittner, D., Mestdagh, P., Denecker, G., Vandesompele, J., Dyer, M.A., and Marine, J.C. (2010). Monoallelic but not biallelic loss of Dicer1 promotes tumorigenesis in vivo. Cell death and differentiation *17*, 633-641.

Lee, D.F., Kuo, H.P., Chen, C.T., Wei, Y., Chou, C.K., Hung, J.Y., Yen, C.J., and Hung, M.C. (2008). IKKbeta suppression of TSC1 function links the mTOR pathway with insulin resistance. Int J Mol Med *22*, 633-638.

Lee, O.H., Kim, H., He, Q., Baek, H.J., Yang, D., Chen, L.Y., Liang, J., Chae, H.K., Safari, A., Liu, D., and Songyang, Z. (2010). Genome-wide YFP fluorescence complementation screen identifies new regulators for telomere signaling in human cells. Mol Cell Proteomics *10*, M110 001628.

Lee, Y.S., Pressman, S., Andress, A.P., Kim, K., White, J.L., Cassidy, J.J., Li, X., Lubell, K., Lim do, H., Cho, I.S., Nakahara, K., Preall, J.B., Bellare, P., Sontheimer, E.J., and Carthew, R.W. (2009). Silencing by small RNAs is linked to endosomal trafficking. Nat Cell Biol *11*, 1150-1156.

Lemmon, M.A., and Schlessinger, J. (2010). Cell signaling by receptor tyrosine kinases. Cell *141*, 1117-1134.

Leung, A.K., and Sharp, P.A. (2007). microRNAs: a safeguard against turmoil? Cell *130*, 581-585.

Leung, A.K., and Sharp, P.A. (2010). MicroRNA functions in stress responses. Molecular cell *40*, 205-215.

Leung, A.K., Vyas, S., Rood, J.E., Bhutkar, A., Sharp, P.A., and Chang, P. (2011). Poly(ADP-ribose) regulates stress responses and microRNA activity in the cytoplasm. Molecular cell *42*, 489-499.

Levitzki, A., and Gazit, A. (1995). Tyrosine kinase inhibition: an approach to drug development. Science *267*, 1782-1788.

Lu, J., Getz, G., Miska, E.A., Alvarez-Saavedra, E., Lamb, J., Peck, D., Sweet-Cordero, A., Ebert, B.L., Mak, R.H., Ferrando, A.A., Downing, J.R., Jacks, T., Horvitz, H.R., and Golub, T.R. (2005). MicroRNA expression profiles classify human cancers. Nature *435*, 834-838.

Maniataki, E., and Mourelatos, Z. (2005). A human, ATP-independent, RISC assembly machine fueled by pre-miRNA. Genes & development *19*, 2979-2990.

Martello, G., Rosato, A., Ferrari, F., Manfrin, A., Cordenonsi, M., Dupont, S., Enzo, E., Guzzardo, V., Rondina, M., Spruce, T., Parenti, A.R., Daidone, M.G., Bicciato, S., and Piccolo, S. (2010). A MicroRNA targeting dicer for metastasis control. Cell *141*, 1195-1207.

Meister, G. (2013). Argonaute proteins: functional insights and emerging roles. Nature reviews Genetics *14*, 447-459.

Melo, S.A., Moutinho, C., Ropero, S., Calin, G.A., Rossi, S., Spizzo, R., Fernandez, A.F., Davalos, V., Villanueva, A., Montoya, G., Yamamoto, H., Schwartz, S., Jr., and Esteller, M. (2010). A genetic defect in exportin-5 traps precursor microRNAs in the nucleus of cancer cells. Cancer cell *18*, 303-315.

Melo, S.A., Ropero, S., Moutinho, C., Aaltonen, L.A., Yamamoto, H., Calin, G.A., Rossi, S., Fernandez, A.F., Carneiro, F., Oliveira, C., Ferreira, B., Liu, C.G., Villanueva, A., Capella, G., Schwartz, S., Jr., Shiekhattar, R., and Esteller, M. (2009). A TARBP2 mutation in human cancer impairs microRNA processing and DICER1 function. Nature genetics *41*, 365-370.

Metivier, R., Penot, G., Hubner, M.R., Reid, G., Brand, H., Kos, M., and Gannon, F. (2003). Estrogen receptor-alpha directs ordered, cyclical, and combinatorial recruitment of cofactors on a natural target promoter. Cell *115*, 751-763.

Michlewski, G., and Caceres, J.F. (2010). Antagonistic role of hnRNP A1 and KSRP in the regulation of let-7a biogenesis. Nature structural & molecular biology *17*, 1011-1018.

Moreno-Manzano, V., Rodriguez-Jimenez, F.J., Acena-Bonilla, J.L., Fustero-Lardies, S., Erceg, S., Dopazo, J., Montaner, D., Stojkovic, M., and Sanchez-Puelles, J.M. (2010).

FM19G11, a new hypoxia-inducible factor (HIF) modulator, affects stem cell differentiation status. J Biol Chem *285*, 1333-1342.

Mori, M., Triboulet, R., Mohseni, M., Schlegelmilch, K., Shrestha, K., Camargo, F.D., and Gregory, R.I. (2014). Hippo signaling regulates microprocessor and links cell-density-dependent miRNA biogenesis to cancer. Cell *156*, 893-906.

Mosesson, Y., Mills, G.B., and Yarden, Y. (2008). Derailed endocytosis: an emerging feature of cancer. Nature reviews Cancer *8*, 835-850.

Nicoloso, M.S., Spizzo, R., Shimizu, M., Rossi, S., and Calin, G.A. (2009). MicroRNAs--the micro steering wheel of tumour metastases. Nature reviews Cancer *9*, 293-302.

Normanno, N., Bianco, C., De Luca, A., Maiello, M.R., and Salomon, D.S. (2003). Target-based agents against ErbB receptors and their ligands: a novel approach to cancer treatment. Endocr Relat Cancer *10*, 1-21.

Olayioye, M.A., Neve, R.M., Lane, H.A., and Hynes, N.E. (2000). The ErbB signaling network: receptor heterodimerization in development and cancer. The EMBO journal *19*, 3159-3167.

Paez, J.G., Janne, P.A., Lee, J.C., Tracy, S., Greulich, H., Gabriel, S., Herman, P., Kaye, F.J., Lindeman, N., Boggon, T.J., Naoki, K., Sasaki, H., Fujii, Y., Eck, M.J., Sellers, W.R., Johnson, B.E., and Meyerson, M. (2004). EGFR mutations in lung cancer: correlation with clinical response to gefitinib therapy. Science *304*, 1497-1500.

Park, J.E., Heo, I., Tian, Y., Simanshu, D.K., Chang, H., Jee, D., Patel, D.J., and Kim, V.N. (2011). Dicer recognizes the 5' end of RNA for efficient and accurate processing. Nature *475*, 201-205.

Parker, R., and Sheth, U. (2007). P bodies and the control of mRNA translation and degradation. Molecular cell *25*, 635-646.

Paroo, Z., Ye, X., Chen, S., and Liu, Q. (2009). Phosphorylation of the human microRNA-generating complex mediates MAPK/Erk signaling. Cell *139*, 112-122.

Qi, H.H., Ongusaha, P.P., Myllyharju, J., Cheng, D., Pakkanen, O., Shi, Y., Lee, S.W., and Peng, J. (2008). Prolyl 4-hydroxylation regulates Argonaute 2 stability. Nature *455*, 421-424.

Reynolds, A.R., Tischer, C., Verveer, P.J., Rocks, O., and Bastiaens, P.I. (2003). EGFR activation coupled to inhibition of tyrosine phosphatases causes lateral signal propagation. Nat Cell Biol *5*, 447-453.

Rudel, S., Wang, Y., Lenobel, R., Korner, R., Hsiao, H.H., Urlaub, H., Patel, D., and Meister, G. (2011). Phosphorylation of human Argonaute proteins affects small RNA binding. Nucleic Acids Res *39*, 2330-2343.

Rybak, A., Fuchs, H., Hadian, K., Smirnova, L., Wulczyn, E.A., Michel, G., Nitsch, R., Krappmann, D., and Wulczyn, F.G. (2009). The let-7 target gene mouse lin-41 is a stem cell specific E3 ubiquitin ligase for the miRNA pathway protein Ago2. Nat Cell Biol *11*, 1411-1420.

Rybak, A., Fuchs, H., Smirnova, L., Brandt, C., Pohl, E.E., Nitsch, R., and Wulczyn, F.G. (2008). A feedback loop comprising lin-28 and let-7 controls pre-let-7 maturation during neural stem-cell commitment. Nat Cell Biol *10*, 987-993.

Sakamoto, S., Aoki, K., Higuchi, T., Todaka, H., Morisawa, K., Tamaki, N., Hatano, E., Fukushima, A., Taniguchi, T., and Agata, Y. (2009). The NF90-NF45 complex functions as a negative regulator in the microRNA processing pathway. Mol Cell Biol *29*, 3754-3769.

Schirle, N.T., and MacRae, I.J. (2012). The crystal structure of human Argonaute2. Science *336*, 1037-1040.

Sharma, S.V., Bell, D.W., Settleman, J., and Haber, D.A. (2007). Epidermal growth factor receptor mutations in lung cancer. Nat Rev Cancer *7*, 169-181.

Shen, J., Xia, W., Khotskaya, Y.B., Huo, L., Nakanishi, K., Lim, S.O., Du, Y., Wang, Y., Chang, W.C., Chen, C.H., Hsu, J.L., Wu, Y., Lam, Y.C., James, B.P., Liu, X., Liu, C.G., Patel, D.J., and Hung, M.C. (2013). EGFR modulates microRNA maturation in response to hypoxia through phosphorylation of AGO2. Nature *497*, 383-387.

Slezak-Prochazka, I., Durmus, S., Kroesen, B.J., and van den Berg, A. (2010). MicroRNAs, macrocontrol: regulation of miRNA processing. RNA *16*, 1087-1095.

Slomiany, M.G., and Rosenzweig, S.A. (2006). Hypoxia-inducible factor-1-dependent and -independent regulation of insulin-like growth factor-1-stimulated vascular endothelial growth factor secretion. J Pharmacol Exp Ther *318*, 666-675.

Sorkin, A., and von Zastrow, M. (2009). Endocytosis and signalling: intertwining molecular networks. Nat Rev Mol Cell Biol *10*, 609-622.

Suzuki, H.I., Arase, M., Matsuyama, H., Choi, Y.L., Ueno, T., Mano, H., Sugimoto, K., and Miyazono, K. (2011). MCPIP1 ribonuclease antagonizes dicer and terminates microRNA biogenesis through precursor microRNA degradation. Molecular cell *44*, 424-436.

Suzuki, H.I., Yamagata, K., Sugimoto, K., Iwamoto, T., Kato, S., and Miyazono, K. (2009). Modulation of microRNA processing by p53. Nature *460*, 529-533.

Tahbaz, N., Kolb, F.A., Zhang, H., Jaronczyk, K., Filipowicz, W., and Hobman, T.C. (2004). Characterization of the interactions between mammalian PAZ PIWI domain proteins and Dicer. EMBO Rep *5*, 189-194.

Tokumaru, S., Suzuki, M., Yamada, H., Nagino, M., and Takahashi, T. (2008). let-7 regulates Dicer expression and constitutes a negative feedback loop. Carcinogenesis *29*, 2073-2077.

Trabucchi, M., Briata, P., Garcia-Mayoral, M., Haase, A.D., Filipowicz, W., Ramos, A., Gherzi, R., and Rosenfeld, M.G. (2009). The RNA-binding protein KSRP promotes the biogenesis of a subset of microRNAs. Nature *459*, 1010-1014.

Tsutsumi, A., Kawamata, T., Izumi, N., Seitz, H., and Tomari, Y. (2011). Recognition of the pre-miRNA structure by Drosophila Dicer-1. Nature structural & molecular biology *18*, 1153-1158.

van Kouwenhove, M., Kedde, M., and Agami, R. (2011). MicroRNA regulation by RNA-binding proteins and its implications for cancer. Nature reviews Cancer *11*, 644-656.

Varallyay, E., Burgyan, J., and Havelda, Z. (2008). MicroRNA detection by northern blotting using locked nucleic acid probes. Nat Protoc *3*, 190-196.

Ventura, A., and Jacks, T. (2009). MicroRNAs and cancer: short RNAs go a long way. Cell *136*, 586-591.

Wang, R., Jiao, Z., Li, R., Yue, H., and Chen, L. (2012). p68 RNA helicase promotes glioma cell proliferation in vitro and in vivo via direct regulation of NF-kappaB transcription factor p50. Neuro-oncology *14*, 1116-1124.

Wang, Y., Roche, O., Yan, M.S., Finak, G., Evans, A.J., Metcalf, J.L., Hast, B.E., Hanna, S.C., Wondergem, B., Furge, K.A., Irwin, M.S., Kim, W.Y., Teh, B.T., Grinstein, S., Park, M., Marsden, P.A., and Ohh, M. (2009). Regulation of endocytosis via the oxygen-sensing pathway. Nat Med *15*, 319-324.

Winter, J., Jung, S., Keller, S., Gregory, R.I., and Diederichs, S. (2009). Many roads to maturity: microRNA biogenesis pathways and their regulation. Nat Cell Biol *11*, 228-234.

Wortham, N.C., Ahamed, E., Nicol, S.M., Thomas, R.S., Periyasamy, M., Jiang, J., Ochocka, A.M., Shousha, S., Huson, L., Bray, S.E., Coombes, R.C., Ali, S., and Fuller-Pace, F.V. (2009). The DEAD-box protein p72 regulates ERalpha-/oestrogen-dependent transcription and cell growth, and is associated with improved survival in ERalpha-positive breast cancer. Oncogene *28*, 4053-4064.

Wu, C., So, J., Davis-Dusenbery, B.N., Qi, H.H., Bloch, D.B., Shi, Y., Lagna, G., and Hata, A. (2011). Hypoxia potentiates microRNA-mediated gene silencing through posttranslational modification of Argonaute2. Mol Cell Biol *31*, 4760-4774.

Wu, H., Sun, S., Tu, K., Gao, Y., Xie, B., Krainer, A.R., and Zhu, J. (2010). A splicing-independent function of SF2/ASF in microRNA processing. Molecular cell *38*, 67-77.

Xia, W., Wei, Y., Du, Y., Liu, J., Chang, B., Yu, Y.L., Huo, L.F., Miller, S., and Hung, M.C. (2009). Nuclear expression of epidermal growth factor receptor is a novel prognostic value in patients with ovarian cancer. Mol Carcinog *48*, 610-617.

Yamagata, K., Fujiyama, S., Ito, S., Ueda, T., Murata, T., Naitou, M., Takeyama, K., Minami, Y., O'Malley, B.W., and Kato, S. (2009). Maturation of microRNA is hormonally regulated by a nuclear receptor. Molecular cell *36*, 340-347.

Yang, J.S., and Lai, E.C. (2011). Alternative miRNA biogenesis pathways and the interpretation of core miRNA pathway mutants. Molecular cell *43*, 892-903.

Yang, L., Lin, C., and Liu, Z.R. (2006). P68 RNA helicase mediates PDGF-induced epithelial mesenchymal transition by displacing Axin from beta-catenin. Cell *127*, 139-155.

Zeng, Y., Sankala, H., Zhang, X., and Graves, P.R. (2008). Phosphorylation of Argonaute 2 at serine-387 facilitates its localization to processing bodies. Biochem J *413*, 429-436.

Vita

Jia Shen was born in Hang Zhou, People Republic of China, on October 22, 1983. She received the degree of Bachelor of Science with a major in Biotechnology from Zhejiang University in 2006 and was honored in Advanced Class of Engineering Education (ACEE), Chu Kochen Honors College of Zhejiang University during the same period. From 2006-2007, she worked as a research assistant in Dr. Jianzhong Shao's laboratory, College of Biosciences, Zhejiang University. In August of 2007, she entered Graduate School of Biomedical Sciences, the University of Texas Health Science Center at Houston to pursue her doctoral degree in Dr. Mien-Chie Hung's laboratory in M. D. Anderson Cancer Center.

Current address:

7901 Cambridge St Apt#102

Houston, TX, 77054